



CENTRALIZED COOPERATIVE CONTROL
FOR ROUTE SURVEILLANCE
WITH CONSTANT COMMUNICATION

THESIS

Joseph D. Rosal, Capt, USAF

AFIT/GE/ENG/09-38

DEPARTMENT OF THE AIR FORCE
AIR UNIVERSITY

AIR FORCE INSTITUTE OF TECHNOLOGY

Wright-Patterson Air Force Base, Ohio

APPROVED FOR PUBLIC RELEASE; DISTRIBUTION UNLIMITED.

The views expressed in this thesis are those of the author and do not reflect the official policy or position of the United States Air Force, Department of Defense, or the United States Government.

CENTRALIZED COOPERATIVE CONTROL
FOR ROUTE SURVEILLANCE
WITH CONSTANT COMMUNICATION

THESIS

Presented to the Faculty
Department of Electrical and Computer Engineering
Graduate School of Engineering and Management
Air Force Institute of Technology
Air University
Air Education and Training Command
In Partial Fulfillment of the Requirements for the
Degree of Master of Science in Electrical Engineering

Joseph D. Rosal, B.S.E.E.
Capt, USAF

March 2009

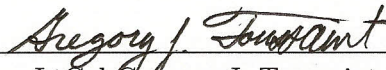
APPROVED FOR PUBLIC RELEASE; DISTRIBUTION UNLIMITED.

CENTRALIZED COOPERATIVE CONTROL
FOR ROUTE SURVEILLANCE
WITH CONSTANT COMMUNICATION

Joseph D. Rosal, B.S.E.E.

Capt, USAF

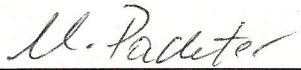
Approved:



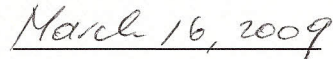
LtCol Gregory J. Toussaint, PhD
(Chairman)



date



Dr. Meir Pachter (Member)



date



Dr. Richard Cobb (Member)



date

Abstract

The route surveillance mission is a new application of unmanned aircraft systems (UASs) to meet the reconnaissance and surveillance requirements of combatant commanders. The new mission intends to field a UAS consisting of unmanned aerial vehicles (UAVs) that can provide day and night surveillance of convoy routes. This research focuses on developing a solution strategy for the mission based on the application of optimal control and cooperative control theory. The route surveillance controller uses the UAS team size to divide the route into individual sectors for each entity. A specifically designed cost function and path constraints are used to formulate an optimal control problem that minimizes the revisit time to the route and the overall control energy of the UAS. The problem complexity makes an analytical solution difficult, so a numerical technique based on the Gauss pseudospectral method is used to solve for the optimal solution. The output trajectories describe a path that each entity could fly to provide surveillance on the route. Simulated and real-world routes containing likely urban and rural characteristics were used to test the controller and show that the developed system provides feasible surveillance solutions under certain conditions. These results represent baseline statistics for future studies in this research area.

Acknowledgements

I would like to thank my thesis advisor and committee for their unrelenting support and guidance through this thesis effort. Ultimately, I could not have accomplished this challenge without the love and support of my wife, parents, and brothers.

Joseph D. Rosal

Table of Contents

	Page
Abstract	iv
Acknowledgements	v
Table of Contents	vi
List of Figures	ix
List of Tables	xii
List of Abbreviations	xiii
 I. Introduction	 1
1.1 Motivation	1
1.2 Route Surveillance Mission	2
1.3 Problem Statement	3
1.4 Thesis Organization	4
 II. Background and Current Research	 6
2.1 Introduction	6
2.2 Cooperative Control	6
2.2.1 Coupling	7
2.2.2 Cooperative search	9
2.3 Gauss Pseudospectral Method	11
2.3.1 General Continuous-time Bolza Problem	13
2.3.2 GPM Discretization	14
2.4 Summary	17
 III. Methodology	 19
3.1 Introduction	19
3.2 Route Surveillance Controller	19
3.3 Input Block	21
3.3.1 Simulated routes	21
3.3.2 Real-world routes	22
3.4 <i>K</i> -means Algorithm Block	22
3.5 Vehicle Dynamics Block	26
3.5.1 TACMAV model	26
3.5.2 Communications Constraint	28
3.5.3 Distance-from-route Constraint	29

	Page
3.6 Cost Function Block	32
3.6.1 Last-visit Time Concept	33
3.6.2 Revisit Cost Function	35
3.6.3 Control Energy Cost Function	40
3.7 Problem Setup Block	41
3.7.1 State, Control, and Path constraint limits . . .	42
3.7.2 Initial guess	44
3.7.3 PSCOL optimization	44
3.8 Summary	45
IV. Analysis and Results	47
4.1 Introduction	47
4.2 Performance Metrics	47
4.3 RS-UAS Controller Test Plan	49
4.4 RS-UAS Controller Results	51
4.4.1 Route Surveillance Coverage	51
4.4.2 Revisit Time	60
4.4.3 Communications Constraint	63
4.5 Summary	64
V. Conclusions and Recommendations	65
5.1 Conclusions	65
5.2 Future Research	67
Appendix A. Dimensionless UAV model	70
Appendix B. Camera Field-of-View Approximation	74
Appendix C. <i>K</i> -means Clustering Algorithm	77
Appendix D. Dudek’s Taxonomy	78
Appendix E. Additional Results	81
E.1 Clicked Route 1	81
E.2 Clicked Route 2	83
E.3 Random Route 1	87
E.4 Texas Route 1	90
E.5 Texas Route 2	94
E.6 Clicked Route 3	97

	Page
Appendix F. Simulation Software	102
F.1 UAV_generalMAIN	102
F.2 UAV_generalCost	103
F.3 UAV_generaldae	104
F.4 UAV_generalConnect	104
F.5 RSconstants and getConfiguration	104
F.6 Create_route	105
Appendix G. PSCOL and TOMLAB Setup	106
Bibliography	108
Vita	111

List of Figures

Figure		Page
2.1.	Example of perimeter surveillance configuration	10
3.1.	RS-UAS controller diagram	20
3.2.	Random data set with K -means clustering applied	24
3.3.	Sample Texas road divided into four sectors	25
3.4.	Simulated UAVs banked at different angles	28
3.5.	UAV parallel to a section of road	30
3.6.	UAV offset from a route	32
3.7.	FOV overlap mapped to one-dimensional road for first pass . .	33
3.8.	FOV overlap mapped to one-dimensional road for return pass .	34
3.9.	Sample augmented UAV history along a route.	36
3.10.	Sample FOV overlap on a route	38
3.11.	Sample last-visit time waveform	39
3.12.	Sample last-visit time waveform propagated in time	39
3.13.	Example state limits for four sectors	42
3.14.	Example turn limits for two sectors	43
3.15.	Example initial guess for two sectors	44
4.1.	Example last-visit time function from a simulation	48
4.2.	Clicked route for Simulation 1	50
4.3.	Clicked route for Simulation 2	50
4.4.	Texas road last-visit time function for Phase 1	53
4.5.	Texas road last-visit time function for Phase 2	53
4.6.	Texas road last-visit time function for Phase 3	54
4.7.	Legendre polynomial used by PSCOL	55
4.8.	Sector 2 trajectory for Simulation 2	56
4.9.	Simulation 4 initial guess and trajectories for Phase 1 and 3 . .	57

Figure		Page
4.10.	Simulation 4 initial guess and trajectories for Phase 1 and 3 . .	58
4.11.	Last-visit time function for Phase 1 and 3 of Simulation 5 . . .	59
4.12.	Simulation 3 route and resulting sector trajectory	60
4.13.	Simulation 6 control energy minimization	62
4.14.	Communications spacing between UAV 1 and 2	64
B.1.	Camera Field-of-view illustration	74
B.2.	Camera Field-of-view corner illustration	75
E.1.	Clicked route from Dayton for two UAVs	81
E.2.	Sector trajectories over clicked Dayton road	81
E.3.	Clicked Road 1 last-visit time function for Phase 1	82
E.4.	Clicked Road 1 last-visit time function for Phase 2	82
E.5.	Clicked Road 1 last-visit time function for Phase 3	83
E.6.	Clicked route from Dayton for four UAVs	84
E.7.	Sector trajectories over clicked road for four UAVs	85
E.8.	Clicked Road 2 last-visit time function for Phase 1	86
E.9.	Clicked Road 2 last-visit time function for Phase 2	86
E.10.	Clicked Road 2 last-visit time function for Phase 3	87
E.11.	Random road divided into three sectors	88
E.12.	Sector trajectories over random road for three UAVs	88
E.13.	Random road last-visit time function for Phase 1	89
E.14.	Random road last-visit time function for Phase 2	89
E.15.	Random road last-visit time function for Phase 3	90
E.16.	Texas road divided into four sectors	91
E.17.	Sector trajectories over Texas road	92
E.18.	Texas road last-visit time function for Phase 1	93
E.19.	Texas road last-visit time function for Phase 2	93
E.20.	Texas road last-visit time function for Phase 3	94
E.21.	Partial Texas road divided into two sectors	95

Figure		Page
E.22.	Sector trajectories over Simulation 2	95
E.23.	Texas road last-visit time function for Phase 1	96
E.24.	Texas road last-visit time function for Phase 2	96
E.25.	Texas road last-visit time function for Phase 3	97
E.26.	Clicked Route 3 divided into three sectors	98
E.27.	Sector trajectories over Clicked Route 3	99
E.28.	Clicked Route 3 last-visit time function for Phase 1	100
E.29.	Clicked Route 3 last-visit time function for Phase 2	100
E.30.	Clicked Route 3 last-visit time function for Phase 3	101

List of Tables

Table		Page
3.1.	Sector lengths corresponding to Figure 3.3	25
3.2.	System specifications for the TACMAV	27
3.3.	Revisit-Cost variable definition	35
3.4.	Path constraint limits	43
4.1.	RS-UAS controller test plan	49
4.2.	Surveillance coverage over the route per phase	52
4.3.	Results from using smaller Δ_{max}	59
4.4.	Surveillance coverage for Simulation 3	60
4.5.	Simulation travel-time ranges for each phase	61
4.6.	Simulation revisit times for each phase	62
D.1.	Dudek’s Taxonomy	80
E.1.	Surveillance coverage for Clicked Route 1	83
E.2.	Surveillance coverage for Clicked Route 2	87
E.3.	Surveillance coverage for random route	90
E.4.	Surveillance coverage for Texas route	94
E.5.	Surveillance coverage for partial Texas route	97
E.6.	Surveillance coverage for Clicked Route 3	101
F.1.	Important simulation software files	102

List of Abbreviations

Abbreviation		Page
AFIT	Air Force Institute of Technology	3
ANT	Advanced Navigation Technology	4
CC	cooperative control	7
DoD	Department of Defense	1
FOV	field of view	2
GPM	Gauss pseudospectral method	15
GPS	Global Positioning System	3
IEDs	improvised explosive device	1
KKT	Karush-Kuhn-Tucker	15
LG	Legendre-Gauss	17
NLP	nonlinear programming problem	15
PSCOL	Gauss pseudospectral optimization program	15
RS	route surveillance	3
RSCC	Route Surveillance Cooperative Control	5
RS-UAS	Route Surveillance-UAS	3
TACMAV	Tactical Micro Air Vehicle	4
UASs	unmanned aircraft systems	1
UAVs	unmanned aerial vehicles	2
3-DOF	3-degree of freedom	14

CENTRALIZED COOPERATIVE CONTROL FOR ROUTE SURVEILLANCE WITH CONSTANT COMMUNICATION

I. Introduction

1.1 *Motivation*

The Department of Defense (DoD) has taken increased interest in the employment of unmanned aircraft systems (UASs) as evidenced by published documents outlining official concept of operations and promoting a department-wide roadmap for future unmanned systems [1, 2]. With benefits such as reducing risk to human life, performing dull, dirty, and dangerous missions, and an unwavering ability to fly sorties without rest, UASs will continue to positively impact current conflicts. During Operations Enduring Freedom and Iraqi Freedom, UASs logged nearly 400,000 flight hours from October 2006 to October 2007 [2]. This statistic is still more impressive with the inclusion of flight hours logged from other operations, and will only increase with future advanced systems fulfilling the requirements established by the “Unmanned Systems Roadmap 2007-2032” [2].

Combatant commanders have identified reconnaissance and surveillance as a principal mission for UASs. Unmanned systems are well suited for this mission since they are an effective tool to help acquire, process, and decipher information that is relevant for today’s warfighter. Research that expands the capabilities of existing UASs could have an immediate impact for current operations.

Improvised explosive devices (IEDs) continue to threaten current operations and are one factor increasing the demand for unmanned systems. Emerging from the need to protect coalition forces, a new concept of a surveillance mission was created to mitigate the IED threat before a device is planted. The new mission attempts to stop and counter the planting of IEDs on roadways by allowing a specifically designed UAS

to surveil routes commonly traveled by coalition forces. The primary objective of this research is to apply optimal control theory and cooperative control theory to allow a UAS to provide persistent surveillance of a roadway. The mission specifications will be discussed in Section 1.2. Section 1.3 provides a problem statement for this research along with assumptions based on the route surveillance mission.

1.2 Route Surveillance Mission

A representative route surveillance mission would be to field a UAS consisting of four unmanned aerial vehicles (UAVs) that can provide day and night surveillance of convoy routes. The system can be controlled from a single ground control unit. The UAS should surveil areas of interest up to 60 miles in length with at least hourly updates to every point along the route. There are two objectives of the proposed UAS that are required for the route surveillance mission. The first is to minimize the re-visit time over the route to better detect the planting of IEDs. The second is to maximize the flight time of the system without losing surveillance of the route.

A requirement of the control algorithm is to automatically adjust coverage routes when UAVs are retasked or need to be refueled. A communication system will provide full bandwidth at a maximum distance of 20 miles. This constraint dictates that the UAVs must reconfigure to maintain full bandwidth to communicate with other vehicles and the ground station at the origin of the route.

The UAS must create a pattern such that each vehicle maintains surveillance of the route and the ability to communicate with other vehicles. Each UAV preserves surveillance by projecting its camera field of view (FOV), defined as the total viewing window of the sensor, on the route at all times. Since the purpose of the surveillance is to detect suspicious activity, the UAVs must stay within a certain distance and height from the route to ensure each camera FOV provides constant imaging of the road. Having identified the relevant aspects of the surveillance mission, the next section will translate these overall objectives into a specific problem statement for this research effort.

1.3 Problem Statement

Given the background information and the mission scenario, an overall problem statement can be formulated as follows: apply optimal control theory to develop UAV trajectories that efficiently meet the objectives of the route surveillance mission. The collective system will be referred to as the route surveillance-UAS (RS-UAS) and must provide constant surveillance on the route in order to achieve the mission objectives. The RS-UAS controller divides each route into sectors and determines appropriate trajectories for the UAS by applying an optimal control technique. The controller is demonstrated by processing simulated and real-world routes to determine if the trajectories provide constant surveillance and if the revisit time is minimized. Since performance is determined through simulations, the routes and UAVs used in the simulations must satisfy a variety of assumptions based on the RS mission and Air Force Institute of Technology (AFIT) resources.

The first assumption is that the routes to be monitored will be well defined for the simulation environment. This research assumes a well-defined route will have a waypoint every quarter of a mile centered on the roadway and that the roadway travels in a straight line between any two waypoints. Although terrain will not be considered, the path shapes of urban and rural routes do differ greatly. The waypoint-defined routes modeled with urban and rural characteristics will be simulated and imported from a global positioning system (GPS) device.

The next assumption is that the UAVs will be treated as point masses controlled by a capable autopilot. The number of UAVs will be capped at four aircraft per team for two reasons. First, the route surveillance mission is intended to primarily operate with team sizes of four aircraft. Second, the amount of processing time required to optimize flight paths for larger team sizes using the current solution technique would be impractical.

The third assumption is that the Tactical Micro Air Vehicle (TACMAV), owned by the Advanced Navigation Technology (ANT) Center, flight characteristics have

been chosen to represent the UAVs modeled in this research. The operational RS-UAS could be implemented as a man-portable weapon system, which is the intended use of the TACMAV platform. Since the TACMAV's camera resolution is much less than the intended sensor for the RS mission, mission altitudes in this research will be decreased to simulate a necessary pixel resolution. Adjusting for the actual camera resolution and UAV can be easily accommodated in the RS-UAS controller.

The tailored mission considered by this research will have the following global attributes:

- The candidate paths will be two-dimensional roads less than 60 miles in length.
- Terrain is assumed to be negligible at flight altitude.
- UAV communication bandwidth is assumed valid at distances less than 20 miles.
- The UAV altitude of 300 feet maintains appropriate pixel resolution.
- Wind will not be a contributing factor in the environment, so it is assumed to be zero.

This research effort is a new investigation into the RS mission, so performance metrics, such as the surveillance coverage and revisit time to the route, cannot be compared to baseline statistics. Instead, the results of the investigation will establish values for the performance metrics that could serve as an initial baseline for future studies. The results show that the overall approach provides a satisfactory solution to the RS problem under certain conditions.

1.4 Thesis Organization

Chapter II will provide key background concepts concerning cooperative control and optimal control problems. The route surveillance mission is categorized as a cooperative search mission and compared to current research for trends in the control architecture. As a result of studying current research with cooperative search mis-

sions, a numerical optimization technique is selected as the solution strategy for this problem.

The RS-UAS controller is developed in Chapter III. The system architecture is introduced and leads to the discussion of the K -means route division and the optimal control problem solved by the numerical optimization software.

Chapter IV will define the metrics used to assess the performance of the controller and present the test schedule developed for the RS-UAS controller. A set of candidate routes that captured likely road shapes were used to demonstrate that the controller can process routes with real-world characteristics. In addition, Chapter IV provides an analysis and discussion of the results.

This research is concluded in Chapter V by offering closing remarks and suggesting methods for expanding upon this research. Recommendations for future work propose methods for improving the RS-UAS controller and taking this research beyond the assumptions outlined in Section 1.3.

II. Background and Current Research

2.1 Introduction

Since the route surveillance problem is a new area of research, this chapter presents cooperative control (CC) search problems to determine a general solution method that can be applied in the RS-UAS controller. As a result, an optimization technique is selected to solve the route surveillance problem. Cooperative control and its complex characteristics are defined in Section 2.2, which continues with an examination of current CC search problems. Section 2.3 discusses the Gauss pseudospectral method and provides reasons for choosing a numerical method to solve the optimal control problem. Section 2.4 summarizes the topics in this chapter used to develop the basis for the methods implemented in the RS-UAS controller.

2.2 Cooperative Control

Cooperative control entails designing algorithms to control interactions between entities in a cooperative system. “A cooperative system is defined to be multiple dynamic *entities* that share information or tasks to accomplish a common, though perhaps not singular, objective” [30]. An example of a cooperative system is a team of UAVs performing a surveillance mission to gain knowledge of an area of operation. The cooperative controller is the mechanism that controls the entities in this example. An important function of an entity within a cooperative system is the capability to communicate with others by actively passing information or passively observing other entities [30]. Communication also plays a large role in identifying the properties and solutions of CC problems.

Cooperative control systems have two general types of control structures: centralized and decentralized. In a centralized approach, a control algorithm is designed to compute a solution assuming it has complete system knowledge. Because all of the system information is available in one central location, this control structure produces optimal solutions for the system. The appropriate solution is transferred to each entity resulting in cooperation.

Conversely, decentralized approaches distribute a copy of the control algorithm throughout the entities in the system. Those embedded control algorithms compute solutions based on necessary information received from other team members. This approach is much harder to design because the embedded controllers cannot make decisions assuming complete system knowledge, making the solutions suboptimal. Unless a consensus building scheme is used to ensure identical information throughout the embedded controllers, the overall cooperation will be limited [6].

Regardless of the control structure, the system achieves cooperation through different methods and conditions of communication. In the centralized case, a form of communication is required between the cooperative controller and the entities for this structure to function. Alternatively, the decentralized structure requires communication between the entities so each embedded controller can function. In most cases, the communication in the system is affected by its environment, which has different impacts on the reliability and robustness of the two structures.

Any cooperative control problem poses its own challenges because of the many driving forces within the system and its environment. Due to this complex nature, designing a general approach for solving CC problems does not exist in the literature. However, Beard, McLain, Chandler, Decker, and Martinez [6, 12, 14, 15, 28, 29] have worked to classify and categorize cooperative search problems. Beard et al. [6] categorized the level of coupling between entity tasks and decisions to help an engineer distill all of the system information down to an essential set required for cooperation. Realizing the amount of coupling in this research effort, which is discussed in the next section, will justify the control structure and methods presented in Chapter III.

2.2.1 Coupling. Defining varying levels of coupling between entities and their tasks provides a method for gaining insight into a CC problem [6]. The four categories that describe the level and type are objective, local, full, and dynamic coupling. This CC characterization is important because the amount of coupling is related to the achievable level of cooperation [6]. If a high degree of coupling exists in a

CC problem, then finding an approach for a valuable solution will be more demanding. If that same CC problem can be translated in a manner which decreases coupling, the solution method that achieves cooperation will be easier to find.

Objective coupling is the simplest and least restrictive incidence of coupling. This situation can be defined when the decisions, costs, and outcomes of an entity do not affect those of the other group members. In essence, the entities have influence on their team members only through the constraint or objective that defines cooperation and not through the direct impact on another entity.

The subsequent level of coupling is local coupling, which shares an attribute with objective coupling. Each entity once again can influence team members through the constraint or objective that defines cooperation. The key difference lies in the fact that local coupling assumes the individual's combined cost to the mission is a function of its decisions and of its *local* neighbors' decisions.

Full coupling represents the highest level of complexity where each entity affects the decisions, costs, and outcomes of itself along with the *entire* group of collaborating entities. In order for a single entity to decide to act, it must have knowledge of the intentions of every other member on the team. The controller approach required for this level of coupling will be highly complex.

The final category of coupling is dynamic coupling. This type is not defined in terms of coupling in constraints or objectives defining cooperation but in terms of coupling between shared physical cooperation. Consider a group of aircraft flying in close formation attempting to benefit from the shared aerodynamics. Local coupling exists between lead and follower aircraft because of the aerodynamic properties affecting the follower and channeling back to the leader. The dynamic coupling in this example is the physical interactions existing between each pair of aircraft in the formation. Because of the physical implications, this category is typically treated in a different manner than CC problems involving the other types of coupling.

Combining this technique of analyzing CC problems in conjunction with Dudek’s taxonomy in Appendix D can provide a powerful advantage in identifying the crucial elements of a CC problem. Determining the level of coupling will help an engineer focus the control efforts on the elements that facilitate cooperation. In other words, those critical characteristics affect the significance of the controlling mechanism. Now that cooperative control has been introduced and a method to identify key elements of CC problems has been discussed, current research in cooperative search missions will be presented and used to select general methods to solve the route surveillance problem.

2.2.2 Cooperative search. Since Decker’s summary of research regarding cooperative search missions, the research focus has shifted from centralized approaches with probabilistic methods [8, 9, 18, 35] to distributed approaches where computation and decision exist at the entity level [4, 6, 13, 19, 24, 25, 28, 29]. Chandler [12] found that the current research using distributed algorithms can undertake increased levels of coupling between local and global neighbors, while making the task of designing useful systems much harder. Three works from current research, all implementing distributed algorithms, have been selected to develop the foundation for the methods implemented in Chapter III.

The work conducted by Kingston et al. [25] on perimeter surveillance with a UAS is the most relevant research for the route surveillance problem. The authors based their solution approach on the principles and perimeter surveillance problem developed by McLain and Beard [6, 29]. Essentially, the general perimeter surveillance problem is reduced to a linear perimeter surveillance problem. Kingston et al. placed the UAVs in a chain along the perimeter as illustrated in Figure 2.1. The UAVs are assumed to communicate at the ends of their respective sectors where the coordination variable (the sector endpoints for each UAV) chosen by Kingston et al. can be communicated. Coordination variables defined by McLain and Beard [6, 29] represent the minimum information required for each entity to decide how to achieve coopera-

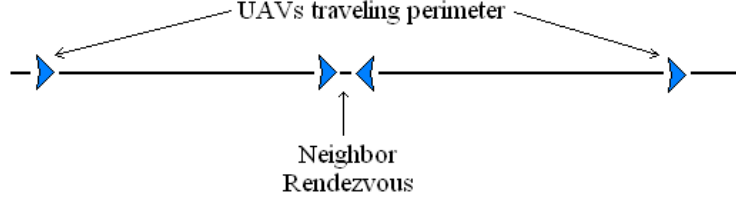


Figure 2.1: Example of perimeter surveillance configuration used by Kingston et al. [25].

tion. The heuristic control law developed by Kingston et al. causes any two neighbors that rendezvous to communicate essential information and then escort the neighbor to the appropriate sector endpoint. Afterwards, the UAVs continue searching their respective sectors. The authors showed that this control law eventually caused the team of UAVs to settle into a balanced surveillance configuration (each UAV traveled a portion of the evenly-divided route) on the perimeter even if some UAVs were spontaneously removed from the system.

The distributed control law developed by Kingston et al. differs from the intended control structure for this research, but the results are applicable. The authors above showed that splitting the route into N sectors (where N is the number of vehicles) produced a steady-state configuration for the UAS to provide surveillance in the perimeter problem. This result will be used in the RS-UAS controller except that communication with the other vehicles and ground control must be preserved while each vehicle travels its sector. However, the type of surveillance in the research above differs from that required in the route surveillance problem. The control algorithm in this research, modeled after the centralized control structure, can provide optimal surveillance trajectories.

The research efforts by McLain and Beard [6, 29] and Martinez et al. [28] aid in selecting a solution approach for the RS-UAS controller. Those authors seek to define cooperation constraints (McLain and Beard) or aggregate objective functions (Martinez et al.) to distill the CC problem into a set of essential information for the collective to obtain for cooperation. The method in which those functions are

produced comes from two distinct fields: one from simply studying and modeling the CC problem under consideration and the other from systems theory or graph-based knowledge. However, both sets of authors have come to the same general structure for distributed algorithms: 1) define a function that captures cooperation, 2) optimize the function that in turn dictates the actions of each entity, and 3) ensure that the collective group comes to a consensus on the essential information. The current research effort is concerned with centralized control algorithms, but the first two steps above will be applied to the RS-UAS controller developed in Chapter III. A function must be created that captures the cooperative surveillance of the collective team. Next, a method is required to optimize the orbit trajectories over the route. The entities do not exchange cooperative information, but the communication between entities must be maintained in order to collectively provide surveillance on the route.

The function created to capture cooperation in this research takes the form of a cost function within an optimal control problem. The next section will describe how a numerical optimization technique is required to overcome problem complexities.

2.3 Gauss Pseudospectral Method

Engineers have taken advantage of optimal control techniques in efforts to find the best method to guide and control aerospace systems. There are two general methods for solving optimal control problems. The first uses conditions for optimality to analytically solve for the optimal control. This approach is feasible for dynamic systems with limited states, controls, and constraints. The second approach uses numerical methods to solve for the optimal control. Although the problems are typically transcribed to some sort of computer language, the classic conditions of optimality are preserved.

In this research, numerical methods were chosen because the potential number of states and controls makes an analytical solution impractical. Each first-order model of the TACMAV includes five states and two control variables. If four UAVs are used to provide surveillance of a route, analytically solving for optimality conditions be-

comes difficult with 20 states and 8 control variables. A 3-degree of freedom (3-DOF) model like the one used by Kim [24] includes seven states and three control variables. In this case, a four-UAV system would include 28 states and 12 control variables. Model complexity only increases with a 6-DOF model. For those reasons, numerical techniques are the preferred solution method, but there are additional design choices required to solve the optimal control problem in this research.

Two general categories for solving continuous-time optimal control problems with numerical techniques are indirect and direct methods. Indirect methods typically use the calculus of variations to derive first-order necessary conditions for optimality. The solutions that result from indirect methods are highly accurate, but require a thorough comprehension of the optimal control problem [7]. In contrast, direct methods convert the continuous-time optimal control problem into a nonlinear programming (NLP) problem [7]. Instead of computing first-order optimality conditions as in an indirect method, the direct method seeks to satisfy the Karush-Kuhn-Tucker (KKT) conditions resulting from an augmented cost function or Lagrangian.

One particular direct method of interest is the pseudospectral method that parameterizes the state and control using global interpolating polynomials. In the case of the Gauss pseudospectral method, the Lagrange interpolating polynomials are used to approximate the state and control. A common problem with direct methods is that they provide either incorrect costate or no costate information, which are often needed to verify optimality [22]. The Gauss pseudospectral method (GPM) marries the pseudospectral method with the Costate Mapping Theorem to convert the KKT multipliers into the Lagrange multipliers [7]. The Costate Mapping Theorem bridges the gap between KKT conditions and first-order necessary conditions. Benson et al. [7] showed that the Costate Mapping Theorem proved equivalence between solving the optimal control problem and computing the continuous-time variational conditions with the Gauss pseudospectral method. This equivalence is important and justifies the use of the GPM because direct methods do not suffer from the same disadvantages of indirect methods and pseudospectral methods converge to a solution at a faster rate.

The numerical method chosen to optimize the route surveillance optimal control problem of Section 3.7.3 is the Gauss pseudospectral optimization program, also called PSCOL. This software package uses the GPM to convert the optimal control problem into an NLP before passing it to an NLP solver. The MATLAB-based NLP solver used for this effort is called SNOPT and it is contained within the TOMLAB Optimization Environment. The remainder of this section will follow the general outline of the Gauss pseudospectral method developed by Benson et al. [7] and employed by PSCOL.

2.3.1 General Continuous-time Bolza Problem. Before the GPM is derived, this section will provide a general definition for a continuous Bolza problem. The Bolza form is an all-encompassing formulation of an optimal control problem. When solving an optimal control problem, the task is to find the state, $\mathbf{x}(\tau)$, the control, $\mathbf{u}(\tau)$, and the initial and final times, t_0 and t_f , respectively, that minimize the cost function

$$J = \Phi(\mathbf{x}(-1), t_0, \mathbf{x}(1), t_f) + \frac{t_f - t_0}{2} \int_{-1}^1 g(\mathbf{x}(\tau), \mathbf{u}(\tau), \tau, t_0, t_f) d\tau \quad (2.1)$$

subject to the constraints

$$\dot{\mathbf{x}}(\tau) = \frac{t_f - t_0}{2} \mathbf{f}(\mathbf{x}(\tau), \mathbf{u}(\tau), \tau, t_0, t_f) \quad (2.2)$$

$$\phi(\mathbf{x}(-1), t_0, \mathbf{x}(1), t_f) \leq \mathbf{0} \quad (2.3)$$

$$\mathbf{C}(\mathbf{x}(\tau), \mathbf{u}(\tau), t_0, t_f) \leq \mathbf{0} \quad (2.4)$$

where $\Phi(\cdot)$ is the Mayer cost, $g(\cdot)$ is the Lagrange cost, $\mathbf{f}(\cdot)$ defines the state dynamics, $\phi(\cdot)$ defines the state boundary constraints, and $\mathbf{C}(\cdot)$ defines the path constraints. Note that PSCOL scales the time interval $t \in [t_0, t_f]$ to $\tau \in [-1, 1]$ via the affine transformation

$$t = \frac{t_f - t_0}{2} \tau + \frac{t_f + t_0}{2} \quad (2.5)$$

During the derivation of the GPM, Equations (2.1)-(2.4) will be referred to as the continuous Bolza problem.

2.3.2 GPM Discretization. The GPM begins with discretizing and transcribing the continuous Bolza problem into an NLP by approximating the state with a basis of $N + 1$ Lagrange polynomials given by

$$\mathbf{x}(\tau) \approx \mathbf{X}(\tau) = \sum_{i=0}^N \mathbf{X}(\tau_i) L_i(\tau) \quad (2.6)$$

where $L_i(\tau)$, for $i = 0, \dots, N$, with N chosen by the user, are defined as

$$L_i(\tau) = \prod_{j=0, j \neq i}^N \frac{\tau - \tau_j}{\tau_i - \tau_j} \quad (2.7)$$

Also, the control is approximated in a similar manner except using a basis of N Lagrange interpolating polynomials given by

$$\mathbf{u}(\tau) \approx \mathbf{U}(\tau) = \sum_{i=1}^N \mathbf{U}(\tau_i) L_i^*(\tau) \quad (2.8)$$

where $L_i^*(\tau)$, for $i = 1, \dots, N$, is equal to

$$L_i^*(\tau) = \prod_{j=1, j \neq i}^N \frac{\tau - \tau_j}{\tau_i - \tau_j} \quad (2.9)$$

Differentiating Equation (2.6) yields

$$\dot{\mathbf{x}}(\tau) \approx \dot{\mathbf{X}}(\tau) = \sum_{i=0}^N \chi(\tau_i) \dot{L}_i(\tau) \quad (2.10)$$

where χ represents the derivative of \mathbf{X} from Equation (2.6). The derivative of the Lagrange polynomials at the N Legendre-Gauss (LG) points can be represented in a differential approximation matrix, which is needed later when Gauss quadrature

is used to approximate the final point \mathbf{X}_f and the cost J . Gauss quadrature is a numerical method for approximating definite integrals with a weighted sum (Gauss weights) of function values within the interval of interest. The LG points are the roots of the Legendre polynomials that form the abscissas for the Gauss quadrature. The differential approximation matrix can conveniently be computed offline as follows

$$D_{ki} = \dot{L}_i(\tau_k) = \sum_{j=0}^N \frac{\prod_{j=0, j \neq i, k}^N \tau_k - \tau_j}{\prod_{j=0, j \neq i}^N \tau_i - \tau_j} \quad (2.11)$$

where $k = 1, \dots, N$ and $i = 0, \dots, N$. The dynamic constraint of Equation (2.2) is converted into an algebraic constraint using the differential approximation matrix as follows

$$\sum_{i=0}^N D_{ki} \chi_i - \frac{t_f - t_0}{2} \mathbf{f}(\mathbf{X}_k, \mathbf{U}_k, \tau_k, t_0, t_f) = \mathbf{0}, \quad k = 1, \dots, N \quad (2.12)$$

where $\mathbf{X}_k \equiv \mathbf{X}(\tau_k)$ and $\mathbf{U}_k \equiv \mathbf{U}(\tau_k)$ for $k = 1, \dots, N$. In addition, $\mathbf{X}_0 \equiv \mathbf{X}(-1)$ and \mathbf{X}_f is defined using the Gauss quadrature given by

$$\mathbf{X}_f \equiv \mathbf{X}_0 + \frac{t_f - t_0}{2} \sum_{k=1}^N w_k \mathbf{f}(\mathbf{X}_k, \mathbf{U}_k, \tau_k, t_0, t_f) \quad (2.13)$$

The continuous cost function in Equation (2.1) is also approximated using Gauss quadrature

$$J = \Phi(\mathbf{X}_0, t_0, \mathbf{X}_f, t_f) + \frac{t_f - t_0}{2} \sum_{k=1}^N w_k g(\mathbf{X}_k, \mathbf{U}_k, \tau_k, t_0, t_f) \quad (2.14)$$

where w_k are the Gauss weights determined using the LG points, \mathbf{X}_k

$$w_k = \frac{2(1 - \mathbf{X}_k^2)}{(k+1)^2 [P_{k+1}(\mathbf{X}_k)]^2} \quad (2.15)$$

where $k = 1, \dots, N$ and P_{k+1} are the Legendre polynomials evaluated at the LG points. The boundary constraints are also discretized at the LG points

$$\phi(\mathbf{X}_k, t_0, \mathbf{X}_f, t_f) = \mathbf{0} \quad (2.16)$$

$$\mathbf{C}(\mathbf{X}_k, \mathbf{U}_k, \tau_k, t_0, t_f) \leq \mathbf{0}, \quad k = 1, \dots, N \quad (2.17)$$

In summary, the PSCOL software package uses the Gauss pseudospectral method defined generally in Equations (2.12)-(2.17) to satisfy the KKT conditions for optimality to *approximate* the optimal solution to the continuous Bolza problem in Section 2.3.2. Benson et al. [7] showed that the approximate optimal solution approaches the exact answer when the number of nodes N increases. Unfortunately, the authors did not suggest a method for determining an appropriate number of nodes other than through heuristic knowledge.

Another benefit to using the GPM employed by PSCOL to solve optimal control problems is that discontinuities in the state or control can be accounted for by splitting the trajectory into phases and then connecting them together by linkage constraints. The problem of interest must first be formulated into a multi-phase continuous Bolza problem as follows. Given a set of P phases, minimize the cost function

$$J = \sum_{p=1}^P J^{(p)} = \sum_{p=1}^P [\Phi^{(p)}(\mathbf{x}^{(p)}(t_0), t_0, \mathbf{x}^{(p)}(t_f), t_f; \mathbf{q}^{(p)}) + \mathcal{L}(\mathbf{x}^{(p)}(t), \mathbf{u}^{(p)}(t), t; \mathbf{q}^{(p)}) dt] \quad (2.18)$$

subject to the dynamic constraint

$$\dot{\mathbf{x}}^{(p)} = \mathbf{f}^{(p)}(\mathbf{x}^{(p)}, \mathbf{u}^{(p)}, t; \mathbf{q}^{(p)}), \quad p = 1, \dots, P \quad (2.19)$$

the state boundary conditions

$$\phi_{min} \leq \phi^{(p)}(\mathbf{x}^{(p)}(t_0), t_0^{(p)}, \mathbf{x}^{(p)}(t_f), t_f^{(p)}; \mathbf{q}^{(p)}) \leq \phi_{max}, \quad p = 1, \dots, P \quad (2.20)$$

the inequality path constraints

$$\mathbf{C}^{(p)}(\mathbf{x}^{(p)}(t), \mathbf{u}^{(p)}(t), t; \mathbf{q}^{(p)}) \leq \mathbf{0}, \quad p = 1, \dots, P \quad (2.21)$$

and the phase continuity or linkage constraints

$$\mathbf{P}^{(p)}(\mathbf{x}^{(p_l^s)}(t), t_f^{(p_l^s)}; \mathbf{q}^{(p_l^s)}, \mathbf{x}^{(p_u^s)}(t_0), t_0^{(p_u^s)}; \mathbf{q}^{(p_u^s)}) = \mathbf{0}, \quad p_l, p_u \in [1, \dots, P]; s = 1, \dots, L \quad (2.22)$$

where $\mathbf{x}^{(p)}(t)$, $\mathbf{u}^{(p)}(t)$, $\mathbf{q}^{(p)}$, and t are the state, control, static parameters, and time in phase p , respectively. L is the number of phases to be linked, $p_l^s \in [1, \dots, P]; s = 1, \dots, L$ are the left phase numbers, and $p_u^s \in [1, \dots, P]; s = 1, \dots, L$ are the right phase numbers. The left and right phase numbers become the first and second phases in time being connected. For example, when connecting phase one and two together, the left and right phase numbers are one and two respectively.

While there are no discontinuities in the route surveillance optimal control problem, the problem does lend itself well to this method because of the natural division of the repeated passes over the route. Each lap (one pass from start to end of the appropriate route sector) taken by the UAVs can be treated as one phase. All the phases are then attached together using linkage constraints. Having discussed the necessary background to understand the methods developed in Chapter III, the next section will summarize the concepts developed throughout this chapter.

2.4 Summary

The route surveillance problem could be postulated in a manner that allows for full coupling to exist and therefore would require a complex decentralized approach. Cooperative control problems can be highly complex when full coupling exists between entity decisions and the mission costs and outcomes. However, the mission requirements outlined in Sections 1.2 and 1.3 dictate that an operator with a computing system monitors the RS-UAS at a single location. This definition suggests that a

centralized approach requiring full system knowledge is an appropriate solution. Since the mission is defined in this manner, an analysis determines that local coupling exists between the decisions of an entity and its neighbors, thereby significantly reducing the coupling. Each UAV is free to fly surveillance on the route as long as it flies within 20 miles of its neighbors ahead and behind.

The linear perimeter surveillance problem considered by Kingston et al. [25] is similar to the RS mission defined in Chapter I. The differences lie in when the entities communicate, the control structure, and the type of perimeters considered. In that problem, entities could travel unconstrained as long as there was a rendezvous with neighbors. The problem in this research has constrained the entities' movement to stay within 20 miles of the neighbors and to ensure that each camera FOV provides constant imaging of the route. The heuristic control law developed by Kingston et al. differs greatly from a centralized approach, but the results of their work show that dividing the route into sectors for each vehicle is a feasible approach for the UAS to provide surveillance of the route.

Three challenges are recognized for this research that stem from the past research in cooperative search problems. The first is designing a cost function that captures the cooperative nature of this mission. Specifically, the cost function should produce a set of trajectories to ensure the collective team provides constant surveillance on the prescribed route. The next challenge needs to constrain the trajectory further by forcing the UAVs to stay within communications range and within range of the route. The final challenge will be to properly formulate an optimal control problem that can be solved by PSCOL.

Chapter III discusses the methods used to solve the route surveillance problem. Chapter IV outlines the steps to validate the methods in Chapter III, discusses the test plan developed to process simulated and real-world routes, and analyzes the results of this research effort.

III. Methodology

3.1 Introduction

This chapter takes the general solution methods outlined in Chapter II and develops the RS-UAS controller that will provide surveillance trajectories for a UAS. The discussion begins with an overview of the system block diagram and continues with subsequent sections covering the details of each subcomponent in the controller.

3.2 Route Surveillance Controller

The RS-UAS controller illustrated in Figure 3.1 is designed to apply the route division idea from research conducted by Kingston et al. and the general solution structure suggested from the cooperative search groundwork. Since the RS-UAS system is a centralized architecture, all of the system information is available to the controller, but after filtering the information, the RS-UAS controller only needs the following information: the number of UAVs and the prescribed waypoint route. The controller operates in a two-step process using the provided information. First, it divides the route into feasible sectors for the size of the UAS. Then, the controller formulates an optimal control problem with a specifically designed cost function and path constraints for PSCOL to optimize. In a real-world environment, the cooperative controller would execute every time the number of UAVs changed. The RS-UAS controller has been designed with a similar purpose automatically executing the two-step process above.

Before any trajectories can be determined, the prescribed route must be partitioned into K sectors, where K is the number of UAVs in operation. The easiest method to partition the prescribed route would be to evenly divide the route into K pieces similar to the linear perimeter surveillance problem discussed in Chapter II. However, a better method considers the route characteristics to shape the sectors to maximize the route coverage. In this research, the K -means clustering algorithm was implemented within the RS-UAS controller to explore a method that would divide the route by analyzing the statistical dispersion of the waypoints defining the route.

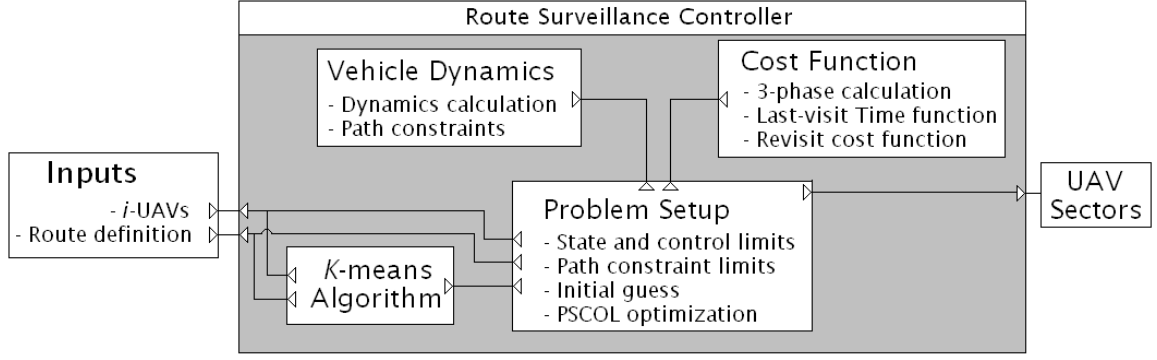


Figure 3.1: The RS-UAS controller diagram.

Section 3.4 will discuss reasons why the K -means algorithm is applicable and show how the algorithm operates to find feasible route sectors.

In Figure 3.1, the Vehicle Dynamics block calculates the UAV dynamics and the path constraints when prompted by the Problem Setup block. This component allows the RS-UAS controller to be customized for different UAV models and path constraints. Section 3.5.1 will discuss the first-order UAV model and provide the parameters taken from the TACMAV. The vehicle path constraint in Section 3.5.2 will ensure that the camera FOV images the route as much as possible. Section 3.5.3 will detail the problem path constraint chosen to restrict the UAS path in order to maintain communication throughout the UAS.

The Cost Function block is responsible for calculating the cost for each phase in the optimal control problem. The route surveillance cost function consists of two components tailored to meet the UAS objectives for the route surveillance mission. First, the revisit cost function uses the last-visit time function to produce a cost for the UAS while traveling along the route. Second, the control energy cost function penalizes the overall energy expenditure of the UAS to ensure maximum system flight time. Section 3.6.1 introduces the last-visit time function concept while Section 3.6.2 provides a method for calculating the revisit cost at each instant in time. Section 3.6.3 demonstrates the method for calculating the cost function used to minimize control inputs.

Once the sectors have been determined, they are passed to the Problem Setup block which contains the PSCOL software. This component receives inputs from the K -means, Vehicle Dynamics, and Cost Function blocks. Most importantly, the Problem Setup block structures the route surveillance problem into a multi-phase optimal control problem as defined in Section 2.3.2. Before PSCOL solves an optimal control problem, two aspects of the problem must be structured. First, all the system states and path constraints must be bounded appropriately. Next, an initial guess must be developed so that PSCOL has a starting point to converge to a solution quickly. Section 3.7.1 explains the structure for constraining the system states and path constraints, and Section 3.7.2 develops the method for estimating the RS initial guess. Lastly, Section 3.7.3 applies the general multi-phase optimal control structure defined in Section 2.3.2 to the RS problem. Before the RS-UAS controller subcomponents are presented, the next section will outline two methods for providing candidate routes.

3.3 Input Block

The primary purpose of creating simulated and real-world candidate routes is to properly show that the developed RS-UAS controller is robust enough to handle various route characteristics. A secondary purpose is to demonstrate potential capabilities of an operational system for the RS mission.

3.3.1 Simulated routes. There are three methods for creating simulated routes for the RS-UAS controller to process. The first method loads a sample map into a MATLAB figure where a user can click a desired path with a mouse along highways in the map. A second method, similar to the first, uses a blank MATLAB figure to allow the user to click a desired path shape. The third method creates randomly generated paths using the assumptions about candidate paths outlined in Chapter I. The first two methods simulate a user having the ability to provide on-the-fly candidate routes. Loading a local map suggests a scenario where an operator has the ability to create a waypoint path based on the local road system. Loading a blank

figure could be used where an area does not have a road system, like the perimeter fence around a base. The random-generated routes allow complex and random route shapes to test system robustness.

3.3.2 Real-world routes. Real-world routes can be recorded with a hand-held GPS device while traveling local roadways. The route chosen for this research effort was designed to manifest likely or common characteristics of urban and rural highways. The test plan in Chapter IV uses a route recorded on a Texas highway, which will serve as a baseline scenario for the RS-UAS controller. It contains appropriate characteristics that meet the route assumptions from Chapter I making it a good candidate for this research effort. Having defined the two methods for creating candidate routes, the next section will explain the K -means clustering algorithm that develops feasible sectors.

3.4 K -means Algorithm Block

The K -means algorithm is a form of a clustering algorithm that seeks to divide M data points, \mathbf{x}_i , into $K < M$ disjoint clusters, S_j [21]. The \mathbf{x}_i 's in this case are the two-dimensional waypoints defining the route. The algorithm minimizes the sum-of-squares metric

$$J = \sum_{j=1}^K \sum_{i=1}^M (\mathbf{x}_i - \boldsymbol{\mu}_j)^T (\mathbf{x}_i - \boldsymbol{\mu}_j) \quad (3.1)$$

where $\boldsymbol{\mu}_j$ is the two-dimensional mean point of the respective cluster S_j . The K -means approach to route division is suitable for this research because it exploits the route characteristics by approximating the information with a multi-mode probability density function. Each route is analyzed by calculating the statistical dispersion of the route and then assigning each waypoint to one of the K clusters.

The form of Equation (3.1) is related to finding the second moment of a set of data, also called the variance of the data. Consider a set of random data points in a

space called H . After determining the mean, the variance of H can be given by

$$\text{VAR}[H] = \sum_{i=1}^M p_i (H_i - \mu)^2 \quad (3.2)$$

where μ is the data mean and p_i is the probability of that data sample occurring. Alternatively, p_i can be interpreted as a weight that describes the importance of the i th sample. In that type of calculation, the data mean is found first and represents the value where the data points in H are centered around. The variance simply determines the variability of the data around the mean. The mean and variance of H can be interpreted in various ways depending on what the data represent.

In this application of the K -means algorithm, the number of UAVs will represent the number of means occurring in the route, which can be interpreted as where the sectors are located in the route. Optimizing the metric in Equation (3.1) will extract the optimal set of waypoints centered around each mean. Two basic sectors arise from this analysis. The first type will have a 2-dimensional variability, meaning the route fluctuates greatly in orthogonal directions. The second type of sector will have a 1-dimensional variability, meaning the route primarily fluctuates in only one direction. The K -means algorithm is useful for extracting different combinations of these two sectors that are likely to be well-balanced, but, as will be explained later, will not necessarily be the optimal partitioning of the route.

The algorithm operates in the following steps (the MATLAB software is listed in Appendix C and comes from the Mathworks File Exchange [11]). Initially, the cluster means are guessed by choosing from two options. The first is randomly choosing means from the data. The second is simply providing an initial guess. Using those initially-guessed means, $\boldsymbol{\mu}_j$'s, each waypoint is assigned to the appropriate cluster mean by the metric given in Equation (3.1). The metric operates by finding the minimum distance from each \mathbf{x}_i (or waypoint) to all of the different cluster means. The \mathbf{x}_i 's are assigned to a group by selecting the closest cluster centroid. The next step is to recompute the centroid of each cluster and then re-assign each data point

to the closest mean. The last two steps are iterated until there are no changes in the cluster means and the waypoint partitions. Figure 3.2 shows four data clusters after the K -means algorithm has been applied. Consider the green cluster at the right of the data spread. All of the data points in that cluster are physically closer to the mean in that local area than the means of the two adjacent blue and red clusters.

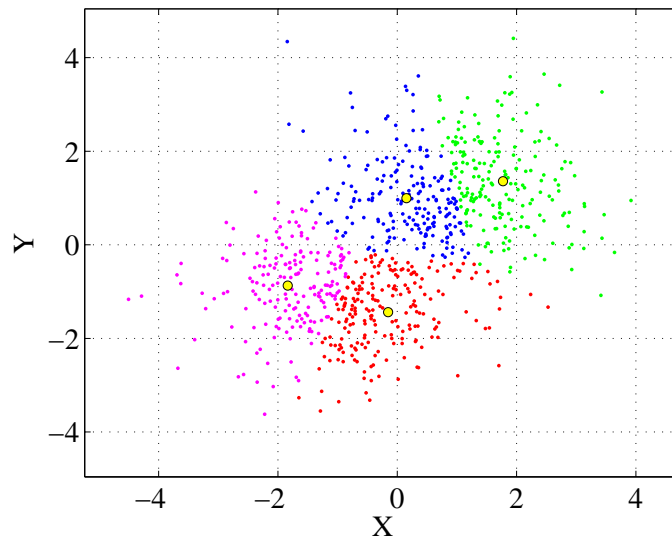


Figure 3.2: Random data set that has been clustered into four groups. The larger yellow points represent the means of the respective clusters.

The performance of the K -means algorithm can be non-optimal because the algorithm typically uses discrete data points for assignment to the closest μ_j , which could cause quantization-like errors to arise. This means that if the data set does not contain sufficient data points relative to the chosen K parameter, the algorithm could return non-optimal clusters. In this application, this error is mitigated because the prescribed routes possess a minimum waypoint resolution ensuring a large data set. If the data set happens to be small, for example the route was generated by a user clicking on a map, then the route can be augmented with waypoints using an interpolation technique. Note that the path is assumed to be a straight line between any two waypoints and the maximum separation between adjacent waypoints will be no more than a quarter of a mile. Figure 3.3 shows the Texas route that has been

partitioned into $K = 4$ sectors. Table 3.1 lists the sector lengths corresponding to Figure 3.3. The endpoint distance refers to the length between the two endpoints of the route.

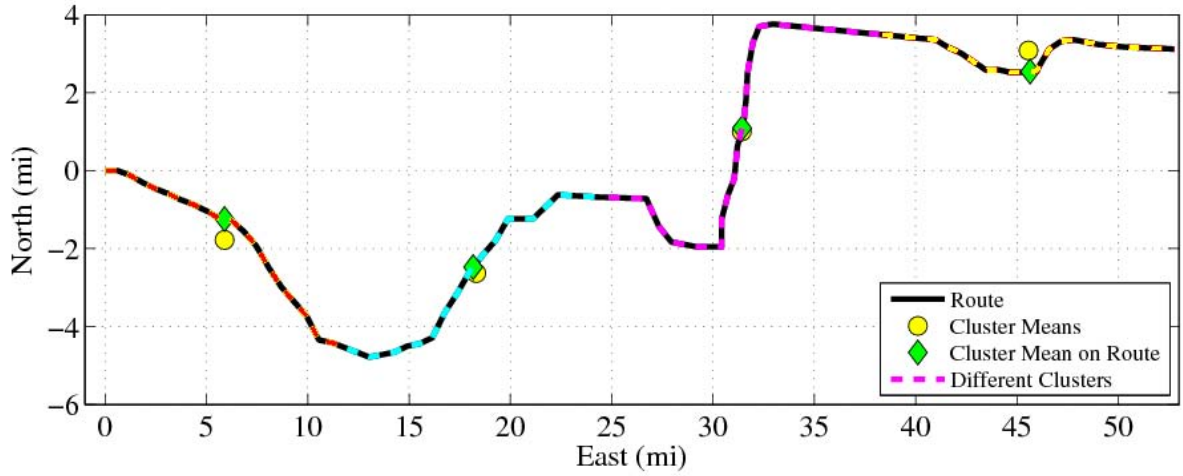


Figure 3.3: Sample Texas road divided into four sectors with K -means algorithm.

Table 3.1: Sector lengths corresponding to Figure 3.3

Sector	Length (mi.)	Color
1	12.98	red
2	14.05	cyan
3	18.04	magenta
4	14.82	yellow
Total Route	59.90	
Endpoint distance	52.88	

Notice that the magenta sector is 18 miles in length and significantly longer than the other three sectors. Studying Figure 3.3 reveals that the magenta sector fluctuates in orthogonal directions because of more bends and transitions in this section of the route. This sector demonstrates the first basic sector (fluctuating in orthogonal directions) example outlined previously. Also, notice that the red, yellow, and cyan

sectors are much straighter demonstrating the second type of basic sector. So for this $K = 4$ case, the output sectors shown in Figure 3.3 are statistically-balanced sectors for the UAVs to fly. However, the sectors would change if the K parameter changed or if the number of waypoints describing the route increased or decreased. Before the sectors of a route are used in the Problem Setup block, the vehicle dynamics and cost function components are discussed in the next two sections.

3.5 Vehicle Dynamics Block

This section presents the vehicle dynamics and path constraints that are calculated throughout the PSCOL optimization. The UAV model is a first-order approximation of the vehicle dynamics used by Kingston et al. [25] and tailored for the TACMAV. The two path constraints are implemented in this controller subcomponent because PSCOL groups all of the path constraints with the equations of motion. The first constraint controls the distance between two neighboring vehicles, while the second constraint governs the UAV distance from the route to ensure the camera FOV is imaging the route whenever possible.

3.5.1 TACMAV model. The TACMAV flight qualities have been chosen to represent the UAVs in this research. The Kestrel autopilot used to control the TACMAV is capable of commanding heading (through bank angle), velocity, and altitude hold, however, since the mission altitude is constant, the two-dimensional dynamics will be modeled by the following dimensionless equations:

$$\begin{aligned}
\dot{p}'_{N,i} &= \frac{T_B V_{max}}{P_{RT}} V_{DL,i} \sin \psi_i \\
\dot{p}'_{E,i} &= \frac{T_B V_{max}}{P_{RT}} V_{DL,i} \cos \psi_i \\
\dot{\psi}_{DL,i} &= \frac{g T_B}{V_{max}} \frac{\tan \phi_i}{V_{DL,i}} \\
\dot{V}_{DL,i} &= \alpha_V T_B (V_{DL,i}^c - V_{DL,i}) \\
\dot{\phi}_{DL,i} &= \alpha_\phi T_B (\phi_i^c - \phi_i)
\end{aligned} \tag{3.3}$$

where $\mathbf{p}' = (p'_N, p'_E)^T$ is the dimensionless inertial position of the UAV, (ψ, ϕ, V) are the heading, roll angle, and airspeed, g is the gravitational constant, and (V^c, ϕ^c) are the airspeed and roll angle commands given by the autopilot. Equation (3.3) has been non-dimensionlized using the process outlined in Appendix A. The first-order response of the autopilot to airspeed and roll angle commands are quantified by the parameters α_V and α_ϕ . Inherently, constraints on the airspeed $-V_{max} \leq V \leq V_{max}$ and roll angle $-\phi_{max} \leq \phi \leq \phi_{max}$ are enforced to ensure the safety of the UAV and to sufficiently model dynamic limitations [25]. Table 3.2 lists relevant specifications of the TACMAV.

Table 3.2: System specifications for the TACMAV

Parameter	Min	Max
Airspeed	$63 \frac{\text{ft}}{\text{s}}$	$90 \frac{\text{ft}}{\text{s}}$
Roll	-45°	45°
Altitude	300 ft	300 ft
α_V		1
α_ϕ		2
Camera FOV (Horiz)		48°
Camera FOV (Vert)		40°
Camera Depression Angle		39°

The sensor that is onboard the TACMAV is a simple fixed-direction camera pointing 90° from the nose of the aircraft towards the left wing. The intent of this research is to design algorithms that ensure the FOV images the roadway so camera resolution is not considered, however, the RS-UAS controller is designed to easily accommodate other UAV models and their sensors. The UAV model and sensor specifications could be replaced with the exact parameters of an operational UAV. For example, the aircraft altitude above ground affects the camera resolution necessary for software identification algorithms so parameters such as this can be tailored for specific situations.

The FOV of the TACMAV was estimated using Terning’s research on FOV approximation [33]. Table 3.2 lists the necessary specifications to approximate the FOV. Appendix B outlines the FOV calculations, including the MATLAB function created by Terning. In this research, Terning’s function was modified to account for vehicle roll, which greatly affects the FOV projection onto the ground. Figure 3.4 depicts two simulated UAVs banked at zero (red trapezoid) and ten (green trapezoid) degrees, respectively. The UAV scale has been increased to demonstrate the FOV orientation. Note that the approximated camera FOVs during the simulations in Chapter IV were restricted to be valid only for distances less than one mile. This restriction ensured that PSCOL could not command maximum positive bank angle throughout the trajectory, effectively imaging large sections of the route in one instant.

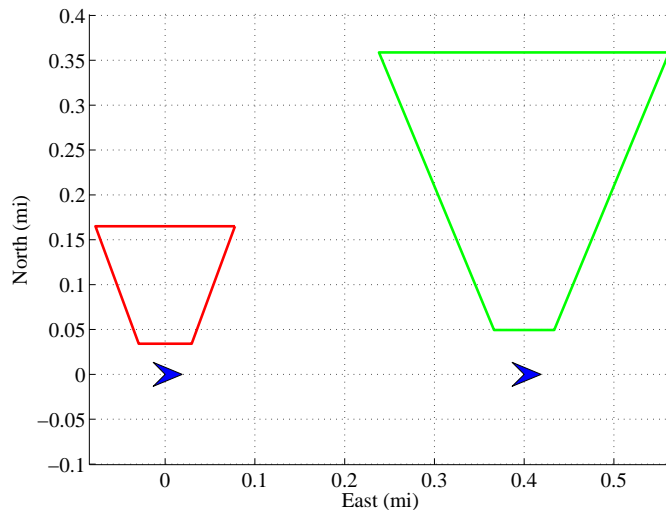


Figure 3.4: Two simulated UAVs banked at zero (red) and ten (green) degrees, respectively. The UAV icons are not to scale.

3.5.2 Communications Constraint. There are two important path constraints that must be evaluated at all times during the optimization. The first is the communications constraint that ensures any two adjacent entities in the system are within 20 miles of each other. The term entity is used here to describe the UAVs as well as the ground station. A simple method for maintaining the communications

constraint is given by

$$\text{ComSpacing}_{i-1} = \| P_{UAV,i} - P_{UAV,i-1} \| \leq 20 \text{ miles} \quad (3.4)$$

where $i = 2, \dots, K$ and K is the number of UAVs on the team and $P_{UAV,i}$ is the i th UAVs position. There will be $K - 1$ ComSpacing calculations for the spacing between UAVs at each instant in time. This equation does not allow the UAVs to fly more than 20 miles apart. Also, the closest UAV to the ground station will not be permitted to fly more than 20 miles away with the following expression

$$\text{ComSpacing}_{GS} = \| P_{UAV,1} - P_{GS} \| \leq 20 \text{ miles} \quad (3.5)$$

where P_{GS} is the position of the ground station. This research will assume the ground station is at the origin of the route. Equations (3.4) and (3.5) will be implemented as a path constraint in the Vehicle Dynamics block, however the constraint limits are applied in the Problem Setup block.

3.5.3 Distance-from-route Constraint. The vehicle path constraint developed to restrict UAV motion seeks to control the cross-track distance of the UAV from the route. The equations developed in this section are based on the following assumption: the route taken between any two waypoints in the path description is assumed to be a straight line. The assumptions in Chapter I ensure sufficient waypoints to accurately describe the path.

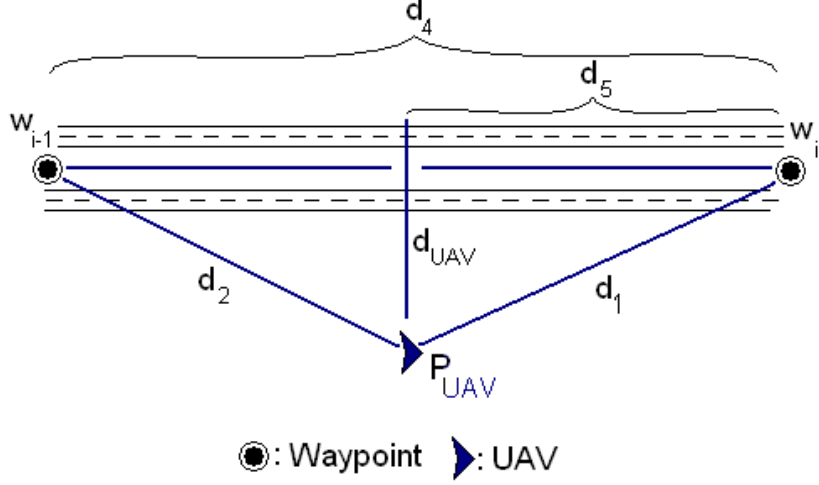


Figure 3.5: Top view of UAV randomly positioned parallel to a section of road.

Considering Figure 3.5, let the i th UAV be at some position P_{UAV} with fixed height. The UAV is moving from waypoint w_{i-1} to waypoint w_i at some velocity. Distances d_1 and d_2 are given by

$$d_1 = \| P_{UAV,i} - w_i \| = \sqrt{(x_i - x_1)^2 + (y_i - y_1)^2} \quad (3.6)$$

$$d_2 = \| P_{UAV,i} - w_{i-1} \| = \sqrt{(x_i - x_2)^2 + (y_i - y_2)^2} \quad (3.7)$$

where $P_{UAV,i} = (x_i, y_i)$, $w_i = (x_1, y_1)$, and $w_{i-1} = (x_2, y_2)$. The distance d_4 should be known, but can be calculated in a manner similar to Equations (3.6) and (3.7). Using a dot product, the component length of the projection of vector $\overrightarrow{P_{UAV}w_i}$ onto vector $\overrightarrow{w_{i-1}w_i}$ is given by

$$d_5 = \overrightarrow{P_{UAV}w_i} \cdot \left(\frac{\overrightarrow{w_{i-1}w_i}}{d_4} \right) \quad (3.8)$$

The right side of the equation converts $\overrightarrow{w_{i-1}w_i}$ into a unit vector before multiplying with $\overrightarrow{P_{UAV}w_i}$. The distance d_{UAV} can now be calculated using the previous quantities

and Pythagorean's Theorem.

$$d_{UAV,i} = \sqrt{d_1^2 - d_5^2} = \sqrt{\|P_{UAV} - w_i\|^2 - \left(\overrightarrow{P_{UAV}w_i} \cdot \left(\frac{\overrightarrow{w_{i-1}w_i}}{d_4} \right) \right)^2} \quad (3.9)$$

where $d_{UAV,i}$ is the i th UAV's distance from the route. Equation (3.9) is converted into a path constraint

$$\Delta_{min} \leq d_{UAV,i} \leq \Delta_{max} \quad (3.10)$$

and implemented in the Vehicle Dynamics block, however the constraint limits are set in the Problem Setup block.

The minimum and maximum offsets of the constraint are based on the approximated FOV projection of the camera mounted on the UAV and can be tailored for any situation. In this research, the path constraint was used to limit the i th UAV's distance from the road to within two-tenths of mile, $\Delta_{max} = 0.2$ mi. This offset was designed to account for positive bank angle while the UAV was traveling the route. Each entity was allowed to fly over the route, $\Delta_{min} = 0$ mi. Figure 3.6 illustrates how the offset values were determined; the scale of the FOV, UAVs, and route (black line) are correct. The Δ_{max} and Δ_{min} variables are only meant to demonstrate how the UAV could be swept close to and away from the route.

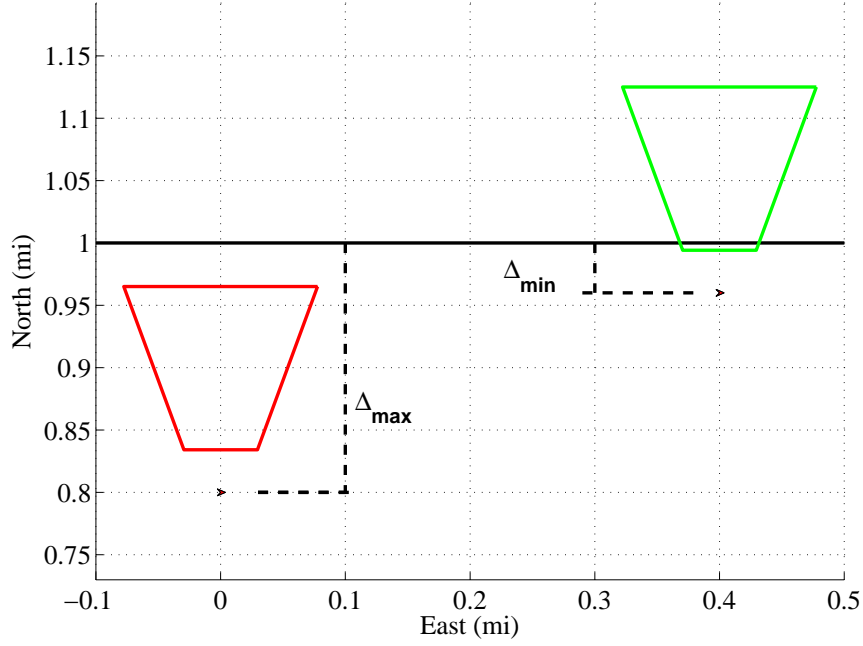


Figure 3.6: Example showing how the UAV offset from the road can be determined by sweeping the vehicle across the route.

This section concludes the discussion on the vehicle dynamics and path constraints, which are only a portion of an optimal control problem. The next section will present the cost function that completes the RS optimal control problem.

3.6 Cost Function Block

The crucial element of the RS-UAS controller is the cost function that captures the cooperative nature of the RS mission. The key to finding an appropriate cost function was incorporating the RS mission objectives: revisit the route as often as possible and maximize the RS-UAS flight time. This section will detail the development of the RS-UAS controller cost function given by

$$\mathcal{J}_T = J_{revisit} + J_{energy} \quad (3.11)$$

The last-visit time concept is developed first and then used to calculate the revisit time cost function, $J_{revisit}$, in Section 3.6.2. Section 3.6.3 will develop the cost function that seeks to minimize control energy, J_{energy} .

3.6.1 Last-visit Time Concept. The RS mission is designed to provide surveillance on a road as often as possible in order to catch suspicious and harmful activity. To increase the probability of observing such acts, each UAV must revisit the road as often as possible. Hence, the RS-UAS cost function requires a function that describes the last-visit time to the road. The essence of the last-visit time function will be explained with a simple example. Imagine a single UAV traveling at constant velocity beside a route at some arbitrary time t_i , where the UAV began its surveillance at $t_0 = 0$. In Figure 3.7, a camera is mounted to the aircraft and is oriented to look at 90° to the left from the vehicle motion (similar to the TACMAV).

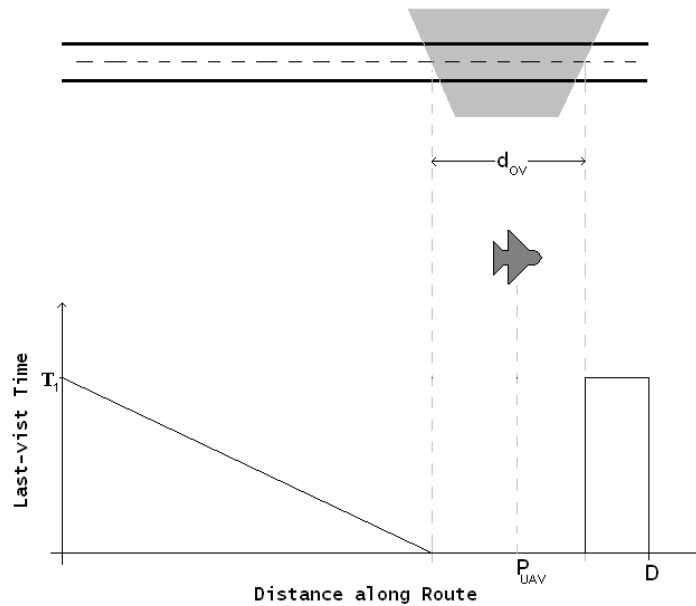


Figure 3.7: A sample FOV overlap has been mapped to a straight line representation of the road where an example last-visit time function has been constructed.

At the time t_i , the camera FOV overlaps a segment of the road that is d_{OV} in length. At this instant in time, the section of road within the FOV has been last

visited at $T = 0$ (where T denotes the time since last visited). The section of road ahead of the UAV has been last visited at $T = t_i$, since the UAV began its surveillance at $t = 0$. The section of road behind the UAV has been last visited at varying T 's. For instance, the beginning of the road was last visited at $T = t_i$ time units ago. The section of road directly behind the UAV was last visited at $T = \frac{d_i}{V_i}$, where d_i is the distance moved by the UAV between $t = t_i$ and $t = t_{i-1}$ and V_i is the velocity at time t_i . As Figure 3.7 depicts, the function takes on a ramp-like shape behind the UAV and a square-like function ahead of the UAV. This overall function shape is only valid when the UAV is making its first pass over the road. All other passes will possess a steady-state last-visit time function depicted in Figure 3.8.

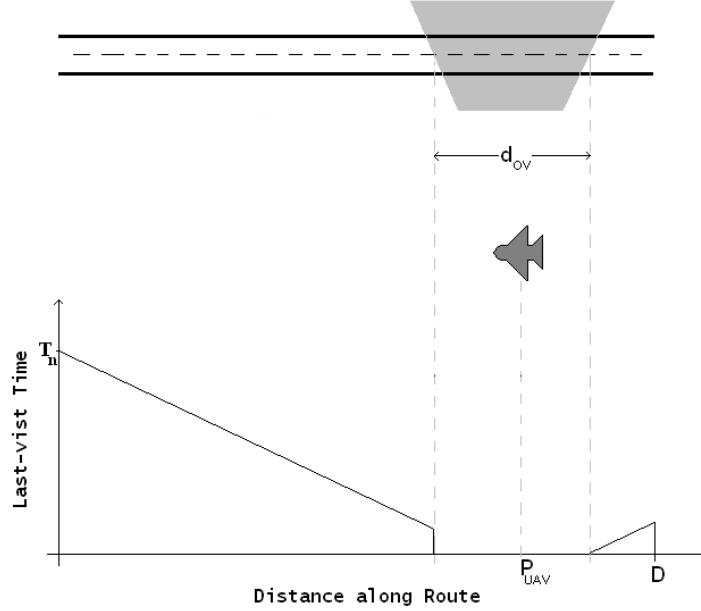


Figure 3.8: A sample FOV overlap has been mapped to a straight line representation of the road where an example last-visit time function has been constructed. This figure depicts a return pass over the road.

By constructing the function at each instant in time, the RS-UAS controller can assign a cost to the time since the last visit by summing all of the last-visit times, T , in the last-visit time function. In Figures 3.7 and 3.8, the last-visit times are represented by the y -axis. The summation of the last-visit times is the total time of

last visit to the road. The key to minimizing the revisit time of the UAS to the road is by effectively driving the overall last-visit time function toward zero. If the road could be viewed in its entirety at each instant in time, the last-visit time function would always be zero. In this case, each UAV is traveling the road with a limited FOV, therefore, the last-visit time function will be manifested as illustrated in Figures 3.7 and 3.8.

The last-visit time function also serves as a convenient method for evaluating the surveillance along the trajectory and can be re-constructed after PSCOL has determined the optimal trajectories. Analyzing the resulting last-visit time function indicates the quality of surveillance on the route. Chapter IV will use this function to judge the performance of the RS-UAS controller. The next section will demonstrate how the revisit cost function is calculated using the last-visit time function.

3.6.2 Revisit Cost Function. Before the revisit cost function is developed, the necessary variables are defined in Table 3.3. The time and state history of the UAVs, t_i and $P_{UAV,i}$, from the past to the current time are assumed to be known. Using this information, necessary quantities (defined in Table 3.3) for constructing the last-visit time function can be calculated for each instant in time. There are two preliminary steps that help calculate the last-visit time function efficiently.

Table 3.3: Revisit-Cost variable definition

Variable	Definition
t_i	Time history of the vehicle motion
$t_{current}$	Current elapsed time since the vehicle began surveillance
$P_{UAV,i}$	i th position of UAV in time
$P_{A-UAV,i}$	augmented position of UAV in time
$d_{OV,i}$	width of i th overlap of FOV
P_{OV}	vector of distance along the route
d_{route}	length of the prescribe route
$d_{OV,i}$	FOV overlap on the route at each instant in time
T_i	Time-since-last-visit history

The first step involves augmenting the state position history between the discrete nodes. Since PSCOL operates with discrete nodes, each UAV's motion will be assumed to move in a straight path between position nodes. A linear approximation can be used to augment the state history, $P_{A-UAV,i}$. This augmentation process affords higher resolution when constructing the last-visit time function. The spacing between the augmented position nodes was chosen to be approximately 200 feet, which is the minimum FOV overlap (defined as the length of road inside the viewing window of the camera) on the road when the vehicle is flying wings level. Section 3.5.3 provides a method for determining the approximate FOV overlaps. Figure 3.9 illustrates a sample UAV trajectory along a prescribed route with nodes spaced at approximately 200 feet.

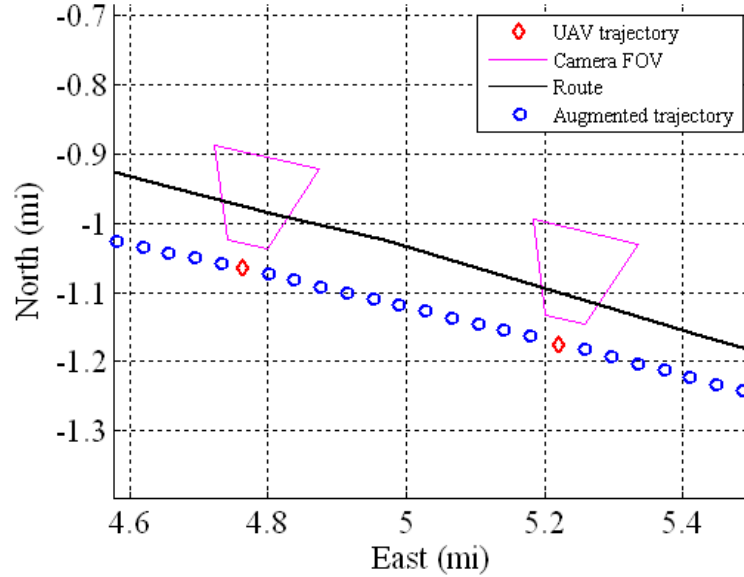


Figure 3.9: Sample augmented UAV history along a route.

The second step must translate the route into one dimension (1-D) representing the distance along the route. The length of the 1-D approximation is the total length of the prescribed route. This will remove road curvature and provide a method for determining the FOV overlap on the road at each instant in time. The 1-D representation is further divided into bins where each bin is also 200 feet in width. P_{OV} is a

vector where each element represents each 200-foot bin along the route. Simultaneously, T_i is a vector the same length as P_{OV} where each element represents the time since last visit for each bin along the route.

Constructing the last-visit time function using the quantities above is done in several steps. At each point in the augmented state history, the FOV is approximated and projected onto the ground. The FOV overlap, $d_{OV,i}$, is determined and translated to a 1-D distance along the route; there will be a trailing and leading edge point representing the overlap. The trailing and leading edge points are compared to the P_{OV} vector to find the bins of the route that were overlapped, $\text{bins} = d_{OV,i} \cup P_{OV}$. Using the overlapped bin element numbers, the time-since-last-visit vector, T_i , is updated. First, the bin times that were not overlapped are updated with the elapsed time since the last augmented UAV position, t_{aug} . Second, the bin elements that were overlapped are set to zero.

$$t_{aug} = t_{current} - t_{i-1} \quad (3.12)$$

$$T_i = T_i + t_{aug} \quad (3.13)$$

$$T_i(\text{bins}) = 0 \quad (3.14)$$

If there is no overlap at the current UAV position, then the time-since-last-visit vector is updated with t_{aug} and no bins are set to zero, and those bins along the route will not be viewed on the current pass over the route. Figure 3.10 demonstrates an example of how a route and an FOV overlap map to a single dimension. In the figure, the red brackets along P_{OV} represent the FOV overlap at the current UAV position along the route. The bins within those brackets correspond to the elements in T_i that are set to zero in Equation (3.14).

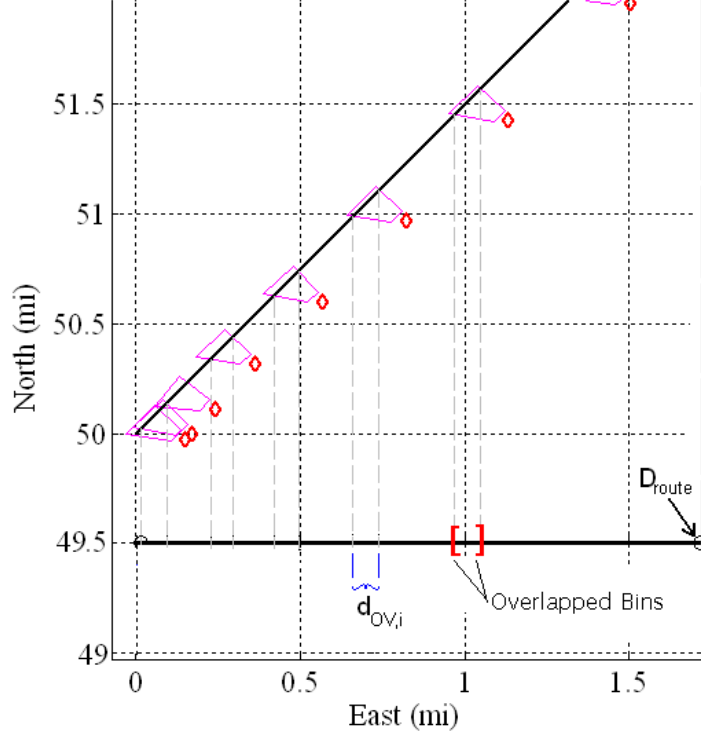


Figure 3.10: Sample FOV overlap history translated to a single dimension (dark flat line). The current overlapped bins are between the red brackets on the route.

The resulting last-visit time function can be illustrated by plotting T_i versus P_{OV} . Figure 3.11 illustrates a sample last-visit time function constructed using the simulated data in Figure 3.10. The plateaus at $T_i = 38$, $T_i = 35$, $T_i = 22$, and $T_i = 0$ seconds represent sections of the road that were overlapped simultaneously at the current time. Those plateaus have varying widths depending on the amount of FOV overlap, $d_{OV,i}$. The sharp transition at $P_{OV} = 0.15$ means the plateaus representing the FOV overlap at $T_i = 35$ and $T_i = 22$ covered some of the same area at two consecutive points in time. Referring back to the reference flight history depicted in Figure 3.10, the bottom left hand corner shows that some of the FOV trapezoids did indeed overlap. The square-like waveform ahead of the current overlap at $T_i = 0$ represents the last-visit time to the route ahead of the current UAV position. Notice that the height of the square-like waveform is derived from the fact that the route

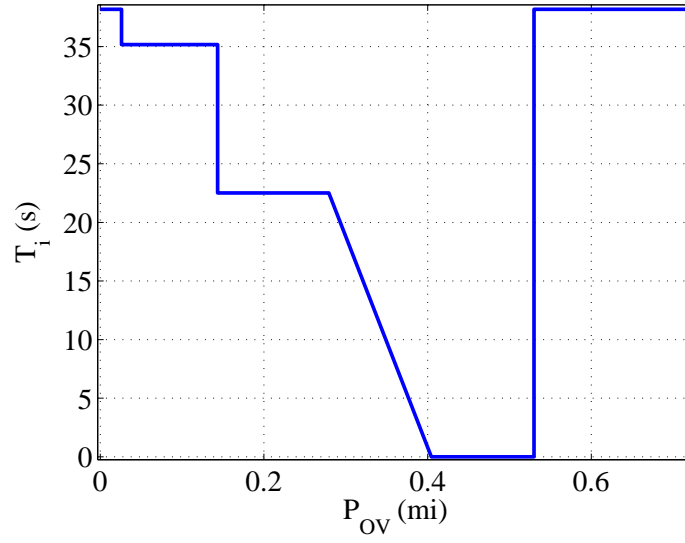


Figure 3.11: Sample last-visit time waveform constructed from time and state history depicted in Figure 3.10.

ahead has not been visited. Figure 3.12 demonstrates the last-visit time function when the UAV has flown further down the route.

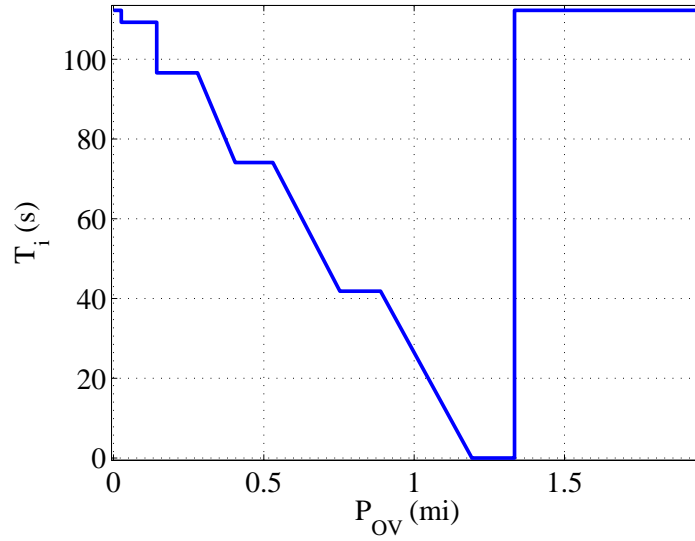


Figure 3.12: Sample last-visit time waveform from Figure 3.11 propagated in time.

The last-visit time function is ready to be used in calculating the $J_{revisit}$ cost function. The last-visit time vector, T_i , at each UAV position in time, like those

illustrated in Figures 3.11 and 3.12, will be summed to produce a revisit time cost for each UAV. The cooperative nature of the route surveillance mission is captured by summing T_i across every UAV sector. All the sectors appended together reconstruct the entire prescribed route. Therefore, summing T_i in this manner assigns a total revisit cost for the collective team of UAVs. The revisit cost function is given by

$$J_{revisit} = \int_0^{t_M^{(p)}} \sum_{j=1}^K \alpha_{ji} \frac{1}{M_{ji}} \sum_{i=0}^{M_i} T_{ji} dt \quad (3.15)$$

where $t_M^{(p)}$ is the total time it takes for the UAVs to simultaneously fly one pass over their sectors of the road, p is the number of phases in the problem (discussed in Section 3.7.3), M_{ji} is the vector length of T_{ji} , and K is the number of UAVs. The weighting parameter $\alpha_{ji} = 1$ when there is currently an overlap and $\alpha_{ji} = c$ when there is currently no overlap on the route. The value of c is determined by recording the amount of UAV positions in the augmented state history that did not have an FOV overlap on the route. As the UAV diverges from the route, c increases at each UAV position because the number of times it is missing the route increases. This weighting scheme adapts to persistent deviations from the route by increasing with each subsequent non-overlap.

A return pass over the route differs from the development above in the assumption of the last-visit time to the route ahead of the current UAV position. In the first pass, the time since the last visit was assumed to be the current elapsed time. However when the UAV has completed a turn and is returning to the origin of the sector, the time since the last visit is now the last T_i vector for the previous pass. In other words, the last-visit vector, T_i , is re-used when each UAV returns back down its sector. The revisit cost function is only one component of \mathcal{J}_T . The next section will develop the second portion of RS-UAS controller cost function.

3.6.3 Control Energy Cost Function. The RS-UAS controller cost function has been augmented with a component to minimize the control energy expended to

perform the surveillance. This portion of the performance metric is taken from the classic linear quadratic regulator cost function. Let the i th UAV's dynamics modeled by the autopilot be given by Equation (3.3). Converting $\dot{V}_{DL,i}$ and $\dot{\phi}_{DL,i}$ into state space

$$\begin{bmatrix} \dot{V}_{DL,i} \\ \dot{\phi}_{DL,i} \end{bmatrix} = \begin{bmatrix} -\alpha_V T_B & 0 \\ 0 & -\alpha_\phi T_B \end{bmatrix} \begin{bmatrix} V_{DL,i} \\ \phi_i \end{bmatrix} + \begin{bmatrix} \alpha_V T_B & 0 \\ 0 & \alpha_\phi T_B \end{bmatrix} \begin{bmatrix} V_{DL,i}^c \\ \phi_i^c \end{bmatrix} \quad (3.16)$$

allows the commanded variables to be gathered into one control vector for the i th UAV

$$u_i = \begin{bmatrix} V_{DL,i}^c \\ \phi_i^c \end{bmatrix} \quad (3.17)$$

Therefore, a quadratic cost function form for minimizing the control energy is given by

$$J_{energy} = \int_0^{t_M^{(p)}} u_i^T \mathbf{R} u_i dt \quad (3.18)$$

where $t_M^{(p)}$ is the total time for the UAV to complete one pass over the sector. \mathbf{R} is a weighting matrix used to penalize control energy where the weights are selected by the following expression [27]

$$R_{ij} = \beta_{ij} \frac{1}{\max(u)^2} \quad (3.19)$$

where $i = j$ and β_{ij} acts as a tuning gain to penalize the vehicle motion. Equation (3.18) normalizes the control energy where β_{ij} acts to add more or less importance to the energy minimization. For the simulations in Chapter IV, β was set to unity gain. Now that the Vehicle Dynamics and Cost Function blocks have been developed, the next section will explain the methods used to synthesize all of the information into a multi-phase optimal control problem.

3.7 Problem Setup Block

This section discusses how the inputs from the K -means, Vehicle Dynamics, and Cost Function blocks are combined into an optimal control problem for PSCOL

to solve. Before this problem is presented, the next section demonstrates the methods for bounding the state dynamics, control inputs, and path constraints. Section 3.7.2 discusses the initial-guess approach used to help PSCOL converge to the optimal solution. The RS optimal control problem is finally presented in Section 3.7.3.

3.7.1 State, Control, and Path constraint limits. PSCOL requires that all state, control, and path constraints be restricted before the optimization program executes. The methods described in this section are for the general case since each scenario differs. First, the position states defined in the UAV model of Section 3.5.1 are constrained by finding the minimum and maximum value of each UAV sector and subtracting or adding one mile, respectively. This method constrains the UAV motion inside an imaginary box around the sector. Although these bounds are necessary for PSCOL, the distance-from-path constraint keeps them from ever being exceeded. Figure 3.13 depicts the Texas route divided into four sectors where boxes have been placed to illustrate state position limits.

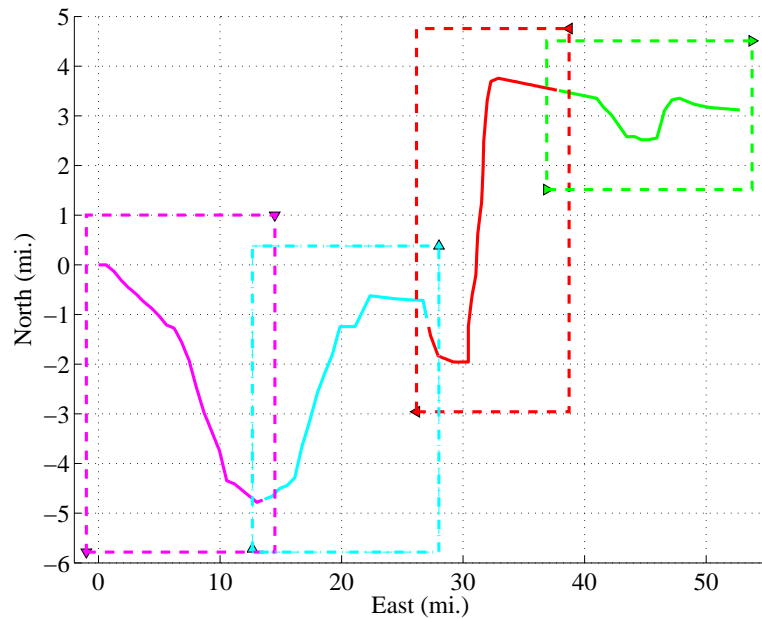


Figure 3.13: Example state limits for four sectors.

The other aircraft states are bounded using the following methods. The UAV heading is constrained so that each UAV cannot perform circles during mid-flight. The only exception is at the ends of the respective sectors. The aircraft velocity, bank angle, and control inputs are constrained with the values in Table 3.2 to simulate the performance limits of the TACMAV.

The trajectory of the UAVs around the ends of their respective sectors (representing the turn-around points) are constrained to a quarter mile East by half mile North box around the sector endpoints and is illustrated for two sectors in Figure 3.14. Each UAV will not fly outside of this box to complete a turn.

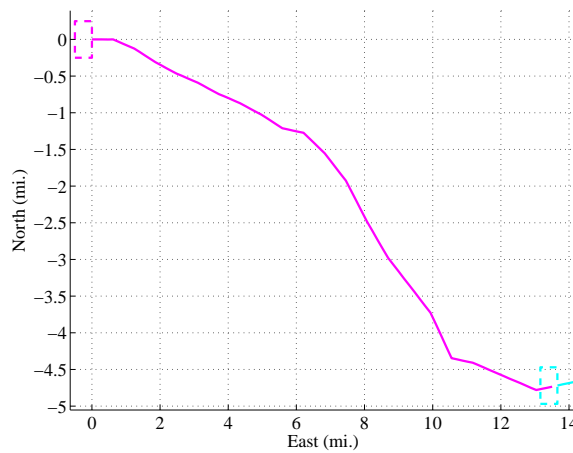


Figure 3.14: Example turn limits for two sectors.

Table 3.4 lists the path constraint limits used for this research. The communications limits are taken from the route surveillance mission defined in Chapter I. The distance-from-path limits are based on projecting the FOV onto the ground and sweeping the UAV across the route (developed in Section 3.5.3).

Table 3.4: Path constraint limits

Path constraint	Min (mi)	Max (mi)
Communication limit	0	20
Distance-from-path limit	0	0.2

3.7.2 Initial guess. PSCOL requires an initial guess for the optimal control problem to enhance the solution and to speed-up processing time. In this research, the initial guess consisted of estimating the UAV trajectories for each sector and phase. Since *a priori* knowledge of each sector existed, the UAV trajectories were approximated by shifting each sector by $\Delta_{max} = 0.2$ miles. While every route is different, a general initial guess calculation is demonstrated in this section.

Consider the route illustrated in Figure 3.15. The solid colored lines represent each sector in the route while the initial guess for each sector is shown as dotted lines. The initial guesses for the first and third phases would take the sector waypoints and shift them South by Δ_{max} . The initial guess for the second phase takes the sector waypoints and shifts them North by Δ_{max} . This initial guess method was chosen because the shifted sectors represent the maximum distance each UAV could travel from the route and the optimal trajectory should converge within the bound created by the initial guess. Now that the problem has been bounded and an initial guess has been determined, the optimal control problem is defined in the next section.

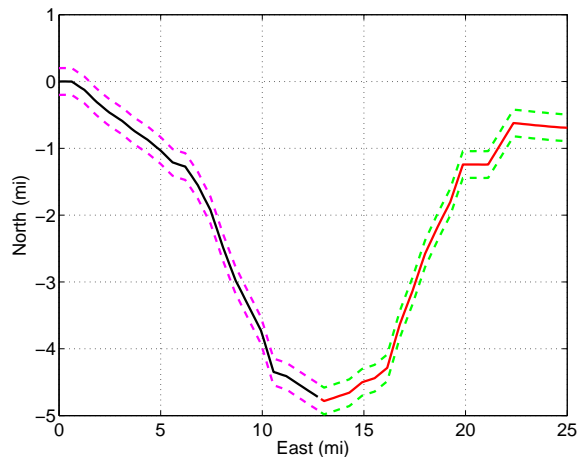


Figure 3.15: Example initial guess for two sectors.

3.7.3 PSCOL optimization. The optimal control problem involved in this research will possess the following multi-phase form. A three-phase approach was chosen to allow the optimization to account for steady-state operation. The assump-

tion is that the second and third passes over the route represent the steady-state orbit over the respective sectors. Note that the GPM performed by PSCOL outlined in Section 2.3 always occurs after the following optimal control problem has been defined. PSCOL will minimize the cost function

$$\mathcal{J}_T = \sum_{p=1}^3 \left[J_{revisit}^{(p)} + J_{energy}^{(p)} \right] \quad (3.20)$$

subject to the dynamics for each UAV in the team as defined by Equation (3.3), the state boundary conditions presented in Section 3.7.1 and defined in Table 3.2, the inequality path constraints defined in Equations (3.4) and (3.9), and the phase linkage constraints

$$\begin{aligned} \mathbf{x}^{(p_l^s)}(t) - \mathbf{x}^{(p_u^s)}(t_0) &= \mathbf{0}, & p_l, p_u &= 1, 2, 3; s = 1, 2 \\ t_f^{(p_l^s)} - t_0^{(p_u^s)} &= 0, & p_l, p_u &= 1, 2, 3; s = 1, 2 \end{aligned} \quad (3.21)$$

where p_l^s and p_u^s are the left and right phases to be connected and s corresponds to the number of phases being linked (Phase 1 to 2 and Phase 2 to 3). Recall that each phase corresponds to one UAS pass over the route. Therefore, three phases will allow the UAS to make three passes over the route. The vehicle dynamics, state boundary conditions, and inequality path constraints do not change during the three phases. Note that the form of J_{energy} will not change during phase transitions. $J_{revisit}$ will change slightly during phase transitions where the changes are outlined in Section 3.6.2.

3.8 Summary

The RS-UAS controller was developed to provide a solution for dividing prescribed routes and optimizing the UAV trajectories over their respective sectors. The Input block used methods for creating simulated and real-world routes to test the controller. The K -means clustering algorithm, the first subcomponent of the con-

troller, was applied to the prescribed routes to explore a different method for dividing routes. The Vehicle Dynamics block uses the TACMAV as the candidate UAV model for the RS-UAS controller. Also within the Vehicle Dynamics block, the communications constraint and the distance-from-path constraint are implemented to restrict the UAV motion to maintain communication with other entities and to ensure the camera FOV images the route. The RS-UAS controller cost function completes the RS optimal control problem and was designed to minimize the revisit time to the route and the overall expended control energy, which achieves the objectives of the route surveillance mission in Chapter I. The Problem Setup block receives inputs from the K -means, Vehicle Dynamics, and Cost Function blocks to synthesize the entire scenario into a three-phase optimal control problem. Chapter IV will present the results of processing selected route scenarios with the RS-UAS controller.

IV. Analysis and Results

4.1 *Introduction*

This research effort culminates with the results and analysis presented throughout this chapter. The RS-UAS controller developed in Chapter III was tested by developing a set of candidate routes that manifested likely urban and rural roadway characteristics. The metrics used to determine the quality of the solution are mapped to the following RS mission objectives outlined in Chapter I: determine if the flight path provides surveillance of the route at all times and determine if the revisit time of the UAS to the path is minimal. Before the test plan is presented, Section 4.2 will discuss how the performance metrics are formulated and used to judge performance. Section 4.3 presents the test plan for the RS-UAS controller and illustrates selected routes from the test plan. Section 4.4 presents the results from the RS-UAS controller and analyzes the quality of the solutions.

4.2 *Performance Metrics*

There are two performance metrics that aid in determining the quality of the surveillance solutions. The first metric calculates the surveillance coverage for each phase within a simulation in percent of the route covered, which should be as close to 100% as possible. The second metric compares the exact travel time of the UAS to the range of travel times allotted for that phase. Since the RS-UAS cost function is minimizing more than one aspect of the problem, the revisit time of the UAS is coupled to the control-energy expenditure. Recall that this research effort is a new investigation, so the coverage values and revisit times throughout the analysis below are not compared to previous work, but establish a baseline for any future efforts.

The last-visit time function introduced in Chapter III is the method for determining the amount of surveillance coverage for each simulation, and is calculated by recording the amount of the route imaged by the UAS and then dividing by the appropriate route length. Figure 4.1 illustrates an example last-visit time function from Phase 3 of Simulation 6 in the test plan. Notice that the third sector's last-visit time

function (in red) is a negatively-sloped line representing a sector that was imaged 100%. The other two sectors (magenta and cyan lines) contain spikes corresponding to sections of the route that were not imaged. This coverage analysis is discussed for a baseline scenario in Section 4.4, which represents typical results from processing the test plan.

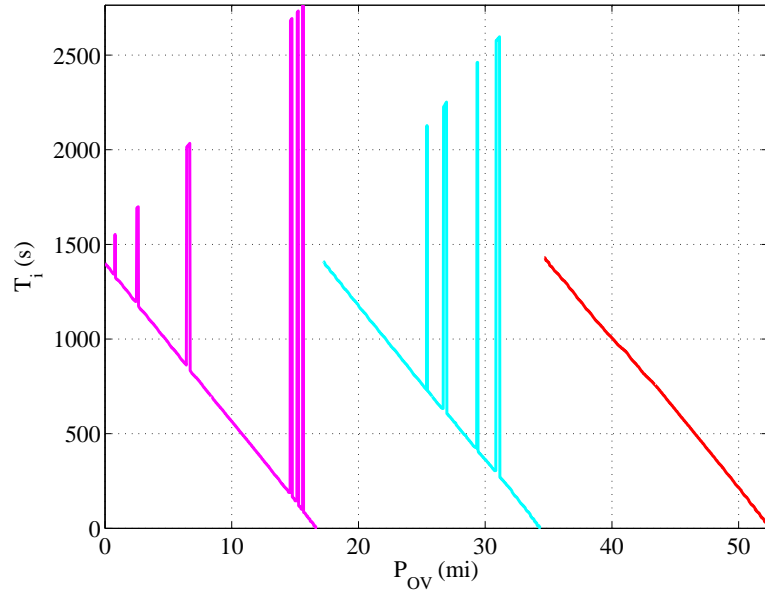


Figure 4.1: Example last-visit time function from a simulation in the test plan.

In each simulation, the range of travel times was determined by finding the absolute minimum and maximum flight times based on dividing the shortest and longest sector lengths by the maximum and minimum velocities of the UAVs, respectively. For example, consider two sectors of a route that are 12 and 12.5 miles in length. The range of travel times for the two-vehicle UAS would be $t_{min} = 12/V_{max}$ and $t_{max} = 12.5/V_{min}$, where V_{min} and V_{max} are the TACMAV velocity constraints. In this case, the revisit time to the route in a phase would be minimized when the travel time of the UAS is t_{min} .

The revisit time to the route for each phase is equivalent to the travel time of the UAS. Since Phase 2 and 3 are assumed to represent the steady-state operation, the revisit times of those phases should settle to a consistent travel time. However,

Section 4.4.2 will show that the revisit times do not settle to constant values and that the minimized control energy of the UAS affects the revisit time by slowing the vehicles to use less energy. Before the results are presented, the next section will detail the test plan for the RS-UAS controller.

4.3 *RS-UAS Controller Test Plan*

The RS-UAS controller was tested by choosing a set of routes from the following three methods: loading a MATLAB figure and clicking a desired route, generating a random route, and loading a pre-existing real-world route from Texas. Table 4.1 lists the test plan and the number of nodes used to describe each UAV trajectory per phase (for example, 30 nodes times 3 phases equals 90 nodes to describe each UAVs total trajectory). The first two simulations demonstrate how a user can provide a clicked route to the controller. The sinusoidal-like random route is meant to show that irregular path shapes (meaning uncommon road shapes) can be processed. Two versions of the Texas route were used to demonstrate the baseline scenario for the RS-UAS controller and that the distance-from-path constraint yields better results. The final clicked route demonstrates a substantial performance increase by doubling the number of nodes describing each UAV’s total trajectory.

Table 4.1: RS-UAS controller test plan

Simulation	Route Type	Team Size	Route Length (mi)	Nodes
1	Clicked	2	34.58	30
2	Clicked	4	57.48	30
3	Random	3	59.86	30
4	Texas	4	59.81	30
5	Texas	2	39.94	30
6	Clicked 3	3	52.34	60

The clicked routes for Simulations 1 and 2 are illustrated in Figures 4.2 and 4.3 and demonstrate the range of complexity for urban and rural environments. Appendix E contains additional results illustrating the other routes from the test plan, their

division, the resulting UAV trajectories, and the last-visit time functions in each phase.

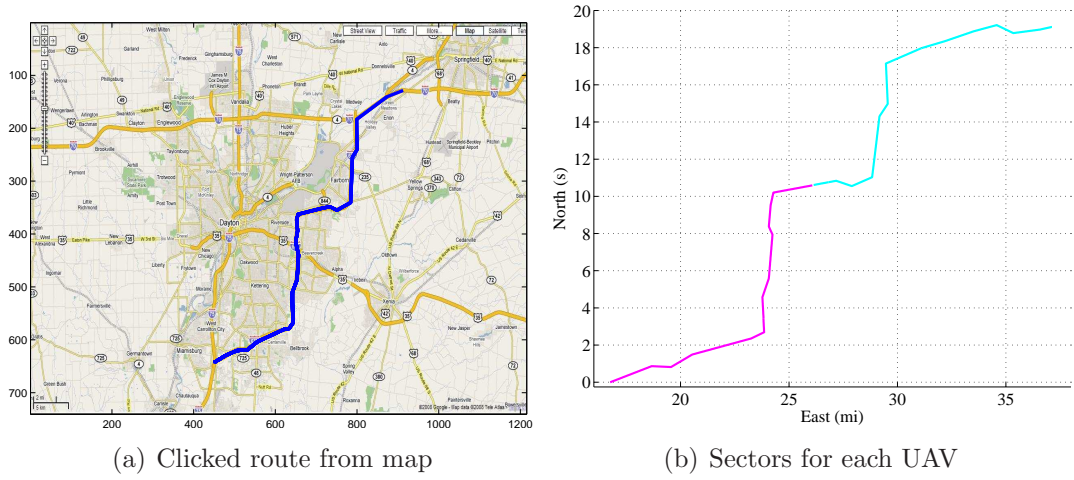


Figure 4.2: Clicked route from Dayton map and resulting sectors for two UAVs.

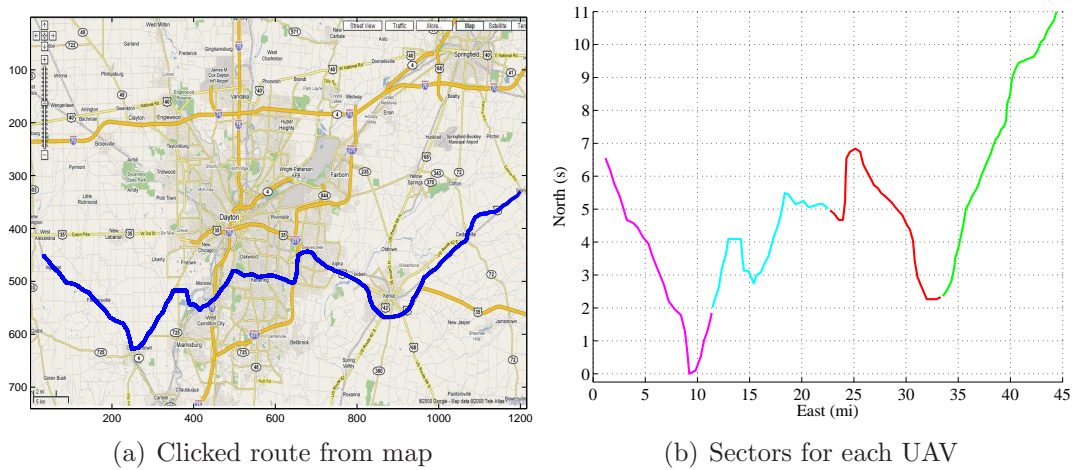


Figure 4.3: Clicked route from Dayton and resulting sectors for four UAVs.

The test plan in Table 4.1 was successfully executed and the results are presented in the remaining sections. General concluding remarks about the performance of the controller are summarized in Section 4.5.

4.4 *RS-UAS Controller Results*

The following sections are organized by discussing each performance metric for the controller and then the factors that affect those metrics. To minimize the number of figures and present a concise description of the performance, two tables list the aggregate surveillance coverage and revisit times for each simulation phase. Also, only Simulations 4 through 6 are discussed in detail throughout the next two sections. The surveillance coverage and revisit time results are presented in Sections 4.4.1 and 4.4.2, respectively. Lastly, Section 4.4.3 demonstrates that the communications constraint was never violated.

4.4.1 Route Surveillance Coverage. After constructing the last-visit time function and recording the amount of road imaged for each simulation phase, the surveillance coverage was calculated and is listed in Table 4.2. The coverage performance was only marginal for Simulations 1 through 4, where generally, surveillance only reached approximately 80% of the route. However, Simulations 5 and 6 show performance increases because the distance-from-path constraint and the number of nodes per phase were tuned as a result of analyzing Simulations 1 through 4. Under the assumptions in Chapter III, the second and third phases offer the best surveillance trajectories since those are meant to represent steady-state operation. Although the overall performance in each phase of Simulations 1 through 4 appears marginal, the coverage across each sector within a phase varied greatly. Since the performance of the first four simulations are related, only the surveillance coverage results of Simulation 4 (baseline scenario) are discussed in detail.

Under the test-plan conditions in Table 4.1, the RS-UAS controller only provided surveillance on the Texas route for 67% in Phase 1, 81% in Phase 2, and 82% in Phase 3. Figures 4.4 through 4.6 illustrate the last-visit time functions for Phases 1 through 3, where the horizontal axis is the distance along the route and the vertical axis is the time since the last visit. Each color-coded section corresponds to the sectors of UAVs 1 through 4, respectively. The best last-visit time function for each phase should be

Table 4.2: Surveillance coverage over the route per phase. The processing time for each simulation is listed in the process column.

	Phase 1	Phase 2	Phase 3	
Simulation	Coverage (%)	Coverage (%)	Coverage (%)	Process (hrs)
1	66	63	70	24
2	65	73	72	30
3	53	81	82	44
4	67	81	82	107
5	71	84	85	40
6	94	96	96	43

four negatively or positively-sloped lines depending on the direction of travel (similar to the example shown in Section 4.2). The frequency of the spikes in the Phase 1 last-visit time function means that the UAS did not image many sections of the route. Phase 2 increased the amount of surveillance on the route slightly, where each sector is beginning to contain larger sections that were viewed 100% as compared to Phase 1. In Phase 3, the collective surveillance coverage did increase from the previous phase, however, there were sections of the route that were never imaged. The spikes in Figure 4.6 rising to a last-visit time of approximately 3500 seconds correspond to those areas of the route that were never viewed and for that reason need to be reduced. The next tier of spikes at last-visit times of approximately 3000 seconds correspond to sections of the road that have not been viewed since Phase 1, and the final tier of spikes varying from 1500 to 2000 seconds correspond to sections of the road that have not been viewed since Phase 2. In spite of this performance, notice that Sector 1 (magenta) of Phase 3 achieved 95% surveillance coverage demonstrating that the RS-UAS controller provides good results under certain conditions.

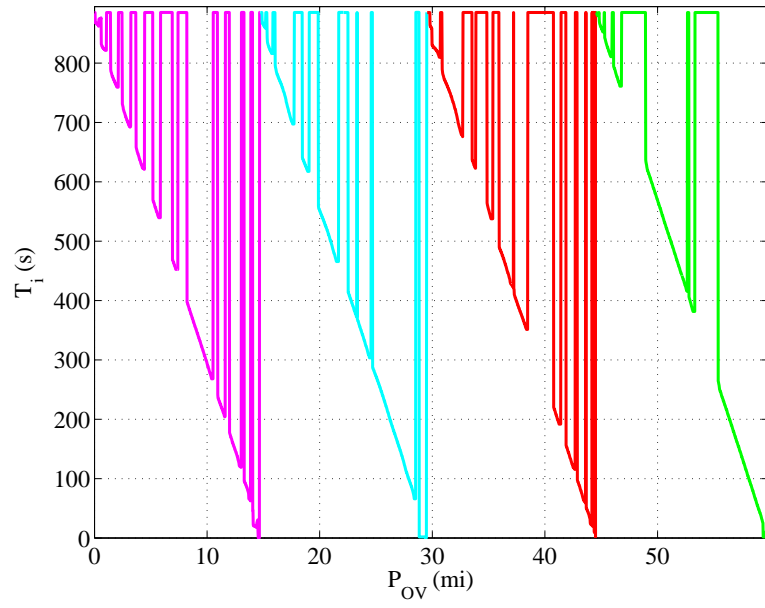


Figure 4.4: Texas road last-visit time function for Phase 1.

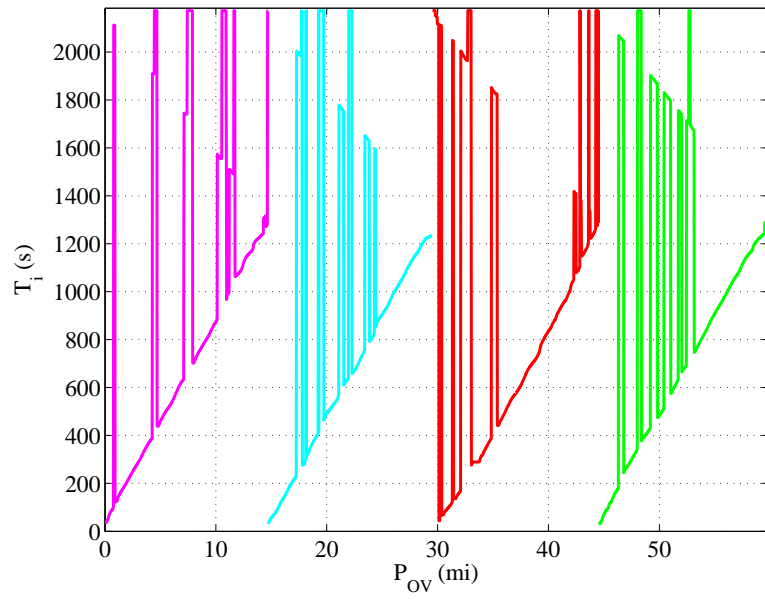


Figure 4.5: Texas road last-visit time function for Phase 2.

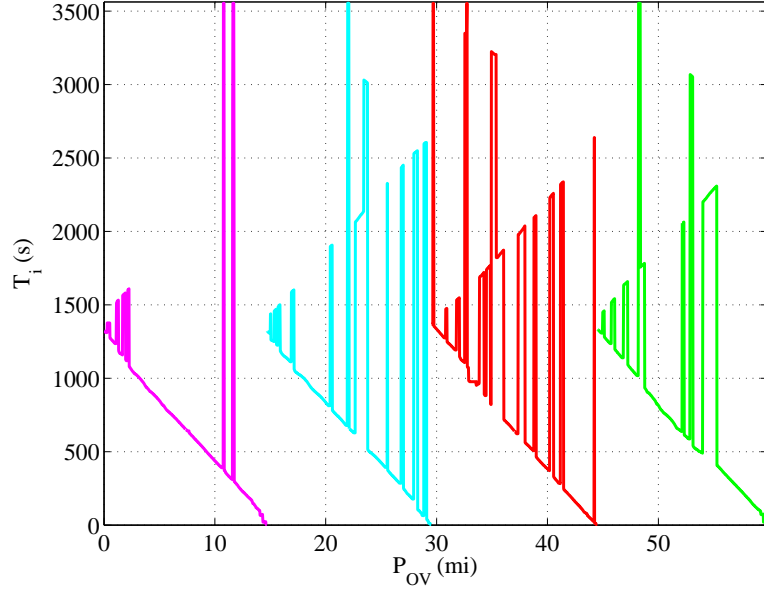


Figure 4.6: Texas road last-visit time function for Phase 3.

There are two factors that affect the surveillance coverage performance in Simulations 1 through 4, both of which, consequently, can be compounded resulting in even worse performance. First, the solutions from PSCOL did not provide good surveillance with 30 nodes describing each UAV trajectory. This meant that PSCOL could not accurately sample the true optimal solution when the route exhibited complex transitions. Second, the initial-guess method from Section 3.7.2 in some cases incorrectly bounded the potential surveillance trajectory, which is crucial for PSCOL to find an optimal solution. If these two factors were not present, the surveillance coverage reached acceptable levels, as in Sector 1 of Phase 3 for Simulation 4. Since each factor has been introduced, the remainder of this section will discuss each in detail.

The first and most important factor affecting the quality of the surveillance is the number of nodes chosen to represent the solution within PSCOL. Recall that PSCOL is a numerical technique that delivers an *approximate* solution for optimal control problems, which Benson et al. [7] showed would approach the exact answer when the number of nodes N increased. The only method of finding an appropriate number of nodes is by heuristically determining when the solution is good enough [22, 23].

Consequently, since each simulation required at least 24 hours of processing time, the number of nodes was not increased for Simulations 1 through 5. As an example, a 30th-order Legendre polynomial (corresponding to 30 nodes) was used by PSCOL to approximate the cost functional, \mathcal{J}_T . The roots (blue circles) in Figure 4.7 illustrate the heavy distribution of the points at both ends of the interval $[-1, 1]$, which is a trait of the Legendre polynomials. When PSCOL converts the solution via the affine transformation in Equation (2.5), the nodes in the middle of the trajectories can now be spread over large distances. This is important because the optimal surveillance trajectories will be improperly sampled during the middle of the trajectory if the number of nodes is too low. In order to demonstrate improper sampling, Figure 4.8

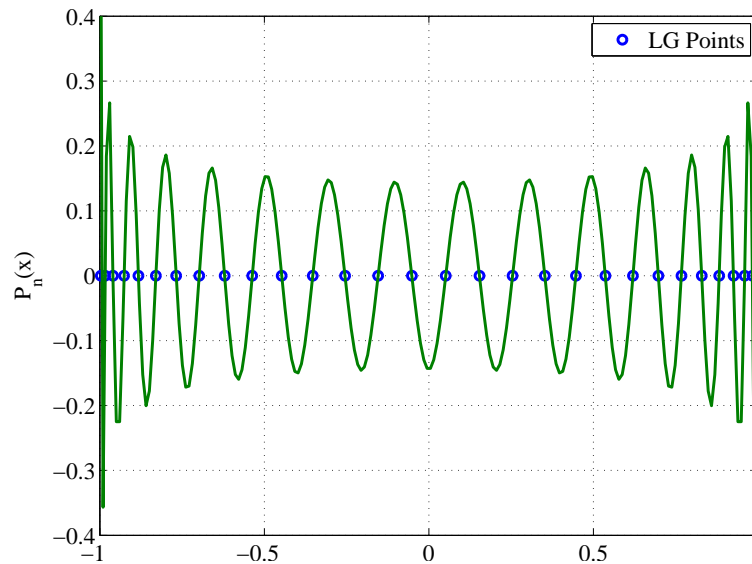


Figure 4.7: 30th-order Legendre polynomial used by PSCOL to approximate the surveillance trajectories of each simulation.

illustrates a sector with transitions that mimic urban roads. Notice that while the overall trajectories in Figure 4.8(a) appear to provide surveillance, a problem between miles 12.5 and 14.5 East is illustrated in Figure 4.8(b). There are not sufficient points to capture the dynamics required to follow the route. This problem is compounded because this research effort assumed the UAV trajectory between two points was a straight line. A spline feature in MATLAB could have been used to better approximate the trajectory between the discrete points, but this is left for future work.

The maximum surveillance coverage for this sector was only 73% and shows how this problem affects coverage for complex routes.

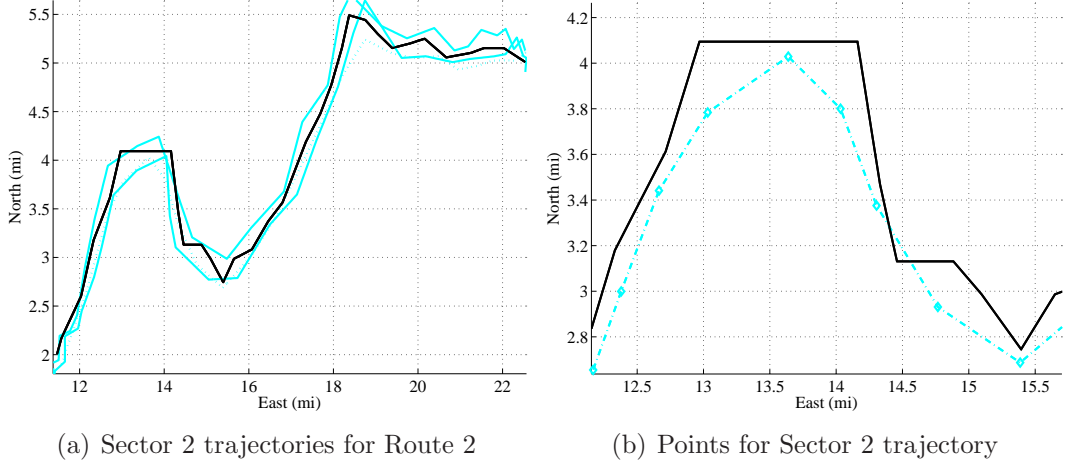


Figure 4.8: Sector 2 trajectory for Simulation 2 showing the solution points.

The second quality factor to affect surveillance was the initial-guess method chosen for this research effort. The surveillance trajectories from PSCOL properly followed the route when the initial guess correctly bounded the paths taken by the UAVs. Two examples will demonstrate how a correct and incorrect initial guess could affect the final surveillance trajectory. Figure 4.9 depicts the Phase 1 and 3 trajectories taken by the first UAV in Simulation 4. Notice that the road moves mostly in the West-to-East direction. Shifting this sector down by $\Delta_{max} = 0.2$ miles properly bounded the surveillance trajectory for most of this section (black dotted line in the figure). However, the portion of road located at mile 10 East is moving nearly south and never gets viewed by the FOV since the trajectory in the figure overlaps the route. Overall, the resulting surveillance coverage in this sector improved from 64% in Phase 1 to 95% in Phase 3. The Sector 1 last-visit time functions (magenta) in Figures 4.4 through 4.6 illustrate the improved surveillance by the decrease of spikes. Notice that at $P_{OV} \approx 11$ miles, the route is missed in all three phases; this corresponds to mile 10 East on the route.

An incorrect initial guess is depicted in Figure 4.10 (dotted black line) for a route section that partly moves from South to North. While later sections of this

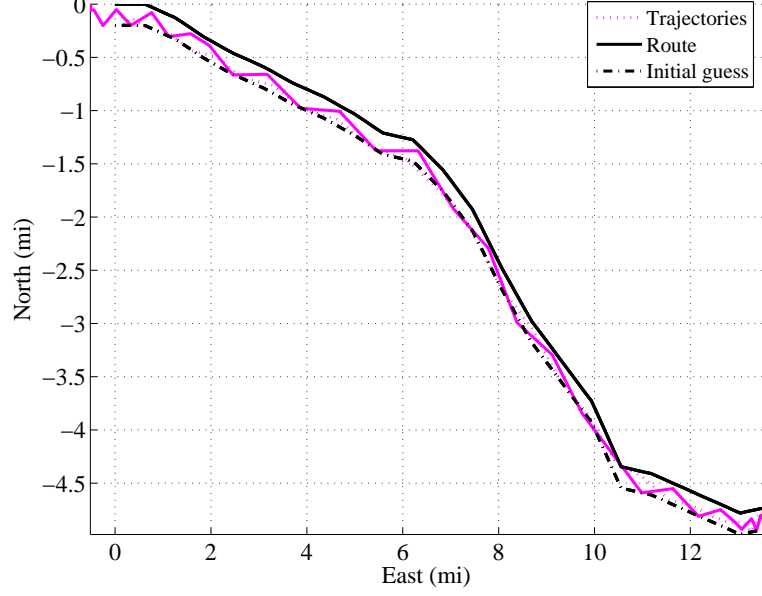


Figure 4.9: Simulation 4 initial guess and trajectories for Phase 1 and 3.

sector better conform to the initial-guess method, the middle of the sector does not. Notice that both of the surveillance trajectories nearly overlap the route above -2 miles North meaning the FOV is not imaging the route. This is caused because shifting the route down by Δ_{max} moves the initial guess only South when it should move in an orthogonal direction from the route by Δ_{max} . This general method caused the initial guess to nearly overlap the route and did not properly bound the potential solution. Because later sections of Sector 3 (red) conform to the initial-guess method, the surveillance coverage, illustrated in Figures 4.4 through 4.6, at the end of the last-visit time function improved. However, the overall coverage in Sector 3 only increased from 60% in Phase 1 to 72% in Phase 3. This coverage did not reach the level that Sector 1 attained because the initial guess was not correct for the entire route.

To counteract the two factors affecting the solution quality, Simulations 5 and 6 were designed to explore two methods that would potentially increase the performance of the RS-UAS controller. The first method decreased the distance-from-path constraint from $\Delta_{max} = 0.2$ miles down to 0.17 miles (forcing the FOV to overlap regardless of the distance from the route) in order to show that the solution could

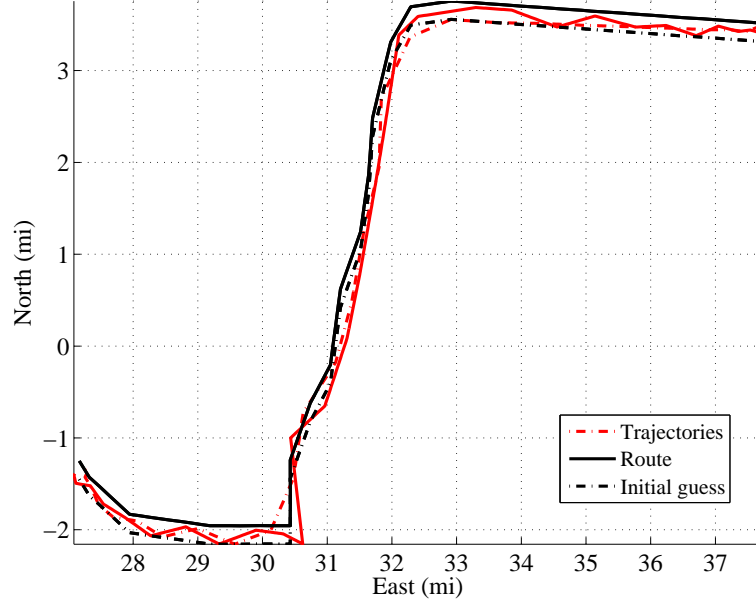


Figure 4.10: Simulation 4 initial guess and trajectories for Phase 1 and 3.

get better without increasing the number of nodes. The second method, employed in Simulation 6, doubled the number of nodes to 60 and used a clicked route that mimics the transitions depicted in Figures 4.8(b), 4.9, and 4.10.

The distance-from-path constraint performed well throughout the simulations maintaining the UAV trajectories close to the prescribed route, nevertheless, the adjustability of the Δ_{max} offset provides room for improvement. Simulation 5 used a portion of the Texas route and decreased the distance-from-path offset down to 0.17 miles. Contrasting Figure 4.11(a) and 4.11(b) to the same route sections in Figures 4.4 and 4.6, demonstrates that decreasing the offset increased the surveillance coverage for the first 20 miles of the Texas route in Simulation 5 (P_{OV} up to 20 miles). Table 4.3 lists the surveillance coverage of the same sections for the two simulations and demonstrates that all three phases of Simulation 5 were a significant improvement over Simulation 4. Although performance did increase, this method cannot overcome the two issues discussed previously. For example, the last-visit time function for Sector 2 (cyan) in Figure 4.11 depicts poor surveillance because this portion of the route contained sections that moved from South to North.

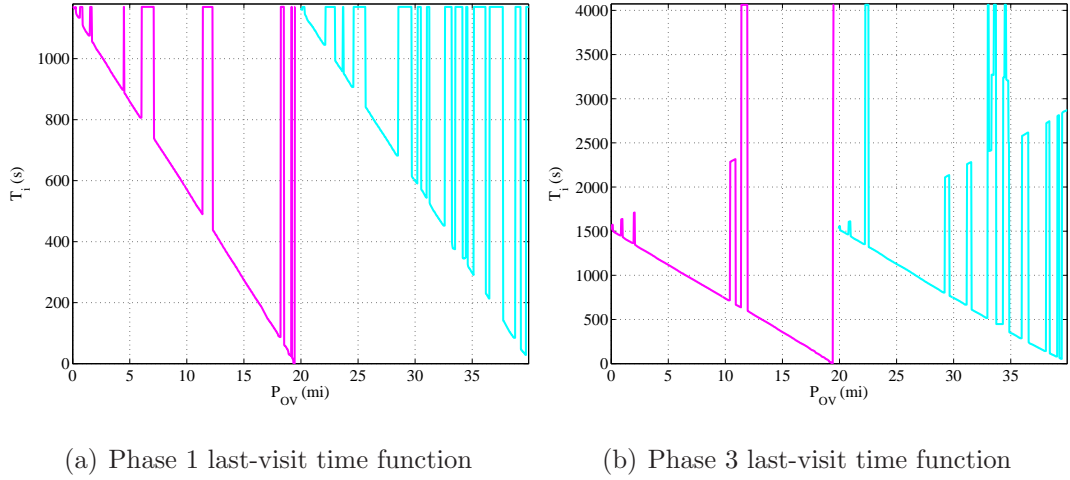


Figure 4.11: Last-visit time function for Phase 1 and 3 of Simulation 5.

Table 4.3: Results from using smaller Δ_{max} over the first twenty miles of the Texas route

Phase	Simulation 4 Coverage (%)	Simulation 5 Coverage (%)
1	67	72
2	82	90
3	82	91

By doubling the number of nodes for Simulation 6, the surveillance results were significantly improved, almost eliminating the effect of the quality factors discussed previously. The clicked route for Simulation 6 is depicted in Figure 4.12(a), while Figure 4.12(b) illustrates the resulting trajectory for UAV 3. Notice that the trajectory encapsulates this route better than the similar sector illustrated in Figure 4.10. Table 4.4 lists the coverage per phase in Simulation 6 and shows that increasing the nodes helped the surveillance coverage stay above 92%. This means that at maximum less than one mile out of seventeen was not imaged. Figure 4.1 illustrates the Phase 3 last-visit time function exhibiting no spikes meaning the sector was imaged 100%. The next section presents results regarding the second performance metric for the RS-UAS controller.

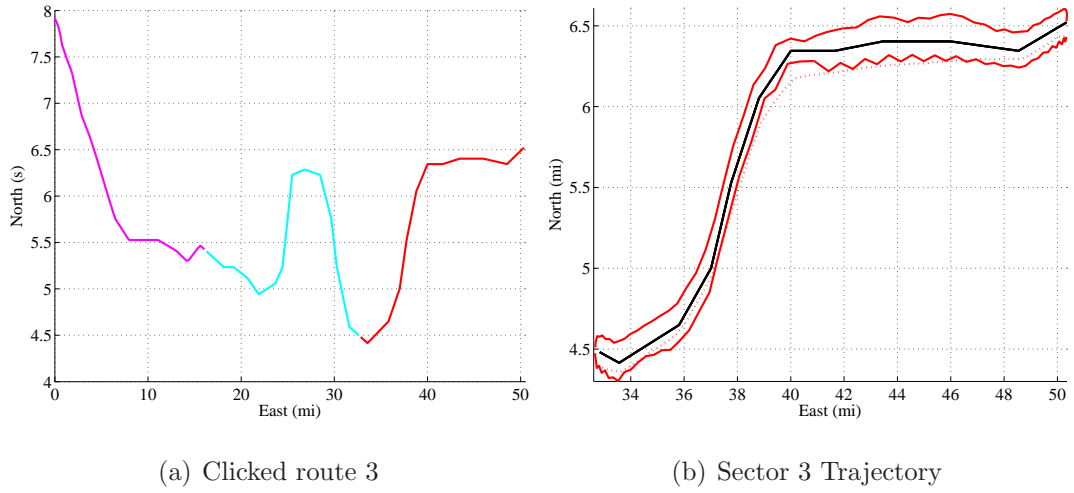


Figure 4.12: Simulation 3 route and resulting Sector 3 trajectory.

Table 4.4: Surveillance coverage for Simulation 3

Sector	Sector Length (mi)	Phase 1 (%)	Phase 2 (%)	Phase 3 (%)
1	17.22	97	97	93
2	17.46	93	98	95
3	17.66	92	94	100

4.4.2 Revisit Time. Before the revisit time performance is assessed for the simulations, it is necessary to compare the travel-time ranges of the UAS to the travel-time ranges of a single UAV flying the same routes from the test plan. Using the method for calculating the travel-time ranges from Section 4.2, Table 4.5 lists the allotted ranges for the UAS (used in PSCOL) and single-UAV cases. The time variable in this section has been converted to the more convenient time unit of minutes (10 minutes versus 600 seconds). Note that no extra simulations were processed for the single-UAV case, so the time ranges for this scenario represent values that would be used in PSCOL under the same conditions of this research. Recall that the RS mission in Chapter I called for, in general, at least hourly visits to points along the route, and in Table 4.5, the single-UAV time ranges are generally hovering around the one-hour limit for Simulations 2 through 4 and 6 (since those routes are nearly

60 miles in length). This suggests that the actual revisit time might fall outside of the RS-mission requirement. In contrast, the travel-time ranges for the UAS indicate a benefit since the travel ranges over the route are much less than the hourly visits required by the RS mission. Table 4.6 lists the actual revisit times for the simulations from the test plan and demonstrates that the revisit times to the route are well under the general limit.

Table 4.5: Simulation travel-time ranges for the UAS and single-UAV cases

	UAS		Single UAV	
Simulation	Min (min)	Max (min)	Min (min)	Max (min)
1	17	27	34	48
2	14	20	56	79
3	19	31	59	82
4	15	25	59	82
5	20	31	39	55
6	17	27	51	72

Having established that a UAS provides an advantage to the RS mission, the revisit time performance can be investigated for the simulations from the test plan. Generally, the revisit times for each phase in Table 4.6 were less than the maximum travel-time ranges, suggesting that the revisit cost function reduces the revisit time to the route. In Phase 1 of all the simulations, the revisit time has been minimized based on the conditions for the minimum travel time in each simulation. However, the surveillance coverage for Phase 1 is poor (except for Simulation 6) as listed in Table 4.2 from Section 4.4.1. In all cases, the revisit time increases for Phases 2 and 3 while the surveillance coverage and control-energy expenditure improve. Figure 4.13 illustrates the normalized control energy during each phase of Simulation 6 (color coded) and shows that the revisit time is coupled to the control energy expended by the UAS. Notice that the control energy is highest in Phase 1, which is expected since

the revisit time is shortest. The spikes at $t = 17$ min and $t = 40$ min correspond to the turn-around points at the end of the sectors.

Table 4.6: Simulation revisit times for each phase

	Phase 1	Phase 2	Phase 3
Simulation	Travel (min)	Travel (min)	Travel (min)
1	17	21	25
2	14	20	20
3	19	25	29
4	15	22	23
5	20	23	26
6	17	24	24

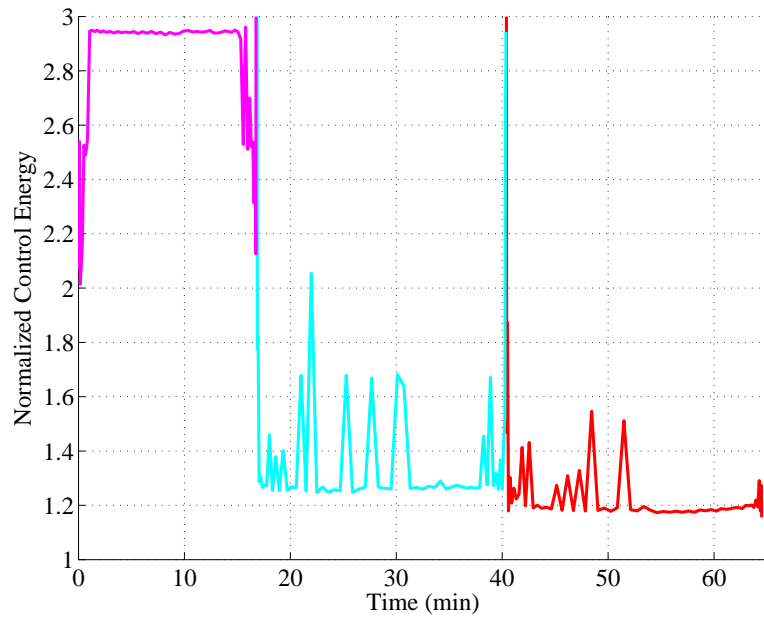


Figure 4.13: Simulation 6 control energy minimization.

In Phases 2 and 3, the revisit times, along with the surveillance coverage and control energy, should settle from a transient-like behavior to a steady-state operation. The two main factors affecting the RS-UAS controller performance were discussed in the previous section and also largely contribute to the unsettled revisit times for Phases 2 and 3. Specifically, the revisit cost function records the last time portions of the route were visited, however, if the surveillance is sporadic, like Simulations 1

through 4, the revisit time will not settle to a constant value. Doubling the nodes in Simulation 6, mitigated the affect of those performance factors on the surveillance coverage as well the revisit time since it settled to a steady-state of 24 minutes. Even though performance improved in the last simulation, the revisit time in Phase 1 is much shorter, which is also common to the first five simulations.

The performance in Phase 1 can be attributed to improper weighting in the first phase of the RS-UAS cost function. Recall that the c parameter in the revisit cost and the β parameter in the control-energy cost seek to place an appropriate importance on the two portions of the overall RS-UAS cost function. Consequently, there is a weighting struggle between the two portions of the cost function. Globally, this weighting issue is overshadowed by the two quality factors in the previous section, and Simulation 6 shows that once those issues are mitigated the revisit time settled appropriately. The next section will briefly discuss the communications constraint before this chapter is summarized in Section 4.5.

4.4.3 Communications Constraint. The communications constraint was never violated throughout the simulations because the routes were properly divided by the K -means clustering algorithm. If the sectors had been unbalanced, the communications constraint would have been violated. Simulation 5 approached the constraint because the sector lengths were close to the 20-mile limit. The peak distance between the two UAVs was 19 miles in phase two. Figure 4.14 illustrates the communications spacing throughout each phase for the two UAVs.

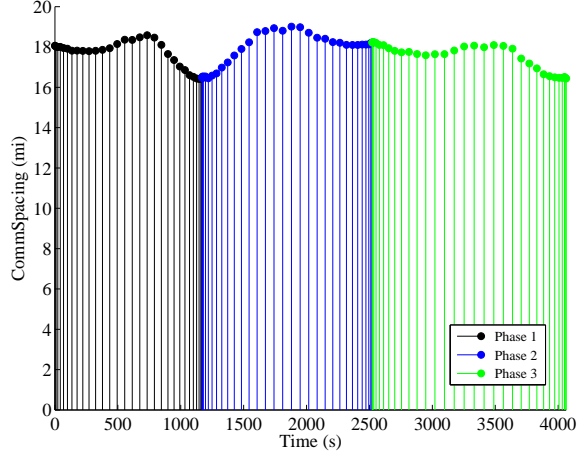


Figure 4.14: Communications spacing between UAV 1 and 2 for Simulation 6.

4.5 Summary

The results outlined in Tables 4.2 and 4.6 demonstrate that the RS-UAS controller performed marginally until the number of nodes was doubled in Simulation 6. The first four routes in the test plan were not provided with persistent surveillance also causing the revisit time not to settle to a constant value. However, the analysis revealed that the number of nodes chosen to represent the surveillance trajectories and the initial-guess method of Section 3.7.2 significantly influenced the quality of the solution. The distance-from-path constraint was found to have a less significant impact on the solution. Chapter V will summarize this research effort, suggest methods to improve the RS-UAS controller, and propose options for future research.

V. Conclusions and Recommendations

This chapter summarizes the research effort used to solve the route surveillance problem. The summarized results are drawn upon to recommend future work intended to improve the RS-UAS controller and take this research beyond the assumptions in Chapter I.

5.1 *Conclusions*

The primary objective of this research was to apply optimal control theory and cooperative control theory to allow a four-vehicle UAS to provide persistent surveillance of a roadway. The route surveillance UAS objectives were to minimize the revisit time to points along the route and to maximize the flight time of the system without losing surveillance. The control algorithm was required to automatically adjust to changes in the number of UAVs to create a pattern such that each vehicle maintains surveillance of the route and the ability to communicate with the other entities in the system.

By applying general approaches from the current cooperative search literature, the RS-UAS controller provided a method for dividing the waypoint-defined route and, more importantly, a method for developing surveillance trajectories to ensure the camera FOV imaged the road. Using the number of UAVs and the route as inputs, the controller autonomously adds resolution to the route as necessary, dissects the route using the K -means clustering algorithm, and constructs an optimal control problem that is solved by the GPM-based optimization software. In order to complete the RS optimal control problem, the overall problem objectives were translated into a cost function and two path constraints. The cost function was developed to minimize the revisit time along the route and the overall control energy of the UAS. Two path constraints restricted the distance between entities and the distance of each UAV from the route. The RS optimal control problem was synthesized into a three-phase optimal control problem compatible with PSCOL, where each phase would represent one collective pass of the UAS over the route.

Using three methods to supply candidate routes, a test plan was created to demonstrate the controller through processing simulated and real-world routes that mimicked urban and rural environments. Two performance metrics ascertained that persistent surveillance coverage was delivered and that the revisit time to the route was reduced. The last-visit time function used to calculate the revisit cost also doubled as a tool to determine the quality of the surveillance. The UAS travel time in each simulation was compared to the single-UAV case to show that the revisit time met the general one-hour requirement of the RS mission. Once the travel-time ranges for each simulation were established, the revisit time in each phase was compared to the maximum allowed travel time to check the revisit time performance.

Results showed that the RS-UAS controller did not provide persistent surveillance in the first four simulations. An analysis of the last-visit time function and resulting UAV trajectories revealed two factors that significantly influenced the quality of the solution. The crucial factor was the number of nodes representing the optimal solution from PSCOL, which posed problems because of the heavy distribution of the points at the two ends of the sector. If the sector had complex transitions in the middle of the route, the solution became sensitive to the number of nodes. The second factor revealed that PSCOL required an initial guess that bounded the potential surveillance trajectory. If the guess was adequate, surveillance reached acceptable levels. But when the guess was inadequate, the route was not imaged consistently. Both of these factors contributed to marginal results, however, further analysis did show that the controller could provide good results.

Two methods were tested to determine if performance could be increased in the last two simulations. The first approach decreased the distance-from-path constraint while holding the number of nodes constant. Performance did increase in a limited case, but the distance-from-path constraint is not an approach to overcome the two issues regarding the number of nodes and the initial guess. The second approach doubled the number of nodes in Simulation 6, which used a route that was similar to sections from the first five simulations. The overall surveillance coverage reached

96% of the route and the revisit time to the route settled to a steady-state value as expected. These results indicate that the approach used in the RS-UAS controller can provide feasible solutions for the route surveillance problem.

In summary, applying optimal control to the route surveillance problem is an appropriate solution method. The cost function and path constraints developed in this research demonstrate that formulating an optimal control problem can provide feasible results. Their potential was realized in only two of the six simulations because of issues specific to the numerical optimization software chosen for this research. Future work is encouraged in order to improve and extend the application of optimal control theory to the route surveillance problem. The next section will suggest avenues of future work to improve upon this new research area.

5.2 *Future Research*

There are two directions for improving upon this research effort. The first direction is aimed at improving the quality of the solutions provided by the current RS-UAS controller. The second direction concentrates on expanding this research's problem statement to include realistic assumptions about the route surveillance mission.

The most significant improvements to the controller developed in this research would be to investigate the feasibility of increasing the number of nodes during simulations and develop a better method for providing a general initial guess to PSCOL. Karasz [23] used an iterative method to quickly solve for the appropriate number of nodes in his application of the GPM. Perhaps, an appropriate distribution of points can be found by iteratively increasing the order of the Legendre polynomials and fitting the location of the roots to the current route under consideration. A better guess allows PSCOL to provide enhanced optimal solutions, therefore, a method that bounds the solution for any route shape should help PSCOL quickly find an accurate solution.

Future work in this area could also take one phase describing a complex sector and split it into multiple phases to increase resolution for that sector. This approach could potentially alleviate the need for increasing the number of nodes per phase (increasing the processing time) and a better initial guess (assuming that the new sectors would be less complex).

The research problem statement in Chapter I addressed a limited portion of the route surveillance mission. Expanding several components of the problem statement opens a whole range of possible future research. First, the candidate routes considered in this research did not include terrain or urban development. The UAVs are assumed to fly at a range of 300 ft above ground level. Mountainous terrain, city buildings, and tall trees in forests could potentially impact the UAV trajectory along the route or impede the camera's view of the route. Future research should expand the route definitions to include environment characteristics other than path shape.

Second, the UAV model and UAS composition are another area to focus future research. The largest limiting assumption of the UAV model in this research is the absence of wind. Even adding constant wind to the problem adds another dimension of complexity. The UAV model should be extended to account for deterministic or stochastic wind models. The first-order UAV model in this research contained a simplified set of states and controls, but model fidelity should be extended to include 3-DOF and 6-DOF models depending on the required level of accuracy. Also, the UAS could be extended to include a heterogeneous team of UAVs that possesses a sensor suite tailored for all types of mission environments, day or night.

Third, the ranges of the routes in this research made a hardware simulation difficult within the test range available to AFIT. In conjunction, UAVs available for academic research at AFIT possess limited maximum flight times depending on the aircraft. Future research could consider decreasing the length of the prescribed routes to fit within a reasonably sized test range to allow multiple passes over the route to be

within the flight times of available UAVs. Performing hardware tests would validate any surveillance trajectories developed by a controller.

Lastly, the problem statement constrained the complexity in the problem to local coupling. Reshaping the mission within the current objectives would certainly lead to a higher degree of coupling between UAV decisions, mission tasks, and mission outcomes. Depending on the amount of coupling, future research could contrast the application of both a centralized and decentralized control approach. In the decentralized case, current cooperative search solutions could be applied to that research effort. This comparison between control architectures could also significantly impact any operational implementation.

Appendix A. Dimensionless UAV model

PSCOL offers an automatic scaling option for optimal control problems. In practice, the automatic scaling has been found to be useful, but it is recommended by the authors of PSCOL to scale and non-dimensionalize the optimal control problem prior to using any numerical technique. Badly scaled problems can cause the software to conclude with infeasible solutions or to continue searching for a non-existent solution. The equations of motion outlined below are badly scaled in the size of the position, velocity, and time values. The dimensionless equations of motion will ensure values between zero and one for the position and velocity states as well as the system time. The equations chosen for modeling the UAV flight dynamics are a first-order approximation and are given by

$$\dot{p}_{N,i} = V \cos \psi_i + w_N \quad (\text{A.1})$$

$$\dot{p}_{E,i} = V \sin \psi_i + w_E \quad (\text{A.2})$$

$$\dot{\psi}_i = \frac{g}{V_i} \tan \phi_i \quad (\text{A.3})$$

$$\dot{V}_i = \alpha_V (V_i^c - V_i) \quad (\text{A.4})$$

$$\dot{\phi}_i = \alpha_\phi (\phi_i^c - \phi_i) \quad (\text{A.5})$$

where $i = 1, \dots, N$ and N is the number of UAVs. The above equations will be non-dimensionalized first for the $i = 1$ general case using the following relationships:

$$V_{DL} = \frac{V}{V_{max}} \quad (\text{A.6})$$

$$p'_N = \frac{p_N}{P_{RT}} \quad (\text{A.7})$$

$$p'_E = \frac{p_E}{P_{RT}} \quad (\text{A.8})$$

$$\tau = \frac{t}{T_B} \quad (\text{A.9})$$

$$V_{DL}^c = \frac{V^c}{V_{max}} \quad (\text{A.10})$$

The subscript DL and the prime superscript are defined as the dimensionless variables. The velocity state and control velocity of each UAV will be scaled and non-dimensionalized by the maximum velocity. The northing and easting positions will be scaled and non-dimensionalized by the maximum route length of 60 miles. Time must also be scaled and non-dimensionalized due to the possibly long flight times, therefore, the scaling factor will be the period of revisit to the route. Notice that heading and roll angle are dimensionless already. The dimensionless time differential operator must be derived first. The derivation begins by considering the relationship

$$\begin{aligned} t &= T_B \tau \\ dt &= T_B d\tau \\ \frac{d\tau}{dt} &= \frac{1}{T_B} \end{aligned} \quad (\text{A.11})$$

The dimensionless differential operator is derived by using the derivative chain rule.

$$\begin{aligned} \frac{d}{dt} &= \frac{d\tau}{dt} \frac{d}{d\tau} \\ \frac{d}{d\tau} &= \frac{dt}{d\tau} \frac{d}{dt} \implies T_B \frac{d}{dt} \end{aligned} \quad (\text{A.12})$$

The dimensionless equations of motion can now be derived.

Northing position:

$$\begin{aligned} \frac{d}{d\tau}(p'_N) &= T_B \frac{d}{dt} \left(\frac{p_N}{P_{RT}} \right) \\ &= \frac{T_B}{P_{RT}} \dot{p}_N \\ &= \frac{T_B}{P_{RT}} [V \sin \psi] \\ \dot{p}'_N &= \frac{T_B}{P_{RT}} V_{DL} V_{max} \sin \psi \end{aligned} \quad (\text{A.13})$$

Easting position:

$$\begin{aligned}
\frac{d}{d\tau}(p'_E) &= T_B \frac{d}{dt} \left(\frac{p_E}{P_{RT}} \right) \\
&= \frac{T_B}{P_{RT}} \dot{p}_E \\
&= \frac{T_B}{P_{RT}} [V \sin \psi] \\
\dot{p}'_E &= \frac{T_B}{P_{RT}} V_{DL} V_{max} \cos \psi
\end{aligned} \tag{A.14}$$

Heading:

$$\begin{aligned}
\frac{d}{d\tau}(\psi) &= T_B \frac{d}{dt}(\psi) \\
&= T_B \dot{\psi} \\
&= T_B \left[\frac{g}{V} \tan \phi \right] \\
\dot{\psi}_{ND} &= \frac{g T_B}{V_{DL} V_{max}} \tan \phi
\end{aligned} \tag{A.15}$$

Velocity:

$$\begin{aligned}
\frac{d}{d\tau}(V_{DL}) &= T_B \frac{d}{dt} \left(\frac{V}{V_{max}} \right) \\
&= \frac{T_B}{V_{max}} \dot{V} \\
&= \frac{T_B}{V_{max}} [\alpha_V (V_i^c - V_i)] \\
\dot{V}_{ND} &= \alpha_V T_B (V_{DL}^c - V_{DL})
\end{aligned} \tag{A.16}$$

Roll rate:

$$\begin{aligned}
\frac{d}{d\tau}(\phi) &= T_B \frac{d}{dt}(\phi) \\
&= T_B \dot{\phi} \\
&= T_B [\alpha_\phi (\phi_i^c - \phi_i)] \\
\dot{\phi}_{ND} &= \alpha_\phi T_B (\phi^c - \phi)
\end{aligned} \tag{A.17}$$

Therefore, the scaled and non-dimensionalized equations of motion for the i th UAV are given by

$$\begin{aligned}
\dot{p}'_{N,i} &= \frac{T_B V_{max}}{P_{RT}} V_{DL,i} \sin \psi_i \\
\dot{p}'_{E,i} &= \frac{T_B V_{max}}{P_{RT}} V_{DL,i} \cos \psi_i \\
\dot{\psi}_{DL,i} &= \frac{g T_B \tan \phi_i}{V_{max} V_{DL,i}} \\
\dot{V}_{DL,i} &= \alpha_V T_B (V_{DL,i}^c - V_{DL,i}) \\
\dot{\phi}_{DL,i} &= \alpha_\phi T_B (\phi_i^c - \phi_i)
\end{aligned} \tag{A.18}$$

Appendix B. Camera Field-of-View Approximation

Using Terning's work [33] as a reference, equations were developed to approximate the sensor footprint projected onto the ground. These relationships will be used to determine suitable equations for the camera FOV overlap on the prescribed path. The following figure will be used for reference throughout the development. In order to calculate the quantities from the equations below, information about the aircraft altitude and attitude must be known. Also, information regarding the camera elevation angle, azimuth angle, and camera FOV must be known.

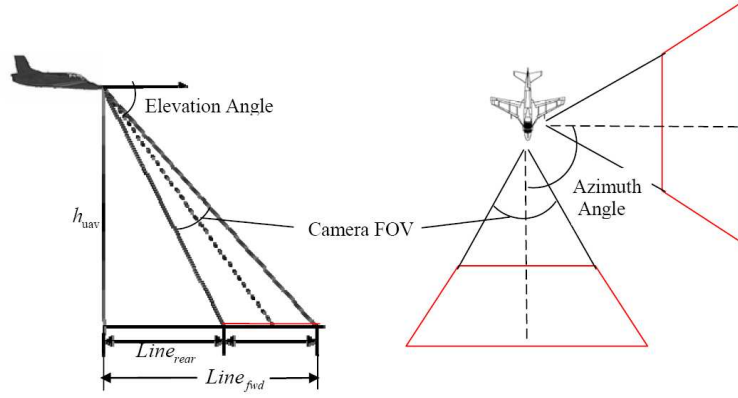


Figure B.1: Camera Field-of-View depiction taken from [33]

In the lefthand image, the $Line_{fwd}$ and $Line_{rear}$ of the sensor footprint are given by

$$Line_{fwd} = \frac{h_{UAV}}{\tan(\theta_{camElevation} - \Phi - \frac{\theta_{VertCamFOV}}{2})} \quad (B.1)$$

$$Line_{rear} = \frac{h_{UAV}}{\tan(\theta_{camElevation} - \Phi + \frac{\theta_{VertCamFOV}}{2})} \quad (B.2)$$

where Φ represents vehicle pitch or vehicle roll depending on approximating the forward or side looking camera FOV (this is the modification to Terning's research). Using Equations (B.1) and (B.2), the corners can be calculated by the following equations for the quantities depicted in Figure B.2. Although the forward-looking case is illustrated, Equations (B.3)-(B.5) are also valid for the side-looking camera

FOV approximation.

$$R_{fwd} = \sqrt{h_{UAV}^2 + Line_{fwd}^2} \quad (B.3)$$

$$Cam_{fwd-LHS} = R_{fwd} \tan\left(\frac{\theta_{HorizCamFOV}}{2}\right) \quad (B.4)$$

$$Cam_{fwd-RHS} = -R_{fwd} \tan\left(\frac{\theta_{HorizCamFOV}}{2}\right) \quad (B.5)$$

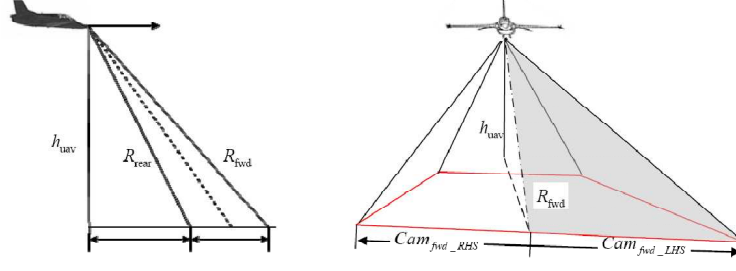


Figure B.2: Camera Field-of-View corner depiction taken from [33]

Listing B.1: This MATLAB function is a modified version of Terning's function used to approximate the camera FOV.

```
function [flines,FOV_PLOT] = createFOV(x_u, y_u, hdg_u,roll, alt_u...
    , camAngle, camElevation, Horiz_camFOV,Vert_camFOV, fieldlimit...
    , plotflag)
%createFOV provides trapezoidal representation of UAV sensor FOV
% Currently does account for bank angle.
% All angles should be in radians
5 % This version accounts for horizontal and vertical FOV angles
%
% Fieldlimit variable needs to be defined in order to scale the ...
%   FOV appropriately within PSCOL

    camElevation_c = camElevation - roll; % Correct the camElevation...
        to account for the bank angle
10 d2r = pi/180;

    up = max(camElevation_c - Vert_camFOV/2,0);
    flines = [alt_u/tan(camElevation_c + Vert_camFOV/2), alt_u/tan(up)...
        ]; % Line_REAR and Line_FWD

15 if abs(flines(2))>fieldlimit,
        flines(2)=fieldlimit;
    end
```

```

range = [norm([flines(1),alt_u]), norm([flines(2),alt_u])]; ...
        % R_rear & R_fwd: Distance from UAV to the ...
        Line_REAR and Line_FWD
20 fRH = [-range(1)*tan(Horiz_camFOV/2), -range(2)*tan(Horiz_camFOV...
        /2)]; % Back and Front CAM_RHS
fLH = [range(1)*tan(Horiz_camFOV/2), range(2)*tan(Horiz_camFOV/2)...
        ]; % Back and Front CAM_LHS
ffarlength = abs(fRH(2) - fLH(2));
fnearlength = abs(fRH(1) - fLH(1));
hyp = [norm([fnearlength/2,range(1)]), norm([ffarlength/2,range(2)...
        ])];
25 %Rotate above shape to desired heading/camera angle combination
rfar = norm([fRH(2),flines(2)]); %projected radial distance to far...
    pt
rnear = norm([fLH(1),flines(1)]); %projected radial distance to ...
    near pt
ranglear = atan2(fRH(2),flines(2));
30 ranglenear = atan2(fRH(1),flines(1));
ranglear2 = [-ranglear+camAngle+hdg_u, ranglear+camAngle+hdg_u...
        ];
ranglenear2 = [-ranglenear+camAngle+hdg_u, ranglenear+camAngle+...
        hdg_u];
FOV1 = [x_u+rfar*cos(ranglear2(2)), (y_u+rfar*sin(ranglear2(2)))...
        ];
    %top RH
35 FOV2 = [x_u+rfar*cos(ranglear2(1)), (y_u+rfar*sin(ranglear2(1)))...
        ];
    %top LH
FOV3 = [x_u+rnear*cos(ranglenear2(2)), y_u+rnear*sin(ranglenear2...
        (2))];
    %bottom LH
FOV4 = [x_u+rnear*cos(ranglenear2(1)), y_u+rnear*sin(ranglenear2...
        (1))];
40 %bottom RH
FOVPL0T=[FOV1;FOV2;FOV4;FOV3;FOV1];

return %createFOV

```

Appendix C. *K*-means Clustering Algorithm

Listing C.1: *K*-means clustering algorithm from Mathworks File Exchange [11].

```
function [gIdx,c]=k_means(X,k)
% K_MEANS    k-means clustering
%   IDX=k_means(X, K) partitions NxP matrix X into K clusters
%   using fully vectorized algorithm, where N is number of data
5 %   points and P is number of variables. The partition minimizes
%   sum of point-to-cluster-centroid Euclidean distances of all
%   clusters. The returned Nx1 vector IDX contains the cluster
%   indices of each point.
%   IDX = k_means(X, C) works with the initial centroids,C,(K x P).
10 %   [IDX,C]=k_means(X, K) returns K centroid locations in KxP ...
%       matrix,C.
%   Version 2.0, by Yi Cao at Cranfield University on 27 March 2008.

% Check input and output
error(nargchk(2,2,nargin));
15 error(nargoutchk(0,2,nargout));

[n,m]=size(X);

% Check if second input is centroids
20 if ~isscalar(k)
    c=k; k=size(c,1);
else
    c=X(ceil(rand(k,1)*n),:);
end
25 % allocating variables
g0=ones(n,1); gIdx=zeros(n,1); D=zeros(n,k);

% Main loop converge if previous partition is the same as current
30 while any(g0~=gIdx)
    g0=gIdx;
    % Loop for each centroid
    for t=1:k
        d=zeros(n,1);
        35 % Loop for each dimension
        for s=1:m
            d=d+(X(:,s)-c(t,s)).^2;
        end
        D(:,t)=d;
    40 end
    % Partition data to closest centroids
    [z,gIdx]=min(D,[],2);
    % Update centroids using means of partitions
    for t=1:k
        45 c(t,:)=mean(X(gIdx==t,:));
    end
end
```

Appendix D. Dudek's Taxonomy

This appendix will provide an overview of Dudek's taxonomy used to facilitate the discussion of multi-agent robotic properties, in this case the RS-UAS. "A key difficulty in the design of multi-agent robotic systems is the size and complexity of the space of possible designs. In order to make principled design decisions, an understanding of the many possible system configurations is essential" [16].

The collective size property categorizes the number of entities acting collaboratively within the environment. A group of autonomous vehicles can range from a single entity to many entities. SIZE-ALONE and SIZE-PAIR are groups of one and two entities, respectively, while SIZE-LIM refers to groups of two or more entities. Dudek included a SIZE-INF category to account for large group numbers that saturate the goals or the environment under consideration.

Communication range applies to entities communicating with other group members, but does not apply to entities communicating with human operators. The COM-NONE category defines a situation when there is no communication between entities. COM-NEAR represents situations when the communication range is limited by hardware or environment. COM-INF assumes there is no limit to communication range but really describes scenarios where the range is much greater than the environment of operation.

Communication topology refers to the manner in which the entities communicate or broadcast information to the rest of the group. TOP-BROAD categorizes situations where an entity can broadcast to other group members within range. TOP-ADD refers to a topology that uses unique identifiers to send information to the entity being identified. This is similar to a computer network using Internet Protocol (IP) addresses to send information to unique computers. TOP-TREE describes topologies that use a static tree communication scheme and, similarly, TOP-GRAPH categorizes scenarios that use a graph topology. Note that the broadcast topology is the most robust scheme since it is not dependent on a single agent passing information.

Communication bandwidth describes how much information can be transmitted for direct and indirect communication. The information transmitted throughout the group carries with it an associated cost for communication, i.e. enemy interception. BAND-ZERO assumes that no communication is possible and therefore dictates that there is no achievable cooperation. BAND-LOW categorizes situations when the communication is highly restrictive due to high consequences of enemy interception. “BAND-MOTION is used to describe network architectures that consider communication cost to be of the same order of magnitude of the cost of moving the robot between locations” [19]. BAND-INF describes scenarios when the communication cost is insignificant.

Collective reconfigurability describes how fast the group can reconfigure itself spatially within the environment. ARR-STATIC describes situations where the group’s configuration is not changing over time. ARR-COM categorizes groups that reconfigure due to cooperation being dependent on communication between entities. ARR-DYN refers to groups that reconfigure indiscriminately.

Processing ability refers to classification of the computational model used by the entities in the group. PROC-SUM processing is a simple non-linear summation while PROC-FSA assumes entities use the finite-state automata. PROC-PDA describes entities that use the push-down automata computation method. PROC-TME is the most common computation method and uses the Turning Machine equivalent.

The final property in Dudek’s Taxonomy is group composition both in the sense of software and hardware. CMP-IDENT describes groups of entities that are all identical, while CMP-HOM refers to groups of entities that only differ in the software being used for control. CMP-HET is a category for groups of entities that are physically different in capabilities, on-board sensors, or both.

Dudek’s Taxonomy is a tool for analyzing an intended system in a CC problem. Table D.1, which was reproduced from [19], concisely outlines Dudek’s Taxonomy.

Table D.1: Dudek's Taxonomy

Property	Description	Subdivision
Collective Size	The number of autonomous agents in the collective	SIZE-ALONE SIZE-PAIR SIZE-LIM SIZE-INF
Communications range	The max distance between 2 elements of the collective such that communications is valid	COM-NONE COM-NEAR COM-INF
Communication topology	The topology used when elements communicate within the range	TOP-BROAD TOP-ADD TOP-GRAPH TOP-TREE
Communication bandwidth	How much information can elements transmit to each other collective	BAND-ZERO BAND-LOW BAND-MOTION BAND-INF
Collective reconfigurability	The rate at which the collective can spatially reorganize itself	ARR-STATIC ARR-COM ARR-DYN
Processing ability	The computational model used by individual elements of the collective	PROC-SUM PROC-FSA PROC-PDA PROC-TME
Collective composition	Are the elements of the collective homogeneous or heterogeneous	CMP-IDENT CMP-HOM CMP-HET

Appendix E. Additional Results

This appendix provides additional results from the six simulations outlined in the test plan of Section 4.3. They are given in the same order as presented in Table 4.1.

E.1 Clicked Route 1

Figure E.1 illustrates the first clicked route from a Dayton area map and the resulting sectors. Figure E.2 illustrates the resulting trajectories from the PSCOL simulations.

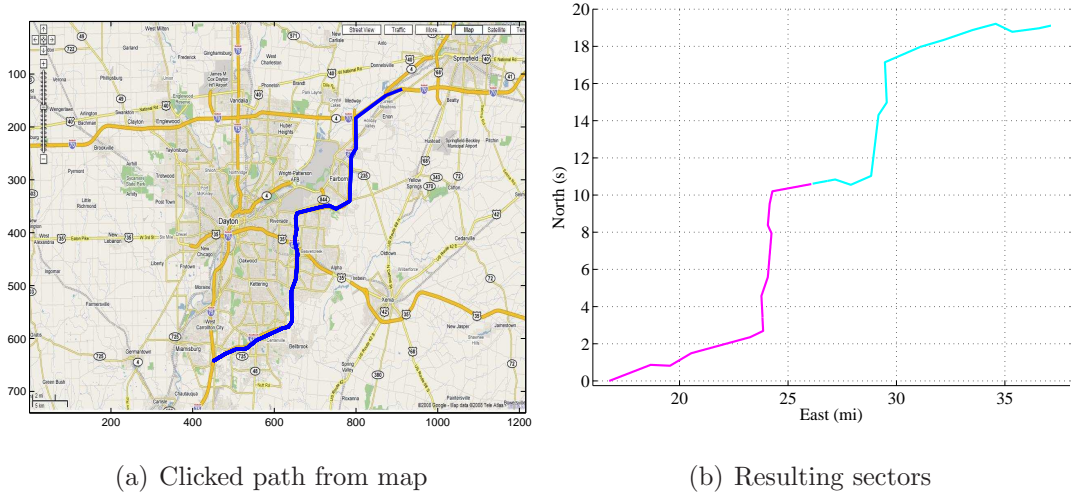


Figure E.1: Clicked route from Dayton for two UAVs and the resulting sectors.

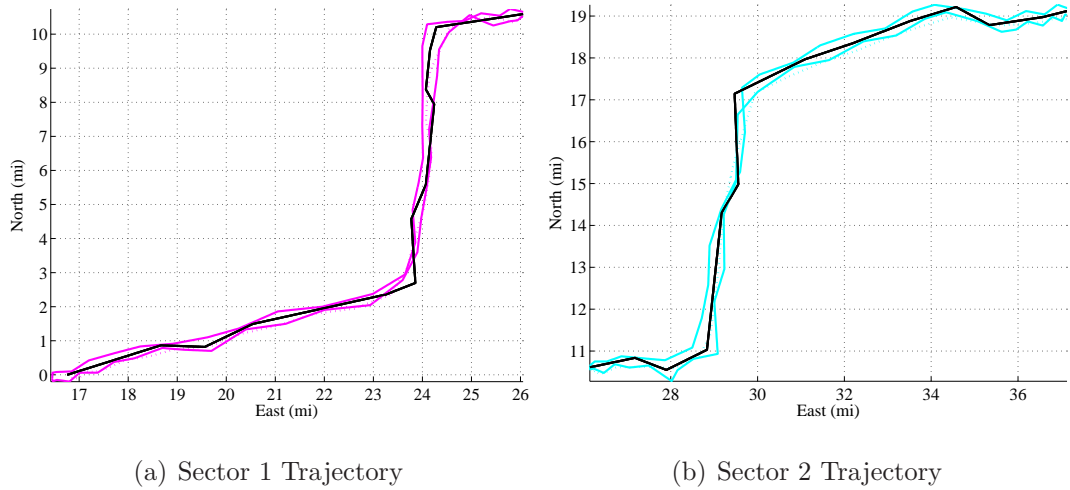


Figure E.2: Sector trajectories over clicked Dayton road.

Figures E.3-E.5 depict the last-visit time functions during the three phases of the problem.

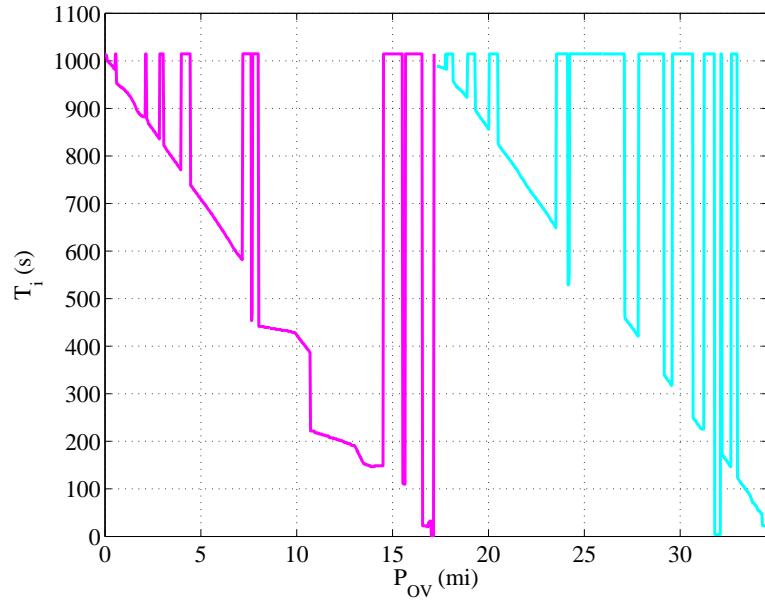


Figure E.3: Clicked Road 1 last-visit time function for Phase 1.

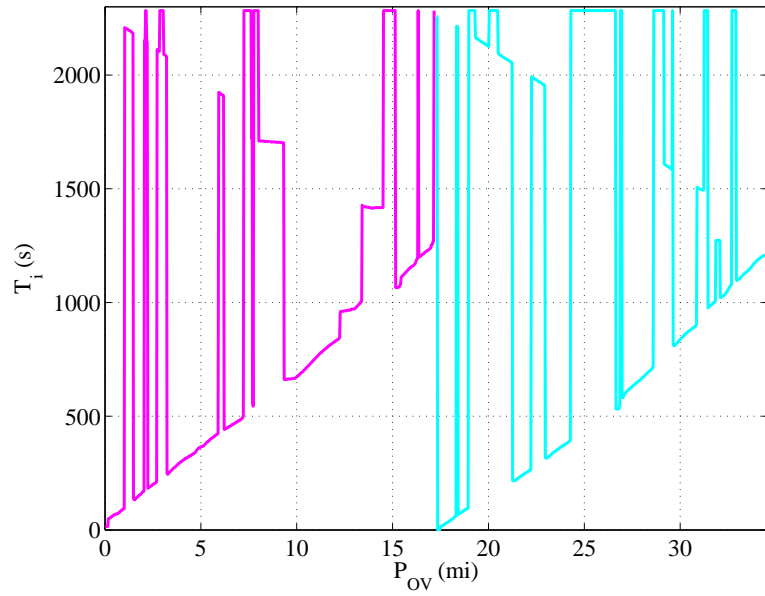


Figure E.4: Clicked Road 1 last-visit time function for Phase 2.

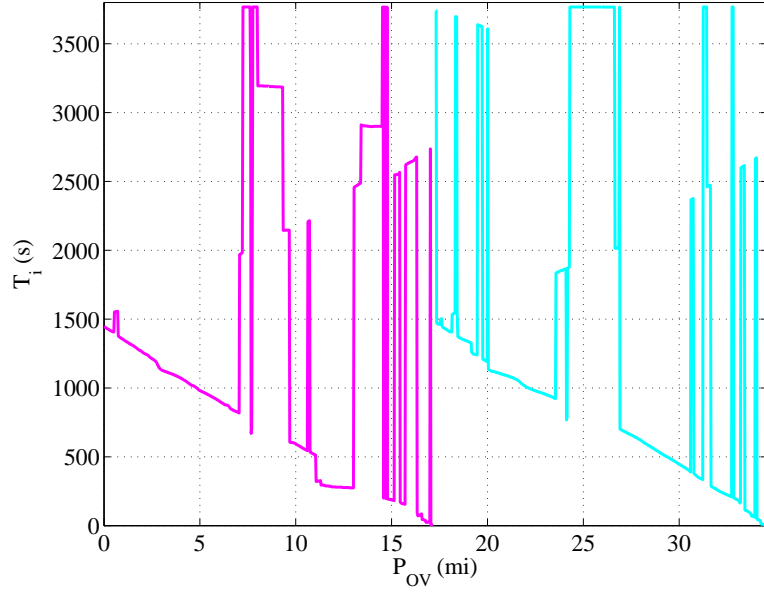


Figure E.5: Clicked Road 1 last-visit time function for Phase 3.

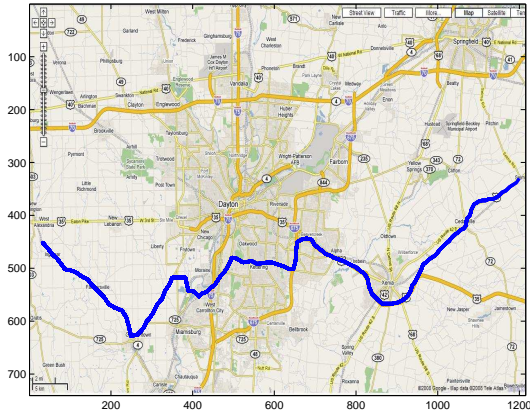
Table E.1 lists the coverage percentage during each phase for both sectors of the route.

Table E.1: Surveillance coverage for Clicked Route 1

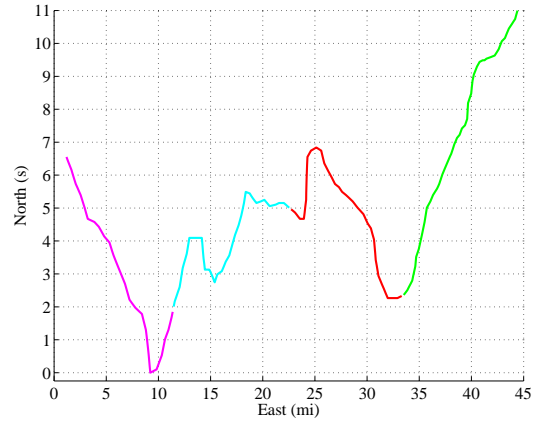
Sector	Sector Length (mi)	Phase 1 (%)	Phase 2 (%)	Phase 3 (%)
1	17.29	79	69	68
2	17.29	54	56	72

E.2 Clicked Route 2

Figure E.6 illustrates the second clicked route from a Dayton area map and the resulting sectors. Figure E.7 illustrates the resulting trajectories from the PSCOL simulations.

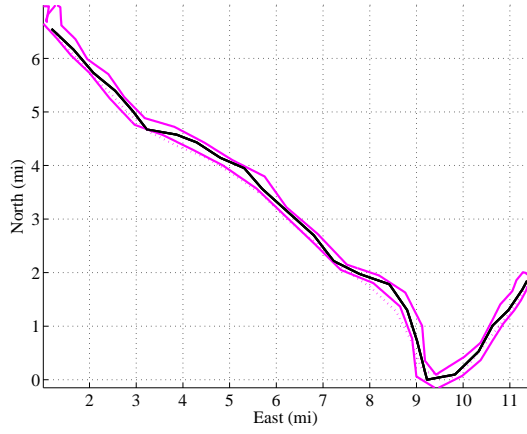


(a) Clicked path from map

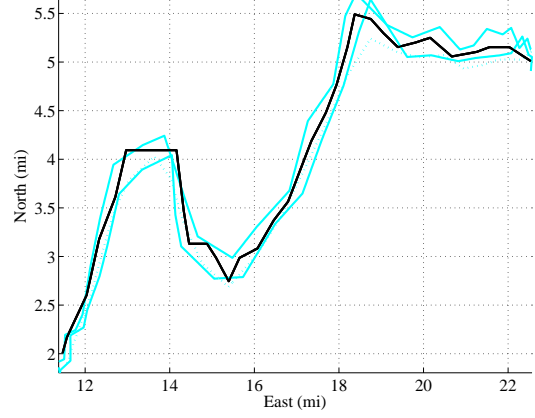


(b) Resulting sectors

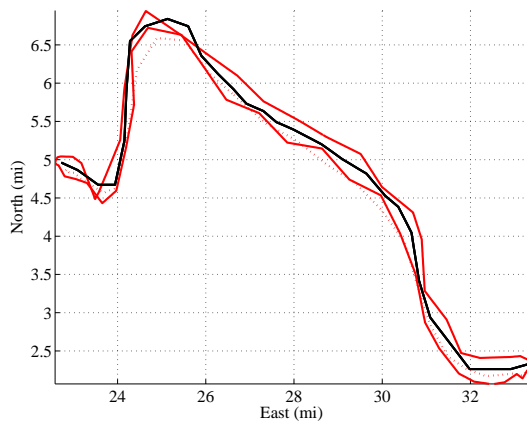
Figure E.6: Clicked route from Dayton for four UAVs and the resulting sectors.



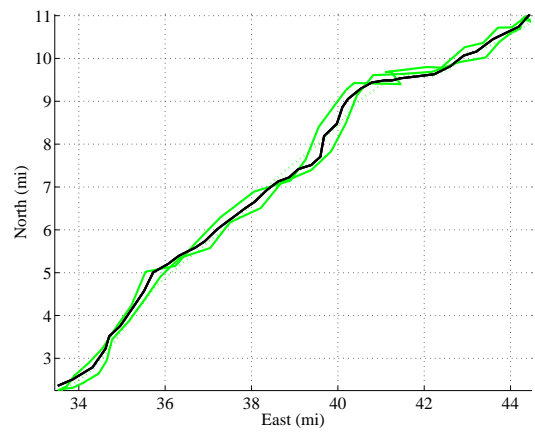
(a) Sector 1 Trajectory



(b) Sector 2 Trajectory



(c) Sector 3 Trajectory



(d) Sector 4 Trajectory

Figure E.7: Sector trajectories over clicked Dayton road for 4 UAV case.

Figures E.8-E.10 depict the last-visit time functions during the three phases of the problem.

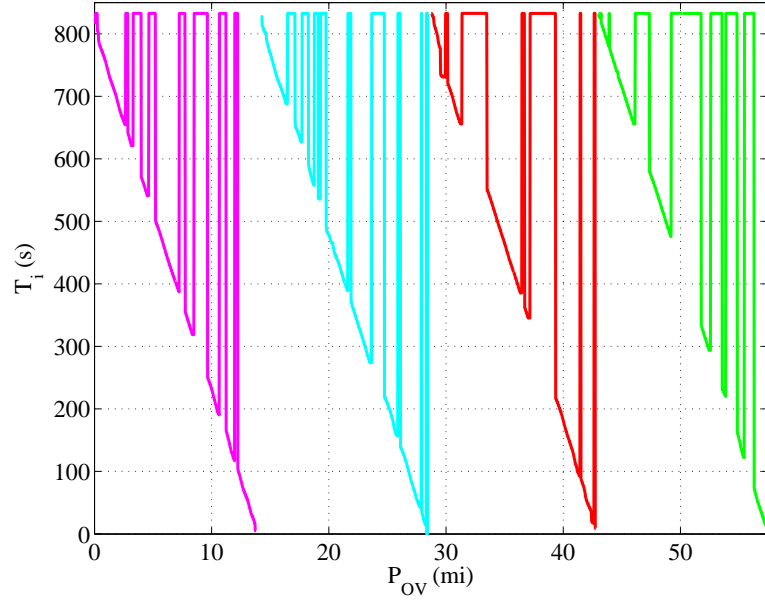


Figure E.8: Clicked Road 2 last-visit time function for Phase 1.

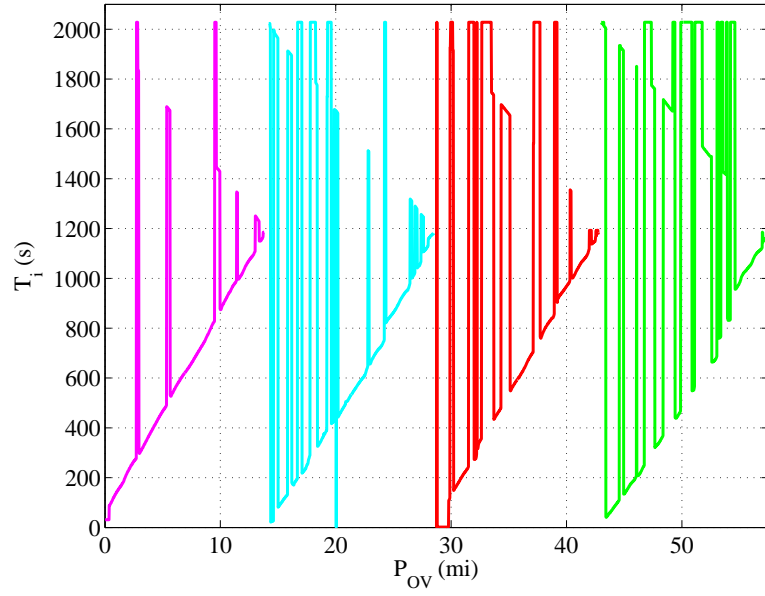


Figure E.9: Clicked Road 2 last-visit time function for Phase 2.

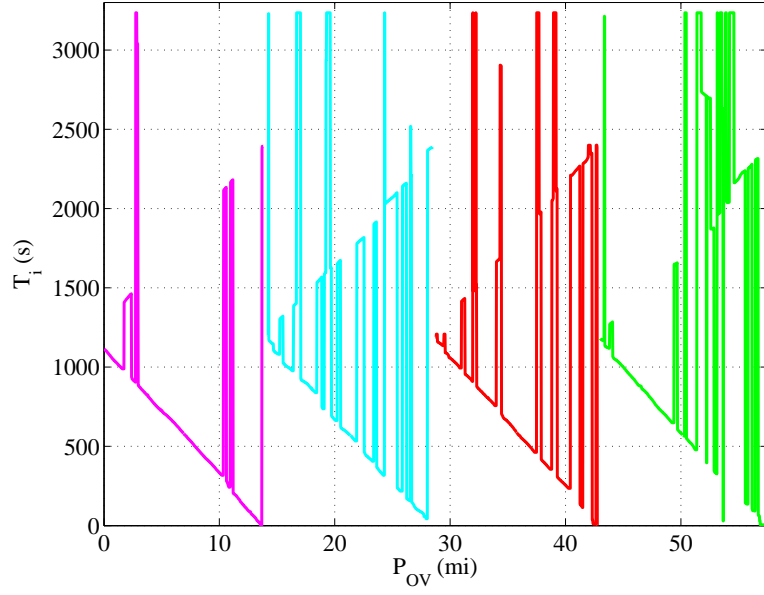


Figure E.10: Clicked Road 2 last-visit time function for Phase 3.

Table E.2 lists the coverage percentage during each phase for both sectors of the route.

Table E.2: Surveillance coverage for Clicked Route 2

Sector	Sector Length (mi)	Phase 1 (%)	Phase 2 (%)	Phase 3 (%)
1	14.19	68	88	87
2	14.52	73	76	63
3	14.29	64	70	72
4	14.48	55	57	65

E.3 Random Route 1

Figure E.11 illustrates a random route divided into three sectors. This route was used for two scenarios where each differed in the implementation of the cost function. The first scenario explained in this section minimized revisit time and control energy. Figure E.12 illustrates the trajectories for each UAV.

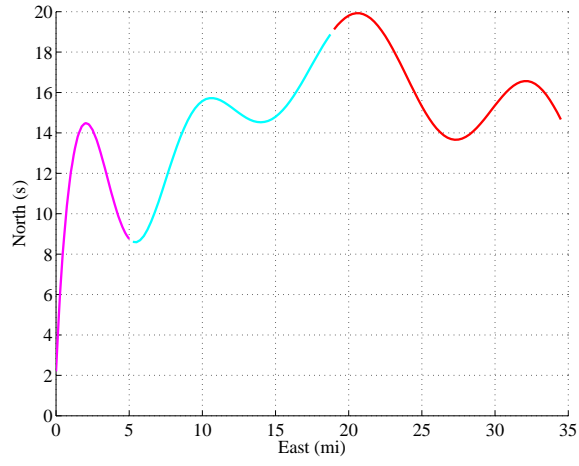
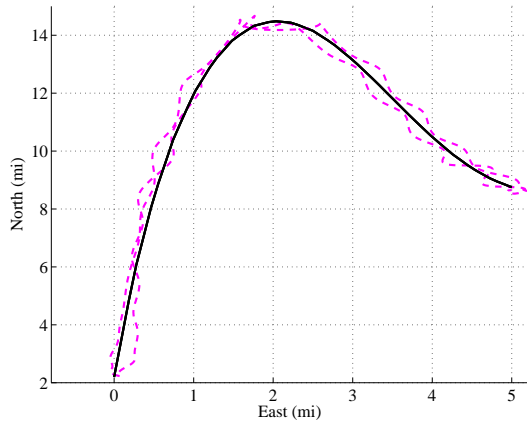
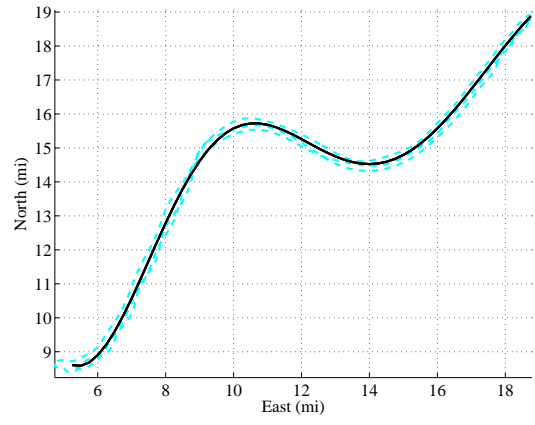


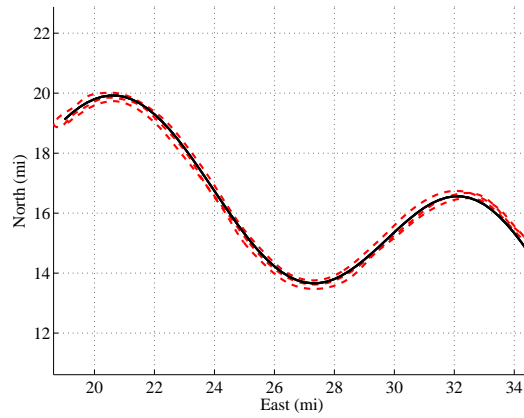
Figure E.11: Random road divided into three sectors.



(a) Sector 1 Trajectory



(b) Sector 2 Trajectory



(c) Sector 3 Trajectory

Figure E.12: Sector trajectories over random road for 3 UAV case.

The last-visit time functions for each phase are illustrated in Figures E.13-E.15.

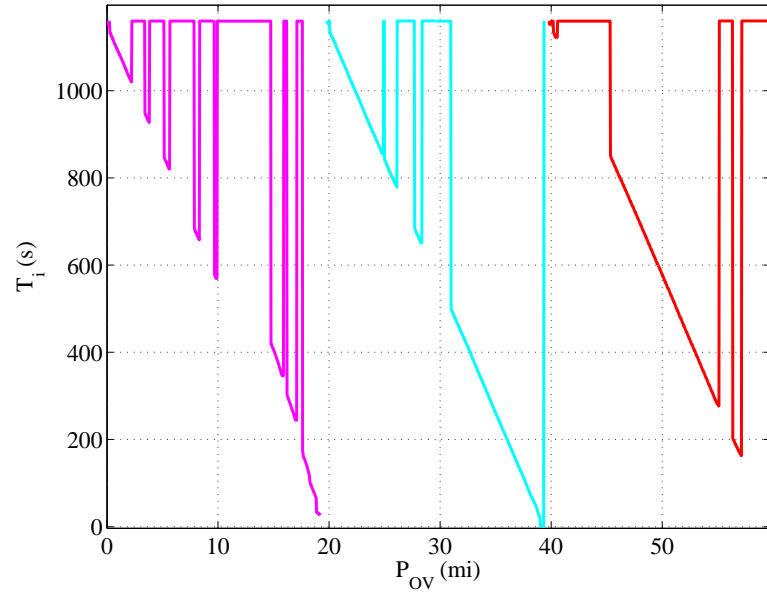


Figure E.13: Random road last-visit time function for Phase 1.

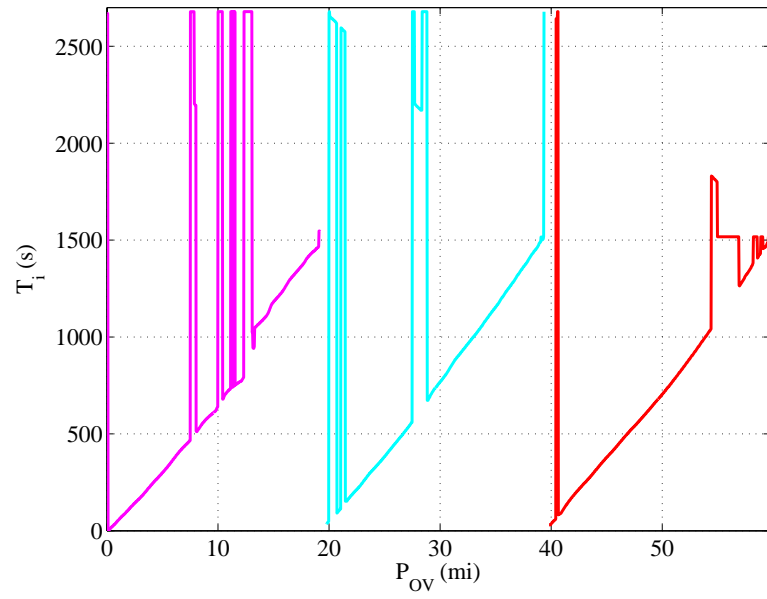


Figure E.14: Random road last-visit time function for Phase 2.

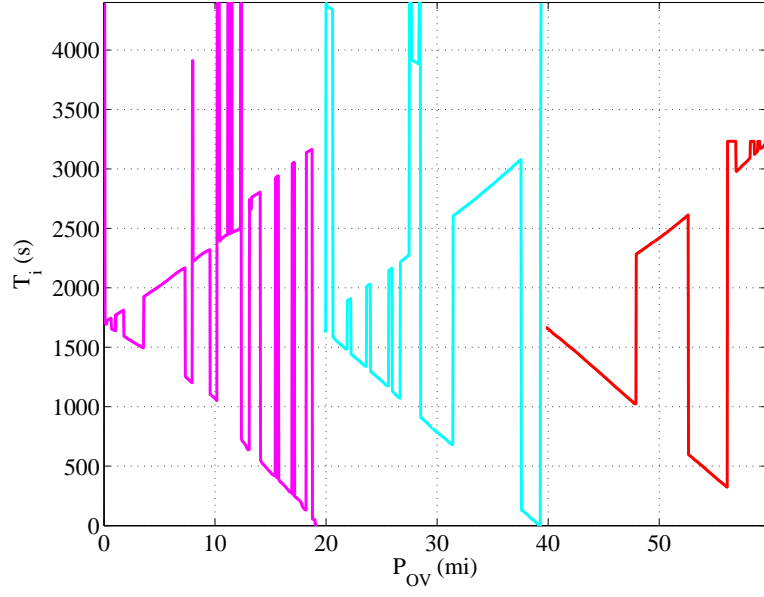


Figure E.15: Random road last-visit time function for Phase 3.

Surveillance coverage per phase outlined in Table E.3.

Table E.3: Surveillance coverage for random route

Sector	Sector Length (mi)	Phase 1 (%)	Phase 2 (%)	Phase 3 (%)
1	19.77	38	86	42
2	20.04	76	85	50
3	19.91	56	97	58

E.4 Texas Route 1

The Texas route served as the baseline scenario for the RS controller. Results were acceptable, but could have been better. The resulting sectors for four UAVs are depicted in Figure E.16.

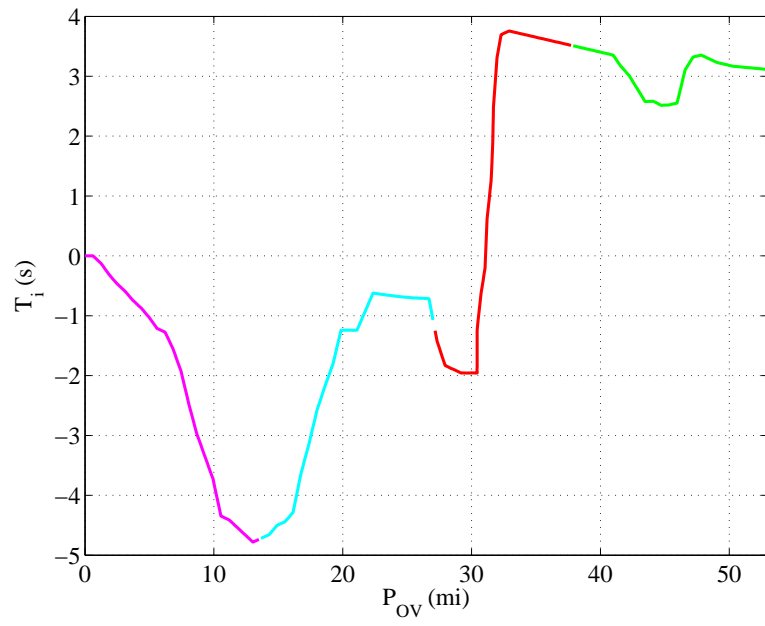


Figure E.16: Texas road divided into four sectors.

Figure E.17 depicts the UAV trajectories over their respective sectors.

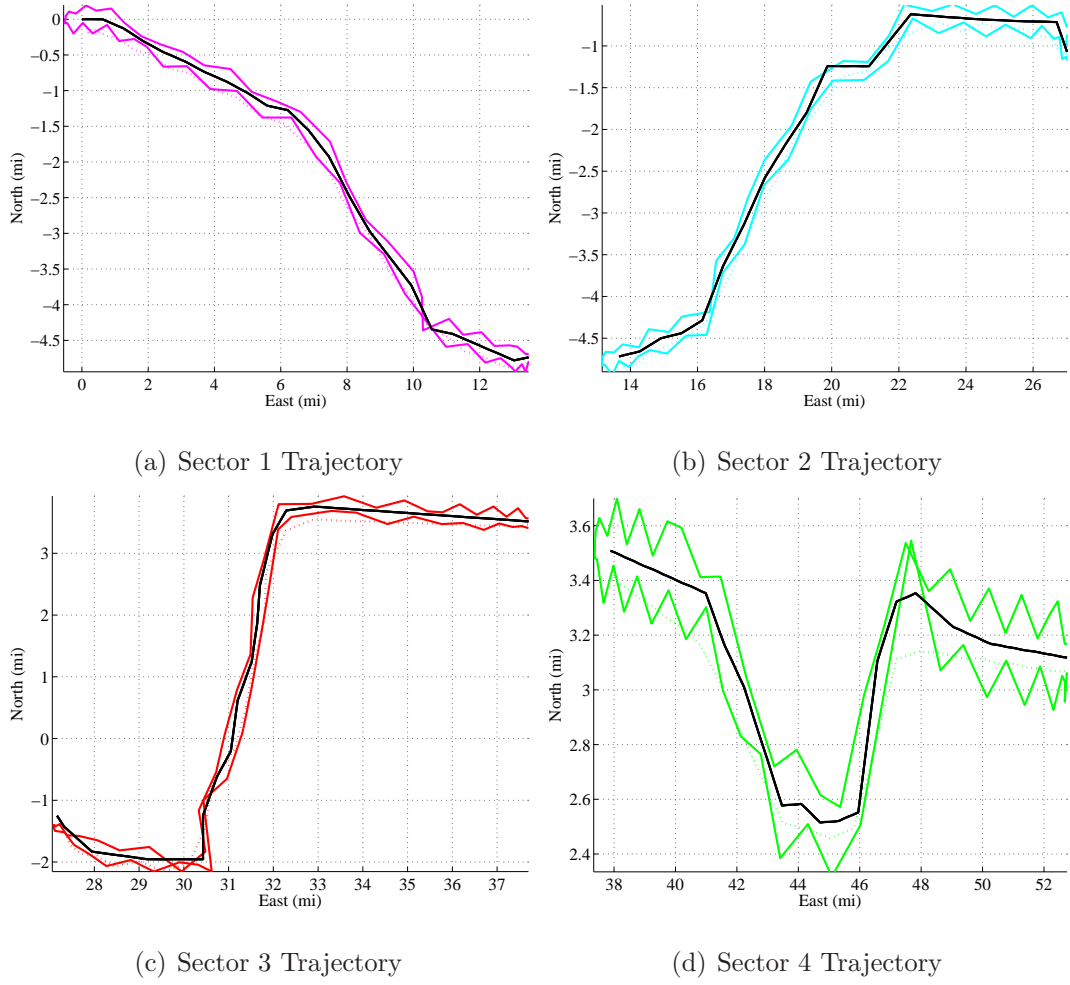


Figure E.17: Sector trajectories over Texas road.

The last-visit time functions for each phase are illustrated in Figures E.18-E.20.

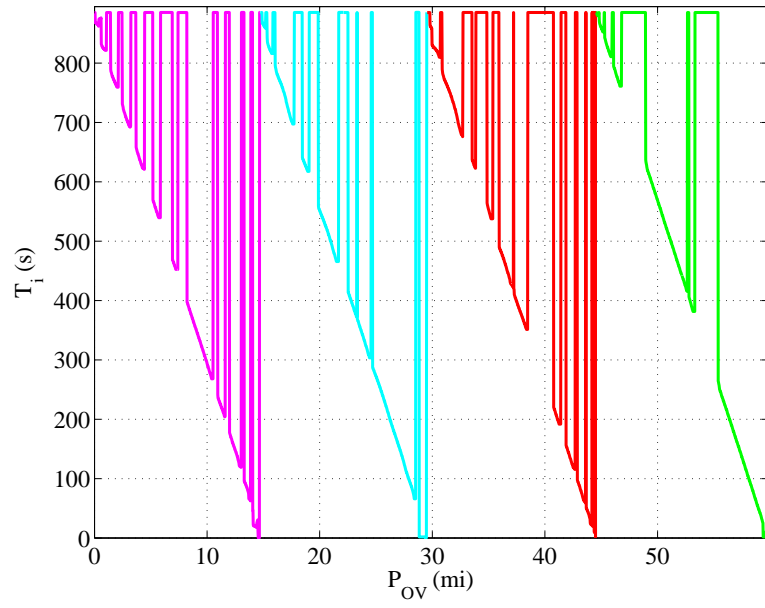


Figure E.18: Texas road last-visit time function for Phase 1.

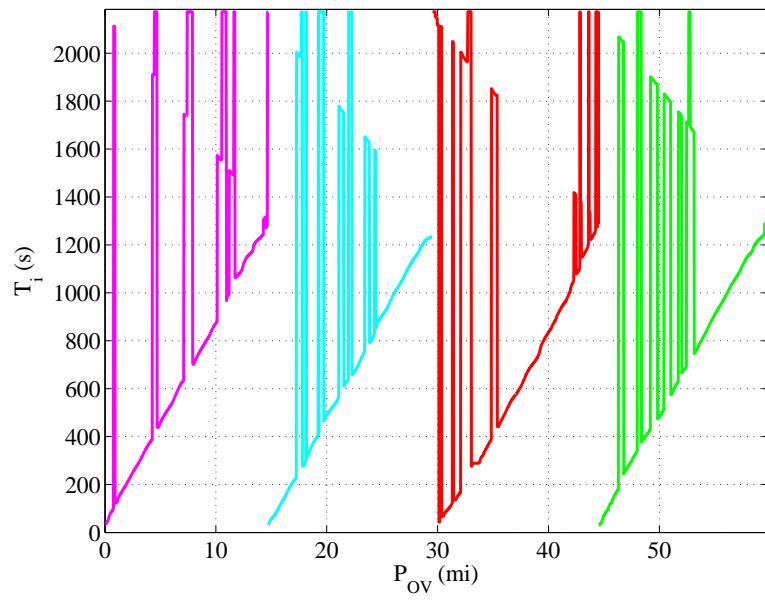


Figure E.19: Texas road last-visit time function for Phase 2.

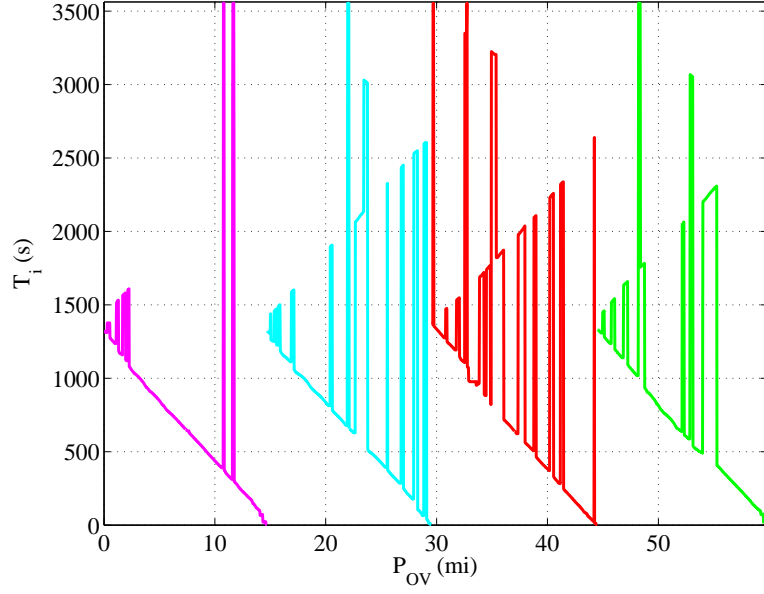


Figure E.20: Texas road last-visit time function for Phase 3.

Table E.4: Surveillance coverage for Texas route

Sector	Sector Length (mi)	Phase 1 (%)	Phase 2 (%)	Phase 3 (%)
1	14.72	65	80	95
2	14.81	78	85	80
3	14.99	60	80	72
4	15.29	70	80	80

E.5 Texas Route 2

This simulation only used a portion of the Texas route because the UAS consisted of only two UAVs. The distance-from-path constraint was decreased in this simulation, and results show that in Sector 1 surveillance coverage increased. However, Sector 2 contained a section that did not conform well to the initial-guess method, and therefore the coverage was marginal. The resulting sectors for two UAVs are depicted in Figure E.21.

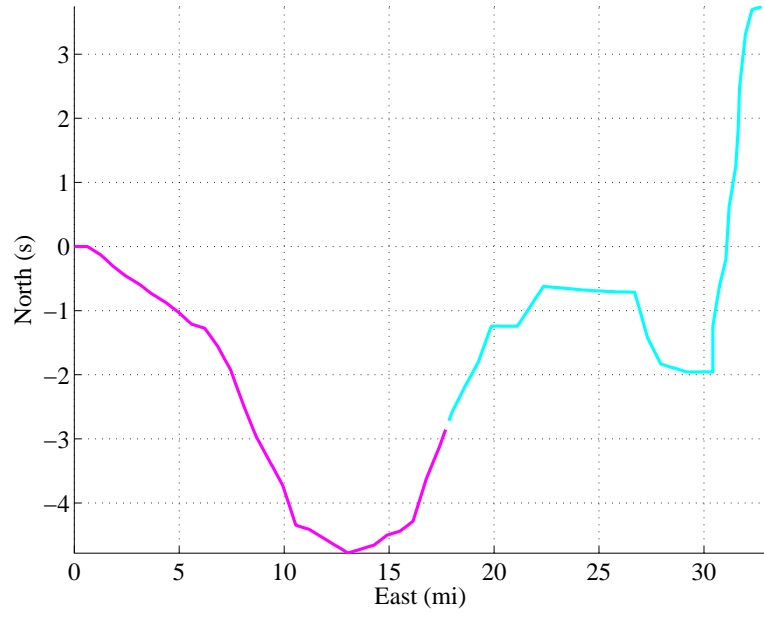
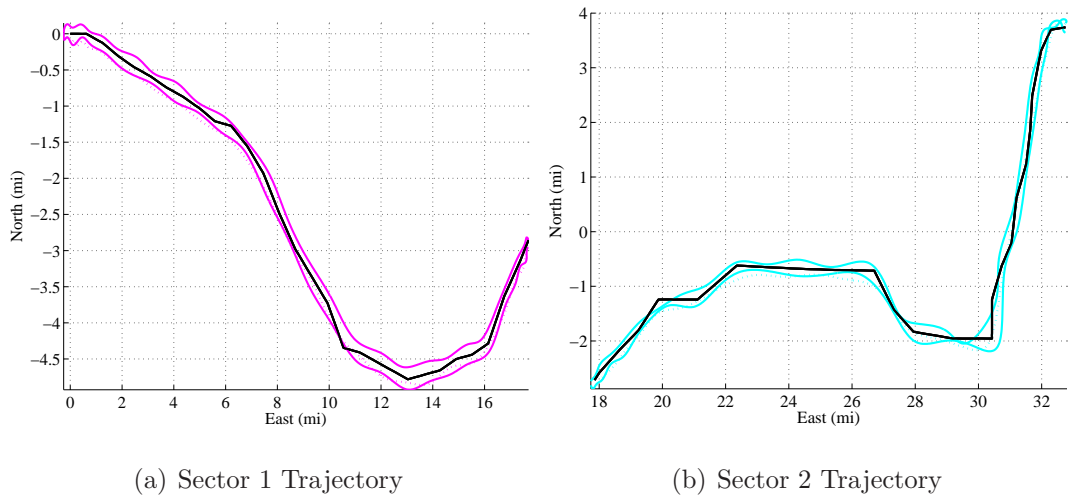


Figure E.21: Partial Texas road divided into two sectors.

Figure E.22 depicts the UAV trajectories over their respective sectors.



(a) Sector 1 Trajectory

(b) Sector 2 Trajectory

Figure E.22: Sector trajectories over Simulation 2.

The last-visit time functions for each phase are illustrated in Figures E.23-E.25.

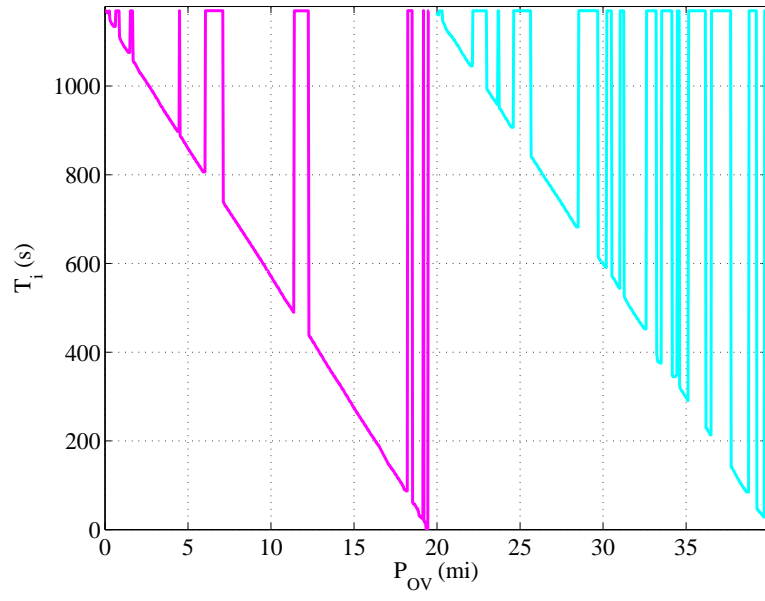


Figure E.23: Texas road last-visit time function for Phase 1.

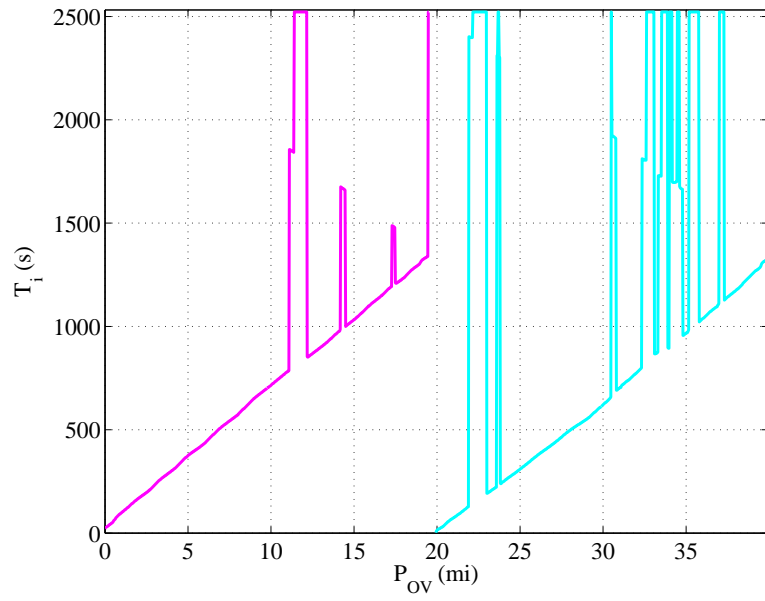


Figure E.24: Texas road last-visit time function for Phase 2.

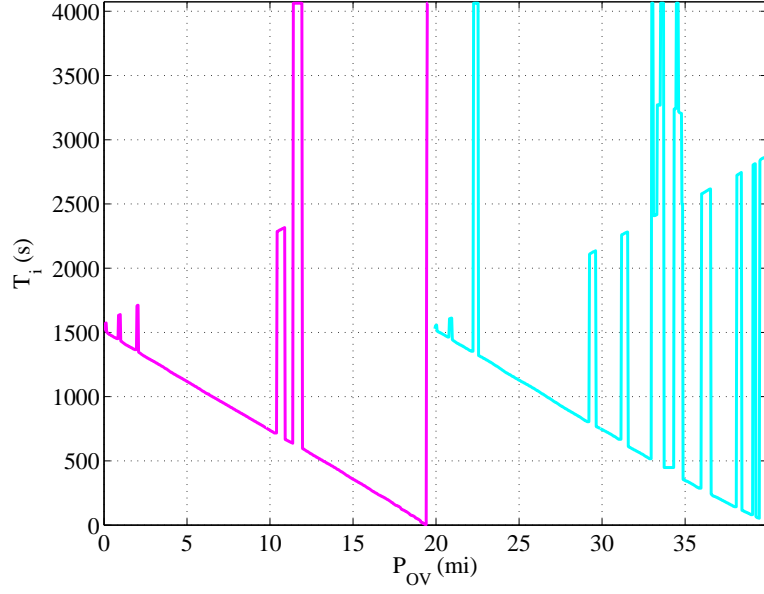


Figure E.25: Texas road last-visit time function for Phase 3.

Table E.5: Surveillance coverage for partial Texas route

Sector	Sector Length (mi)	Phase 1 (%)	Phase 2 (%)	Phase 3 (%)
1	19.93	84	90	91
2	20.01	60	78	80

E.6 Clicked Route 3

This third clicked route served as the simulation that investigated raising the number of nodes to sixty. While the performance was of high quality, a section of the route in Sector 2 did not conform well to the initial-guess method. As a result, there were some sections of the route that were missed in Phases 1 and 3. The resulting sectors for three UAVs are depicted in Figure E.26.

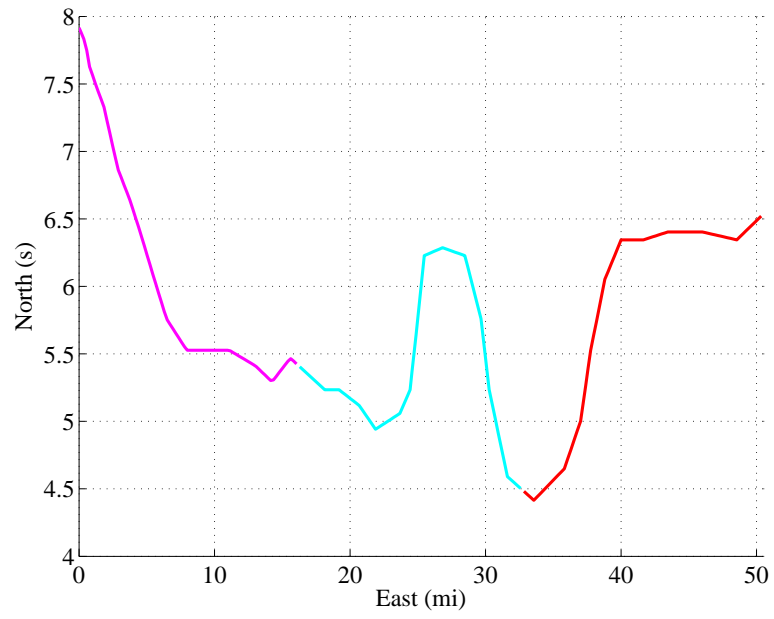


Figure E.26: Clicked Route 3 divided into three sectors.

Figure E.27 depicts the UAV trajectories over their respective sectors.

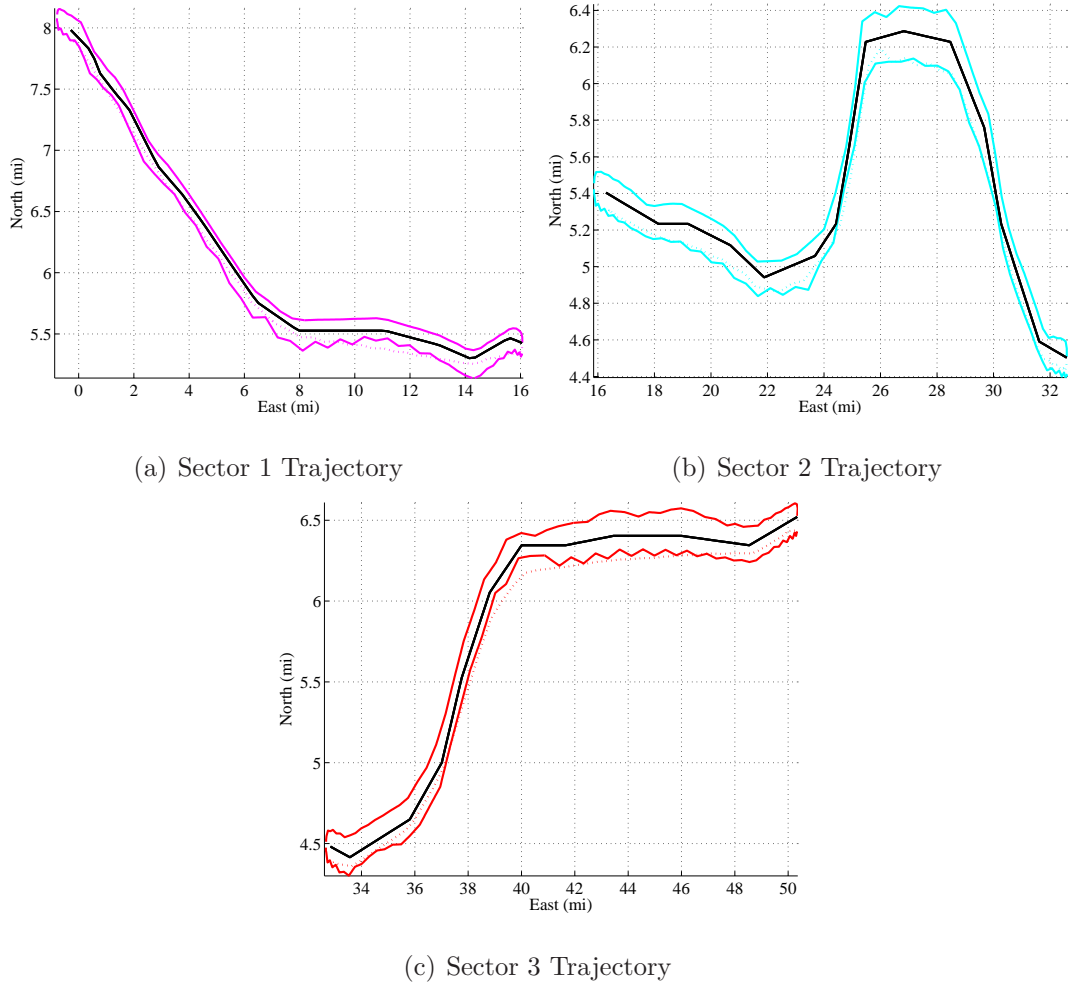


Figure E.27: Sector trajectories over Clicked Route 3.

The last-visit time functions for each phase are illustrated in Figures E.23-E.25.

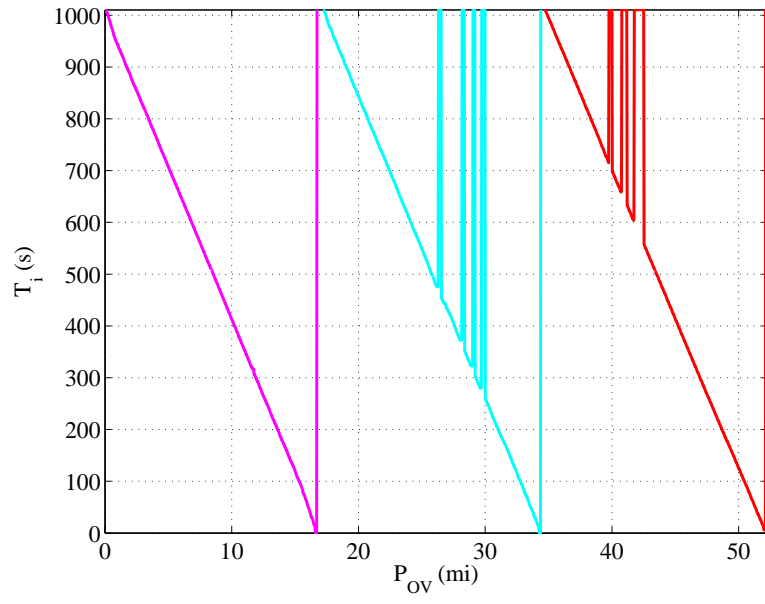


Figure E.28: Clicked Route 3 last-visit time function for Phase 1.

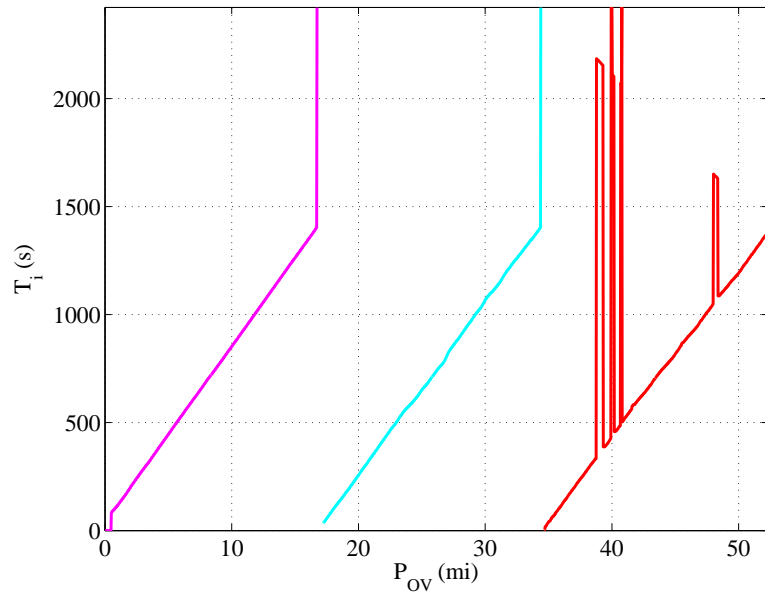


Figure E.29: Clicked Route 3 last-visit time function for Phase 2.

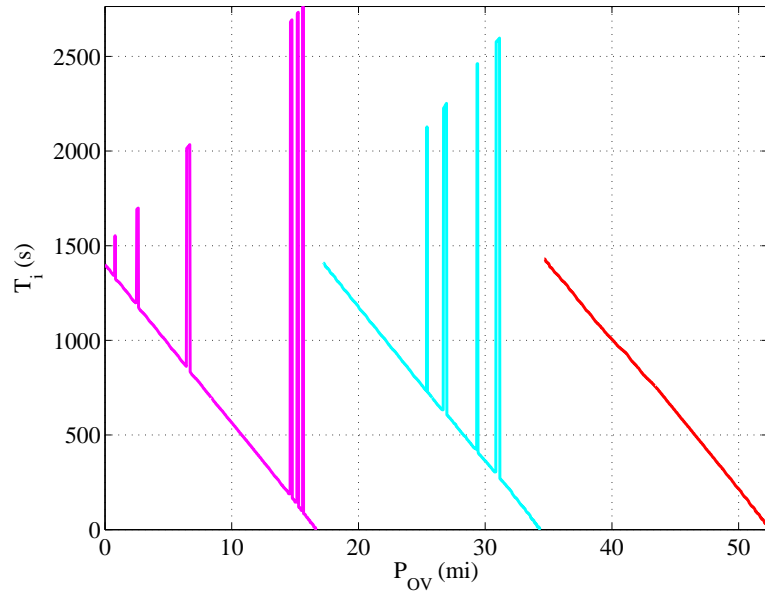


Figure E.30: Clicked Route 3 last-visit time function for Phase 3.

Table E.6: Surveillance coverage for Clicked Route 3

Sector	Sector Length (mi)	Phase 1 (%)	Phase 2 (%)	Phase 3 (%)
1	17.22	97	97	93
2	17.46	93	98	95
3	17.66	92	94	100

Appendix F. Simulation Software

This appendix will provide a description of the simulation software structure. The software will be available by contacting any of the thesis advisors.

This section will assume that the TOMLAB software environment has been installed to function with MATLAB. The user must ensure that the SNOPT solver has been installed within TOMLAB. In this research effort, the PSCOL directory was added to the MATLAB search path. Other versions of PSCOL might require installation. Refer to the software installation instructions for further details. Also, it is encouraged to read the PSCOL User's manual before attempting to decipher the simulation software discussed below.

Recall that the RS-UAS controller was structured to mimic PSCOL, so the main simulation software files use the general structure defined in the PSCOL User's manual supplied with the software. Table F.1 lists the main software files. There are other peripheral functions that were created, however those are not discussed because they are straightforward. Each file will be discussed in the following sections.

Table F.1: Important simulation software files

File	Description
UAV_generalMAIN	Synthesizes the problem and calls the other UAV-general files
UAV_generalCost	Contains the cost function formulation
UAV_generaldae	Contains the UAV model and all path constraints
UAV_generalConnect	Defines the linkage constraints
RSconstants	Defines all the problem constants
getConfiguration	Imports the global constants into each function
create_route	Prompts the user to create a route definition

F.1 UAV_generalMAIN

This file is the largest component of the simulation software where the RS optimal control problem is synthesized to be compatible with PSCOL. There are four basic steps: define the route definition, divide the route, build the problem cell arrays that PSCOL requires, and execute PSCOL.

First, the constants file is called to load the problem constants into a global variable called ‘Constants’, which is a MATLAB structure array. The create_route file is called to prompt the user for a route definition type while augmenting the Constants variable with the waypoints from the route and the route length. Note that resolution is added within the file that creates the routes.

Second, the route definition is divided depending on the team size. For team sizes greater than a single UAV, the K -means clustering algorithm divides the route. Since the K -means function does not sort the sectors, a secondary file sorts the sectors in the correct order. The last requirement in this section is to calculate the sector lengths and required heading to fly the route (used in the initial guess).

Third, the time, problem limits and initial guess are created for each phase. Using the ‘pscollInitialize’ file, the limits and guess are structured using the standard PSCOL structure. Also, the linkage connections are declared here using the structure in the PSCOL manual.

Lastly, the problem parameters are structured into cell arrays in a variable called ‘setup’. PSCOL is called and the solution is saved to file before being plotted. The plot-results file grabs the required variables and plots the trajectory in each phase.

F.2 UAV_generalCost

The cost function file receives two inputs: the current solution and the phase number. The structure of the current solution is given in the PSCOL User’s manual. After importing the global constants with ‘getConfiguration’, the current solution is broken out into individual variables. The revisit cost function for each phase is calculated first and then appended to the control energy cost at the end of the file.

The revisit cost is calculated in the following general steps. The current UAV states are augmented using a built-in MATLAB function. The last-visit time and route-distance vectors are created for simulation speed. Using the augmented state history, the overlap bins are found by projecting the FOV onto the ground and finding

the intersections points using the ‘polyxpoly’ function in MATLAB. After, the last-visit time vector is updated appropriately. The revisit cost is calculated at each instant in time of the original trajectory solution. These steps are iterated throughout the augmented state history for each UAV in the phase. The output is a $1 \times N$ vector, where N is the number of nodes in the problem.

F.3 UAV_generaldae

The dynamics file calculates the dynamics and path constraints using the current solution. The phase number is not used in this file although it is required in the function declaration. After importing the global constants, the state dynamics are calculated using the dimensionless equations outlined in this research. Next, the vehicle path constraint used to restrict the UAV distance from the path is calculated. Conveniently, the ‘dsearchn’ function is used to find the two closest waypoints to the current UAV position. Lastly, the communications constraint is calculated between each UAV. PSCOL requires that the state dynamics and path constraints be formulated into one large output matrix using the structure in the PSCOL User’s manual. The output is a $N \times (7 \cdot K - 1)$ matrix, where N is the number of nodes and K is the number of UAVs.

F.4 UAV_generalConnect

The connections file is typically the same for any multi-phase problem in PSCOL; the syntax was copied from the PSCOL User’s manual. The linkage constraints connect the states, controls, and time in Phases 1 to 2 and Phases 2 to 3.

F.5 RSconstants and getConfiguration

The constants file conveniently places the problem constants in one location under the variable called ‘Constants’, which is a MATLAB structure. Every simulation file requires this global variable to function properly. The file ‘getConfiguration’ is used to import this variable into each simulation function.

F.6 Create_route

The route creation file prompts the user to select from four methods of creating a route: click a route from a map, click a route from a blank figure, create a random route, or load a predefined route file. Once the user has selected a type, the vector of waypoints describing the route is augmented with the appropriate waypoint resolution. The outputs of this file include the route definition, route length, and the exact distance between all of the waypoints.

Appendix G. PSCOL and TOMLAB Setup

Before the RS-UAS software can be executed, the end user must ensure that PSCOL and TOMLAB are correctly installed. Air Force Institute of Technology (AFIT) government students and faculty have access to both PSCOL and TOMLAB. Other users will need to acquire a license for both PSCOL and TOMLAB. The following instructions were created by Major Tim Jorris and assume both software packages have been acquired. Installing PSCOL and TOMLAB are completed in the following manner:

- Close MATLAB and navigate to the executable file: tomlab-win32-73-setup.exe for MATLAB 7 through 2006b or tomlab-win32-setup-2007a.exe for MATLAB 2007a
- Select custom install
- Choose an install directory, e.g. C:\tomlab\
- Select the following options to successfully execute the RSCC algorithm (other options are not needed):
 - TOMLAB Base Module
 - TOMLAB Minos
 - TOMLAB Sol: with SNOPT and NPSOL
 - TOMLAB Mad
 - TOMLAB GPOCS
- Click next and then install
- Copy the tomlab.lic file to the installed directory for TOMLAB

After TOMLAB has completed installation, open MATLAB and type the following at the command line: 'run('C:\tomlab\startup.m')' or wherever the directory for TOMLAB is located. The startup file will confirm a correct installation and add the TOMLAB directories to the MATLAB search directories.

Once TOMLAB has been installed with MATLAB, the next step is to add the PSCOL libraries to the MATLAB search directories. The ‘addpath’ command in MATLAB can be used.

Bibliography

1. *Joint UAS Concept of Operations*. Technical report, Office of the Secretary of Defense, Department of Defense, March 2007.
2. *Unmanned Systems Roadmap 2007-2032*. Technical report, Office of the Secretary of Defense, Department of Defense, Oct 2007.
3. Anderson, E.P., R.W. Beard, and T.W. McLain. “Real-time dynamic trajectory smoothing for unmanned air vehicles”. *Control Systems Technology, IEEE Transactions on*, 13(3):471–477, May 2005. ISSN 1558-0865.
4. Barooah, P. and J.P. Hespanha. “Estimation on Graphs from Relative Measurements”. *Control Systems Magazine, IEEE*, 27(4):57–74, Aug. 2007. ISSN 0272-1708.
5. Beard, R., D. Kingston, M. Quigley, D. Snyder, R. Christiansen, W. Johnson, T. McLain, and M. A. Goodrich. “Autonomous vehicle technologies for small fixed-wing UAVs”. *Journal of Aerospace Computing, Information and Communication*, (JA):92 – 108, 2005. ISSN 1542-9423.
6. Beard, R.W., T.W. McLain, D.B. Nelson, D. Kingston, and D. Johanson. “Decentralized Cooperative Aerial Surveillance Using Fixed-Wing Miniature UAVs”. *Proceedings of the IEEE*, 94(7):1306–1324, July 2006. ISSN 0018-9219.
7. Benson, D., G. Huntington, T. Thorvaldsen, and A. Rao. “Direct Trajectory Optimization and Costate Estimation via an Orthogonal Collocation Method”. *AIAA Guidance, Navigation, and Control Conference and Exhibit, 2006*, 1435–1440, November-December 2006.
8. Bethel, R.E. and G.J. Paras. “A PDF Multitarget Tracker”. *IEEE Transactions on Aerospace and Electronic Systems*, 30(2):386–403, 1994.
9. Borrelli, F., D. Subramanian, A.U. Raghunathan, and L.T. Biegler. “MILP and NLP Techniques for centralized trajectory planning of multiple unmanned air vehicles”. *American Control Conference, 2006*, June 2006.
10. Bryson, A.E. and Yu-Chi Ho. *Applied Optimal Control: Optimization, Estimation, and Control*. Blaisdell Pub. Co., 1969.
11. Cao, Yi. “Efficient K-Means Clustering using JIT”. *MATLAB Central*. [Online]. Available: <http://www.mathworks.com/matlabcentral/fileexchange/19344>. [Accessed: October 2009].
12. Chandler, P.R. “Cooperative control of a team of UAVs for tactical missions”. volume 1, 7 – 15. Chicago, IL, United States, 2004.

13. Chandler, P.R., M. Pachter, and S. Rasmussen. "UAV cooperative control". volume 1, 50 – 55. Arlington, VA, 2001. ISSN 0743-1619. URL <http://dx.doi.org/10.1109/ACC.2001.945512>.
14. Chandler, P.R., M. Pachter, S. Rasmussen, and Schumacher C. "Distributed Control for Multiple UAVs with Strongly Coupled Tasks". American Institute of Aeronautics and Astronautics, 2003.
15. Decker, D. *Decision Factors for Cooperative Multiple Warhead UAV Target Classification and Attack with Control Applications*. Ph.D. thesis, Air Force Institute of Technology (AETC), Wright-Patterson AFB, OH, October 2005. AFIT/DS/ENY/05-04.
16. Dudek, G., M.R.M Jenkin, Milios E., and Wilkes D. "Taxonomy for multi-agent robotics". *Autonomous Robots*, 3(4):375–397, Dec 1996.
17. Earl, M.G. and R. D'Andrea. "Modeling and control of a multi-agent system using mixed integer linear programming". *Decision and Control, 2002, Proceedings of the 41st IEEE Conference on*, 1:107–111 vol.1, Dec. 2002. ISSN 0191-2216.
18. Flint, M., E. Fernandez, and M. Polycarpou. "Stochastic Models of a Cooperative Autonomous UAV Search Problem". *Military Operations Research*, 8(4):13–32, 2003.
19. Gurfil, P. and E. Kivelevitch. "Flock properties effect on task assignment and formation flying of cooperating unmanned aerial vehicles". *Journal of Aerospace Engineering, IME*, 221(4):401–416, Jun. 2007. ISSN 0954-4100.
20. Hansen, J., M. Pachter, D. Jacques, and Blue P. "Optimal Guidance of a Relay MAV for ISR Support Beyond Line-of-Sight". *AIAA Guidance, Navigation, and Control Conference and Exhibit, Honolulu, Hawaii*, August 2008.
21. Hartigan, J.A. *Clustering Algorithms*. John Wiley and Sons, Inc., New York, 1975.
22. Jorris, T. *Common Aero Vehicle Autonomous Reentry Trajectory Optimization Satisfying Waypoint and No-fly Zone Constraints*. Ph.D. thesis, Air Force Institute of Technology (AETC), Wright-Patterson AFB, OH, September 2007. AFIT/DS/ENY/07-04.
23. Karasz, W.J. *Optimal Re-entry Trajectory Terminal State Due to Variations in Waypoint Locations*. Master's thesis, Air Force Institute of Technology (AETC), Wright-Patterson AFB, OH, December 2008. AFIT/GA/ENY/08-D01.
24. Kim, S. and Y. Kim. "Three Dimensional Optimum Controller for Multiple UAV Formation Flight Using Behavior-based Decentralized Approach". *International Conference on Control, Automation and System*, Oct. 2007.
25. Kingston, D., R. Holt, R. Beard, T. McLain, and D. Casbeer. "Decentralized perimeter surveillance using a team of UAVs". volume 1, 128 – 134. San Francisco, CA, United States, 2005.

26. Klavins, E. "Programmable Self-Assembly". *Control Systems Magazine, IEEE*, 27(4):43–56, Aug. 2007. ISSN 0272-1708.
27. Luo, J and C.E. Lan. "Determination of weighting matrices of a linear quadratic regulator". *Journal of Guidance, Control, and Dynamics*, 18(6):1462–1463, Dec. 1995. ISSN 0731-5090.
28. Martinez, S., J. Cortes, and F. Bullo. "Motion Coordination with Distributed Information". *Control Systems Magazine, IEEE*, 27(4):75–88, Aug. 2007. ISSN 0272-1708.
29. McLain, T.W. and R.W. Beard. "Coordination variables, coordination functions, and cooperative-timing missions". *Journal of Guidance, Control, and Dynamics*, 28(1):150 – 161, 2005. ISSN 0731-5090.
30. Murphey, R. and P.M. Pardalos. *Cooperative Control and Optimization*. Kluwer Academic Publishers, 1st edition edition, 2002.
31. Rosario, R.A. *Optimal Sensor Threshold Control and the Weapon Operating Characteristic for Autonomous Search and Attack Munitions*. Master's thesis, Air Force Institute of Technology (AETC), Wright-Patterson AFB, OH, March 2007. AFIT/GAE/ENG/07-02.
32. Solmon, C. "Cooperation of LP solvers for solving MILPs". *Tools with Artificial Intelligence, 1997. Proceedings., Ninth IEEE International Conference on*, 240–247, Nov 1997.
33. Terning, N.A. *Real-time Flight Path Optimization for Tracking Stop-and-Go Targets with Micro Air Vehicles*. Master's thesis, Air Force Institute of Technology (AETC), Wright-Patterson AFB, OH, March 2008. AFIT/GAE/ENY/08-M28.
34. Weisstein, Eric W. "K-Means Clustering Algorithm". *MathWorld—A Wolfram Web Resource*. [Online]. Available: <http://mathworld.wolfram.com/K-MeansClusteringAlgorithm.html>. [Accessed: October 2009].
35. Yang, Y., M. Minai, and M. Polycarpou. "Decentralized Cooperative Search in UAV's Using Opportunistic Learning". *AIAA Guidance, Navigation, and Control Conference and Exhibit, Monterey, CA, Aug. 5-8, 2002*, Aug 2002.

Vita

Captain Joseph Rosal grew up in Pensacola, Florida where he attended the University of West Florida. In December 2003 after transferring to the University of Florida, he graduated with a Bachelor of Science Degree in Electrical Engineering and was commissioned from the AFROTC program as a 2nd Lieutenant, United States Air Force. His first assignment was as an Antenna Systems Engineer at the Air Force Research Laboratory, Hanscom Air Force Base, Massachusetts. After completing his tour at Hanscom Air Force Base, he was accepted to the Air Force Institute of Technology at Wright-Patterson Air Force Base, Ohio. Upon graduation, he will be assigned to the 46th Test Wing at Eglin Air Force Base, Florida.

REPORT DOCUMENTATION PAGE					Form Approved OMB No. 0704-0188	
<p>The public reporting burden for this collection of information is estimated to average 1 hour per response, including the time for reviewing instructions, searching existing data sources, gathering and maintaining the data needed, and completing and reviewing the collection of information. Send comments regarding this burden estimate or any other aspect of this collection of information, including suggestions for reducing this burden to Department of Defense, Washington Headquarters Services, Directorate for Information Operations and Reports (0704-0188), 1215 Jefferson Davis Highway, Suite 1204, Arlington, VA 22202-4302. Respondents should be aware that notwithstanding any other provision of law, no person shall be subject to any penalty for failing to comply with a collection of information if it does not display a currently valid OMB control number. PLEASE DO NOT RETURN YOUR FORM TO THE ABOVE ADDRESS.</p>						
1. REPORT DATE (DD-MM-YYYY)		2. REPORT TYPE		3. DATES COVERED (From — To)		
14-03-2009		Master's Thesis		Aug 2008 — Mar 2009		
4. TITLE AND SUBTITLE Centralized Cooperative Control For Route Surveillance With Constant Communication				5a. CONTRACT NUMBER		
				5b. GRANT NUMBER		
				5c. PROGRAM ELEMENT NUMBER		
				5d. PROJECT NUMBER		
6. AUTHOR(S) Rosal, Joseph D. Capt, USAF				5e. TASK NUMBER		
				5f. WORK UNIT NUMBER		
7. PERFORMING ORGANIZATION NAME(S) AND ADDRESS(ES) Air Force Institute of Technology Graduate School of Engineering and Management (AFIT/EN) 2950 Hobson Way WPAFB OH 45433-7765				8. PERFORMING ORGANIZATION REPORT NUMBER AFIT/GE/ENG/09-38		
9. SPONSORING / MONITORING AGENCY NAME(S) AND ADDRESS(ES) Air Force Research Laboratory Attn: Alok Das 2241 Avionics Circle WPAFB, OH 45433 937-674-9882; alok.das@wpafb.af.mil				10. SPONSOR/MONITOR'S ACRONYM(S) AFRL/RY		
				11. SPONSOR/MONITOR'S REPORT NUMBER(S)		
12. DISTRIBUTION / AVAILABILITY STATEMENT Approval for public release; distribution is unlimited.						
13. SUPPLEMENTARY NOTES						
14. ABSTRACT The route surveillance (RS) mission is a new application of unmanned aircraft systems (UASs) to meet the reconnaissance and surveillance needs of combatant commanders. This mission intends to field a four-vehicle UAS that can provide surveillance of convoy routes. This research focuses on developing a solution strategy based on the application of optimal control and cooperative control theory. The RS controller uses the UAS team size to divide the route into sectors for each entity. A specialized cost function and path constraints are used to formulate an optimal control problem that minimizes revisit time to the route and overall control energy of the UAS. The problem complexity makes an analytical solution difficult, so a numerical technique based on the Gauss pseudospectral method is used to solve for the optimal solution. The output trajectories represent paths that the UAS could fly to provide constant surveillance. Simulated and real-world routes containing likely urban and rural characteristics are used to test the controller and show that the developed system provides feasible solutions under certain conditions.						
15. SUBJECT TERMS route surveillance, cooperative control, unmanned aerial vehicle						
16. SECURITY CLASSIFICATION OF:			17. LIMITATION OF ABSTRACT	18. NUMBER OF PAGES	19a. NAME OF RESPONSIBLE PERSON	
a. REPORT	b. ABSTRACT	c. THIS PAGE			LtCol. Gregory J. Toussaint, AFIT/ENG	
U	U	U	UU	126	19b. TELEPHONE NUMBER (include area code) (937)255-3636 x7257;gregory.toussaint@afit.edu	